

國立臺灣大學工學院化學工程研究所

碩士論文

Department of Chemical Engineering

College of Engineering

National Taiwan University

Master Thesis



具拉伸及生物可相容性之水膠：製備、特性分析及於  
電阻式記憶體應用

Fabrication and Characterization of a Stretchable and  
Biocompatible Pseudo-Hydrogel for Resistor Memory  
Device Applications

吳加恩

Mercedes Wu

指導教授：陳文章 博士

Advisor: Wen-Chang Chen, Ph.D

中華民國 106 年 7 月

July, 2017

## Acknowledgments



I would like to thank Professor Wen-Chang Chen for the support and advice during my graduate studies. I would also like to thank Dr. Chien Chung Shih for the extremely helpful suggestions, discussions, and tutelage during the entire course of my thesis project. I felt that Dr. Shih went above and beyond to help this project. I would like to thank Professor Guo, Professor Lee, and Professor Chiu for being in my defense committee and giving great advice and suggestions.

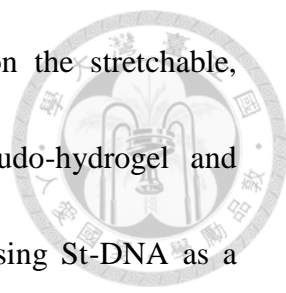
I would also like to thank 徐聖甯 for teaching me about ultrasonic spray-coating, AFM, alpha-step, and the PVA:PMAA polymer system for dielectric use when I arrived in this lab. Many thanks to 張晉榮 for helping me with all of the documentation and paperwork for my graduate studies. Many thanks as well to Hsu Li-Che, Sophia Huang, and Hsieh Hui-Ching for teaching and helping me run various analysis tools like DSC, TGA, XRD, etc... I would also like to thank Dr. Jung Yao Chen and Dr. Mengyao Gao for their help and advice during my graduate studies. Much gratitude for Ender Ercan and 林俊延 for being able to work together during late hours. Final thanks to 劉欣瑜, 謝昀庭, 吳炳翰, Chiang Yun-Chi, 吳欣叡, 曾尹澤, 王燕婷, 林彥丞, Eric Tsai, 蔡長紘, 洪誌鍵 and 曾建偉 for all their help in making the lab a friendly and easy to communicate place.

## Abstract



Biodegradable/biocompatible organic materials are a safe, non-toxic, renewable, and low-cost alternative to traditional inorganic and plastic options. In the world of electronic substrates, hydrogels are a viable “green” alternative to traditional stretchable electronic substrates but lack a direct integration pathway because of intrinsic properties like solvent evaporation, high water content, and poor mechanical characteristics. If these weaknesses were overcome, a suitable scaffold for fully stretchable, non-toxic, and biocompatible electronics could be recognized.

In the first part of the thesis (chapter 2), a biocompatible, non-toxic, self-healing, mechanically tough, vapor absorbing and retaining, and recyclable PVA:PMAA pseudo-hydrogel is easily fabricated. TGA, DSC, XRD, FTIR, and self-healing testing were used to confirm that the full blending of PVA and PMAA polymers as well as give insight on the strong hydrogen cross-link bonding between them. Stress-strain curves, relaxation times, loading and unloading mechanical testing revealed the high elongation, fast recovery, and tunable mechanical properties which helped confirm the 3D gel network of the pseudo-hydrogel structure. The pseudo-hydrogel interactions with water were especially important as the gel was able to absorb and retain water vapor which is a novel property. The gel was also able to dissolve fully in water which is important for recycling and biodegradable pathways.



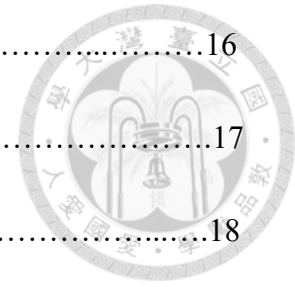
In the second part of the thesis (chapter 3), we built upon the stretchable, biocompatible, nontoxic, and water-soluble nature of the pseudo-hydrogel and fabricated a high performance resistive DNA memory device. Using St-DNA as a charge trapping and transporting layer, the memory device was fabricated using a structure of 1:1 pseudo-hydrogel/1:4 PEDOT:PU/St-DNA/1:4 PEDOT:PU to preserve the “green” properties of the pseudo-hydrogel. The device exhibited WORM memory characteristics similar to literature findings with a  $V_{c,ON}$  of 2V, a high ON/OFF current ratio of  $10^4$  and a long retention time of  $10^4$ s. The device also retained these memory characteristics under 10, 30, and 50% strain as well as 1000 strain cycles at 30% strain. The device could be easily dissolved in DI water, which opens up recyclability, bioresorbability, and biodegradability potential.

Keywords: stretchable, biocompatible, disintegratable, hydrogel, resistor memory

# Contents

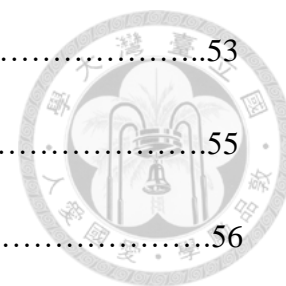


<b>Abstract.....</b>	<b>II</b>
<b>Table Captions.....</b>	<b>VIII</b>
<b>Figure Captions.....</b>	<b>IX</b>
<b>Chapter 1. Introduction.....</b>	<b>1</b>
1.1 Introduction to Biodegradable/Biocompatible Organic Electronics.....	1
1.1.1 Hydrogels.....	2
1.1.1.1 Tough Double-network Hydrogels.....	2
1.1.1.2 Hybrid Hydrogels.....	4
1.1.1.3 Self-healing Hydrogels.....	5
1.1.2 Organogels.....	6
1.1.3 Biodegradable “Green” Substrates.....	8
1.2 Introduction to Polymer Memory.....	10
1.2.1 Resistor-type Polymer Memory Device Structure and Fabrication...	11
1.2.2 Resistor-type Memory Classifications.....	12
1.2.3 Operating Mechanism of Polymer Resistor-type Memory.....	13
1.2.3.1 Filamentary Conduction Mechanism.....	13
1.2.3.2 Charge Transfer (CT) Mechanism.....	14
1.2.3.3 Charge Trapping-Detrapping Mechanism.....	15

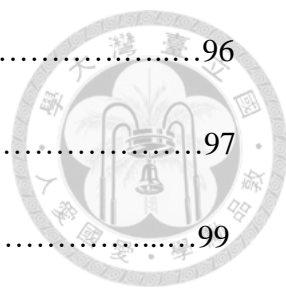


1.2.3.4 Conformational Change.....	16
1.2.4 Polymer Materials for Resistor-type Memory.....	17
1.2.4.1 Polyimides.....	18
1.2.4.2 $\pi$ -Conjugated Polymers.....	19
1.2.4.3 “Green” and Biocompatible Polymers.....	20
1.2.4.4 Polymer Composites.....	21
1.3 Research Objectives.....	24
1.4 References.....	26
<b>Chapter 2. Fabrication and Characterization of PVA:PMAA Pseudo-Hydrogels for Biocompatible and Stretchable Electronic Substrates.....</b>	<b>46</b>
2.1 Introduction to PVA:PMAA Pseudo-Hydrogel.....	46
2.2 Experimental.....	47
2.2.1 Materials.....	47
2.2.2 Characterization.....	47
2.2.3 Fabrication of Pseudo-Hydrogels.....	48
2.3 Results and Discussion.....	49
2.3.1 Pseudo-hydrogel Analysis.....	49
2.3.1.1 Thermogravimetric Analysis (TGA).....	49
2.3.1.2 Differential Scanning Calorimetry (DSC).....	50
2.3.1.3 X-ray Diffraction (XRD).....	52

2.3.1.4 Infrared Spectroscopy (FTIR).....	53
2.3.1.5 Self-healing Properties.....	55
2.3.2 Water and Pseudo-hydrogel interactions.....	56
2.3.2.1 Water Vapor Absorption and Equilibrium.....	57
2.3.2.2 Recycling and Biodegradable Potential.....	60
2.3.2.3 Effect of Vapor Content on Mechanical Properties.....	61
2.3.3 Mechanical Properties.....	62
2.3.3.1 Stress-Strain Curves and Relaxation Times of Pseudo-hydrogel Blends .....	62
2.3.3.2 Relaxation Times and Load-Unload Cycles.....	64
2.3.3.3 Effect of Different Cross-linking Times and Temperatures....	65
2.4 Conclusion.....	66
2.5 References.....	68
<b>Chapter 3. Biocompatible and Stretchable DNA Memory fabricated on a PVA:PMAA Pseudo Hydrogel.....</b>	<b>90</b>
3.1 Introduction to Biocompatible Memory Devices.....	90
3.2 Experimental.....	93
3.2.1 Materials.....	93
3.2.2 Characterization.....	93
3.3.3 Fabrication and Measurement of Memory Devices.....	94



3.3 Results and Discussion.....	96
3.3.1 Pseudo-hydrogel Surface Morphology.....	97
3.3.2 Memory Device Characterization.....	99
3.3.2.1 Memory Device Performance Under Strain.....	100
3.3.2.2 DNA Memory Mechanism.....	100
3.3.3 Memory Device Dissolution in Water.....	102
3.3.4 Conclusions.....	103
3.4 References.....	104
<b>Chapter 4. Conclusion and Future Work.....</b>	<b>112</b>





## Table Captions



<b>Table 1-1.</b> Chemical structures of electroactive layers and their memory characteristics.....	34
<b>Table 2-1.</b> Effect of vapor content on the Young’s modulus of a 1:1 pseudo-hydrogel .....	72
<b>Table 2-2.</b> Stress-strain curve data for PVA, PMAA, and pseudo-hydrogel blends casted in EG.....	72
<b>Table 2-3.</b> Strain-relaxation curves from 25% strain for pseudo-hydrogel blends.....	73
<b>Table 2-4.</b> Stress-strain curve data for different cross-linking times of a 1:1 pseudo-hydrogel blend.....	73
<b>Table 2-5.</b> Strain-relaxation curves from 25% strain for different cross-linking times of a 1:1 pseudo-hydrogel blend.....	74

## Figure Captions



**Figure 1-1.** Double-Network hydrogel diagrams in an (a) alginate–polyacrylamide double-network gel and (b) polymer-supramolecular polymer double-network gel.....39

**Figure 1-2.** Stretchable and dehydration resistant hydrogel-elastomer hybrid.....40

**Figure 1-3.** Self-healing A6ACA hydrogels containing dangling side chains with carboxyl groups.....40

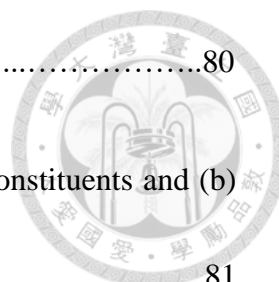
**Figure 1-4.** Environmentally stable PEDOT:PSS-PAAm organogels before and after being stored in a vacuum for 22 hours.....41

**Figure 1-5.** Examples of biodegradable substrates used to make electronic devices which include: (a) organic transistor active-matrix driver on a paper substrate, (b) organic thin film transistor fabricated on resorbable PLGA, (c) Organic resistive memory fabricated on DNAC substrate.....42

**Figure 1-6.** Device structure of resistor-type memory: (a) MIM test cell and (b) cross-point array.....43

**Figure 1-7.** Device structure of stretchable memory device with a structure of PDMS/CNTs/MH-b-P<sub>12.6k</sub>/Al.....43

<b>Figure 1-8.</b> Class architypes of polymer resistive memories.....	44
<b>Figure 1-9.</b> Schematics of the switching effects of (a) carbon-rich filaments and (b) metallic filaments.....	44
<b>Figure 1-10.</b> Mechanisms of electric field-induced charge transfer.....	45
<b>Figure 1-11.</b> Example of conformational change memory behavior using the (a) chemical structure of PCz and (b) current voltage characteristics.....	45
<b>Figure 2-1.</b> Facile fabrication of PVA:PMAA pseudo-hydrogel.....	75
<b>Figure 2-2.</b> Plotted (a) TGA and (b) DTG thermogram of PVA casted in EG and Water. (c) TGA and (d) DTG of PMAA casted in EG and Water. (e) TGA and (f) DTG of PVA, PMAA, and pseudo-hydrogel blends casted in EG.....	75
<b>Figure 2-3.</b> DSC thermograms of (a) PVA casted in EG and Water (b) PVA, PMAA, and pseudo-hydrogel blends casted in EG.....	77
<b>Figure 2-4.</b> XRD diagrams of (a) PVA casted in EG and Water (b) PVA, PMAA, and pseudo-hydrogel blends casted in EG.....	78
<b>Figure 2-5.</b> FTIR spectra of PVA casted in water, DMSO, and EG in (a) overlay, (b) offsets, and (c) close-up of 1200 to 600 $\text{cm}^{-1}$ .....	79
<b>Figure 2-6.</b> FTIR spectra of (a) PMAA casted in water and DMSO and (b) PMAA	



casted under different durations at 200 °C in EG.....80

**Figure 2-7.** FTIR spectra of (a) pseudo-hydrogels and their pure constituents and (b) close-up of the pseudo-hydrogel blends.....81

**Figure 2-8.** FTIR spectra of (a) 1:1 PVA:PMAA pseudo-hydrogel at different cross-linking temperatures and times and b) the change in  $A_{3320}/A_{2930}$  ratio and  $A_{1710}/A_{2930}$  as a function of cross-linking temperature and duration. ....82

**Figure 2-9.** Picture of (a) cut and self-healed under ambient condition pseudo-hydrogel casted at 200 °C with (b) strain testing.....83

**Figure 2-10.** Picture of (a) cut and self-healed under 60 °C and high humidity pseudo-hydrogel casted at 150 °C and its corresponding (b) stress-strain curve.....84

**Figure 2-11.** Water vapor absorption of PVA, PMAA, and pseudo-hydrogel blends casted in EG .....85

**Figure 2-12.** Water vapor retention of three 1:1 pseudo-hydrogel samples.....85

**Figure 2-13.** Recycling through dissolution in DI water of 1:1 pseudo-hydrogel.....86

**Figure 2-14.** Effect of vapor content on the Stress-strain curve of a 1:1 pseudo-hydrogel.....86

**Figure 2-15.** Stress-strain curves of PVA, PMAA, and pseudo-hydrogel blends casted



in EG.....87

**Figure 2-16.** Strain-relation curves at 25% strain of pseudo-hydrogel blends.....87

**Figure 2-17.** (a) Load-unload cycles of 1:1 pseudo-hydrogel and (b) stress relaxation curves for 1:1 pseudo-hydrogel. ....88

**Figure 2-18.** Stress-strain curves of a 1:1 pseudo-hydrogel at different cross-linking temperatures and times. ....89

**Figure 2-19.** Strain-relation curves at 25% strain of a 1:1 pseudo-hydrogel at different cross-linking temperatures and times. ....89

**Figure 3-1.** Diagram (a) and picture (b) of stretchable DNA memory device.....107

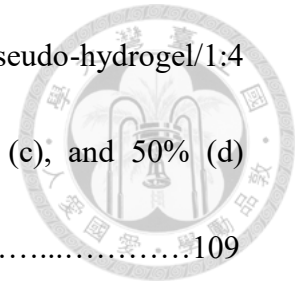
**Figure 3-2.** AFM topographies and phase images of 1:1 pseudo-hydrogel at an area of (a) 25  $\mu\text{m}^2$  and (b) 100  $\mu\text{m}^2$ .....107

**Figure 3-3.** I-V curves (a) and retention times (b) of the St-DNA (sodium salt) memory devices fabricated on a device structure of 300nm silicon oxide/Al/St-DNA/Al.....108

**Figure 3-4.** I-V curves (a) and retention times (b) of the St-DNA (sodium salt) memory devices fabricated on a device structure of 1:1 pseudo-hydrogel/1:4 PEDOT:PU/St-DNA/1:4 PEDOT:PU.....108

**Figure 3-5.** I-V curves and retention times (read at 1 V) of the St-DNA (sodium salt)

memory devices fabricated on a device structure of 1:1 pseudo-hydrogel/1:4 PEDOT:PU/St-DNA/1:4 PEDOT:PU at 0% (a), 10% (b), 30% (c), and 50% (d) strain.....109



**Figure 3-6.** Compilation of I-V curves (a) and retention times (read at 1 V) (b) of the St-DNA (sodium salt) memory devices at 0%, 10%, 30%, and 50% strain.....110

**Figure 3-7.** ON state retention of stretchable DNA resistor device after 500 cycles of 30% strain and relax.....111

**Figure 3-8.** DNA device dissolution in DI water over 24 hours.....111

# Chapter 1

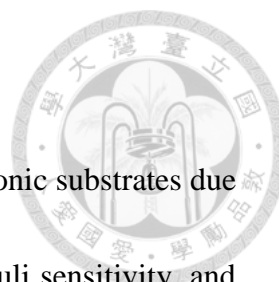


---

## Introduction

### 1.1 Introduction to Biodegradable/Biocompatible Organic Electronics

Biodegradable/biocompatible organic materials are a safe, non-toxic, renewable and low-cost alternative to traditional inorganic and plastic options. With the steady rise in consumer electronics as well as the decrease in electronic lifetimes, a sustainable and environment friendly alternative should be transitioned into.<sup>1-4</sup> Furthermore, green organic materials offer unique advantages over inorganic and plastic based electronics with their ability to increase in material flexibility, stretchability, bioresorbability and mechanical robustness.<sup>2</sup> An increase in the mechanical properties of biomaterials is especially important in the field of wearable electronics where inorganic materials are no longer attractive options due to their inherent rigidity.<sup>4</sup> The ultimate goal of research into “green” materials is to not only utilize their intrinsic advantages like low toxicity, low-cost, flexibility/stretchability, and biodegradability/biocompatibility, but also provide exceptional and unimaginable functionalities compared over traditional materials.



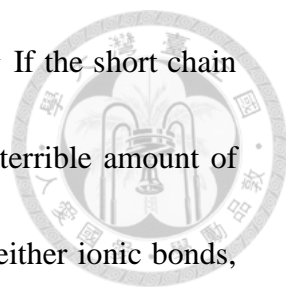
## 1.1.1 Hydrogels

Hydrogels are a new and exciting biomaterial option for electronic substrates due to their high stretchability, biocompatibility, biodegradability, stimuli sensitivity, and self-healing potential.<sup>5-11</sup> Traditionally, hydrogels are classified as a three-dimensional network of polymers that possess a high degree of flexibility due to their large water content.<sup>9</sup> However, hydrogels pose problems for direct integration into high performance electronics due to their poor mechanical properties, water loss, high water content, weak interfacial bonding and low fracture toughness.<sup>5, 6, 7, 11</sup> Many techniques have been applied to hydrogels to overcome these problems and increase their viability in flexible and stretchable electronics.

### 1.1.1.1 Highly Stretchable and Tough Double-network Hydrogels

Forming double-network hydrogels is an innovative way to improve the mechanical properties of hydrogels. Double-network hydrogels are typically formed by two covalently connected networks comprising of one with short chains and the other with longer chains.<sup>10</sup> One major theory behind the toughness of double-network hydrogels is the sacrificial bond principle. It states that gel toughness comes from the breaking weak bonds in the short chains before the stronger bonds in the longer, more densely cross-linked, chains. This prevents gel fracture by delaying chain scission along





the fracture interface of the more strongly bonded chain network.<sup>11</sup> If the short chain bonds are not reversible, double-network hydrogels suffer from a terrible amount of hysteresis.<sup>10</sup> This can be remedied by using sacrificial network of either ionic bonds, hydrophobic interactions, crystallites or hydrogen bonds to improve the recovery of mechanical stability.<sup>10, 11</sup> Out of these Hydrogen bonding improves mechanical recovery speed the greatest.<sup>11</sup> By combining strong and weak cross-links, double-network hydrogels can possess greatly improved mechanical properties such as, elongation, fracture energy, gel toughness and responsiveness, compared to their pure constituents.<sup>7</sup> Interestingly, combining these two polymer networks usually results in an extreme improvement in mechanical properties, usually eclipsing their pure constituents.<sup>7, 12</sup> Figure 1-1, shows schematics of typical double-network hydrogels.

Double-network hydrogels possess a wide range of impressive mechanical properties. They can be tough enough to withstand impacts from a golf club and resist slicing with a cutter at stresses as high as 25 MPa.<sup>11, 12</sup> Double-network gels can withstand large elongations greater than 500% as well as have high fracture energies, even high enough to become notch-insensitive under strain.<sup>7</sup> By combining two individual networks that are mechanically weak, with the first one stiff and brittle, and the second, soft and ductile, the resulting double-network gel is an extreme mechanical improvement in becoming stiff and ductile.<sup>12</sup>

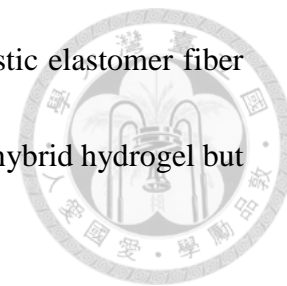


### 1.1.1.2 Hybrid Hydrogels

Hydrogels suffer from two main disadvantages in their suitability as substrates for green electronics, water loss and poor mechanical properties. The inability for hydrogels to retain their water content in ambient conditions is one of the largest and most disadvantageous properties of hydrogels. Loss of water affects the size, the shape and, most importantly, the mechanical properties of a hydrogel. Furthermore, water loss is intrinsic to most hydrogels. Elastomers remain stable in various environments due to their lack of solvent and have a wide range of mechanical properties. Inspired by the structures of mammalian skins, Yuk, et al. were able to successfully assemble pre-shaped elastomers and tough hydrogels to form a hydrogel-elastomer hybrid that was dehydration resistant.<sup>5</sup> A schematic of this structure can be seen in Figure 1-2. Water loss was successfully retarded by binding and encapsulating their PAAm-alginate hydrogel in an Ecoflex sheet.<sup>5</sup> Their work is the one of the first demonstrations of a stable hydrogel in ambient conditions.

Hydrogels have also been combined with inorganic materials to increase their suitability for green electronics. Lee et al. were able to combine single wall carbon nano-tubes, graphene and silver nanowires with a borax-PVA self-healing hydrogel to form an extremely stretchable self-healing strain sensor capable of over 1000% strain.<sup>13</sup>

Zhao et al. combined double-network hydrogels with a thermoplastic elastomer fiber mesh on a macroscopic scale to not only increase the toughness of hybrid hydrogel but also increase their Young's moduli to over 6 MPa.<sup>14</sup>

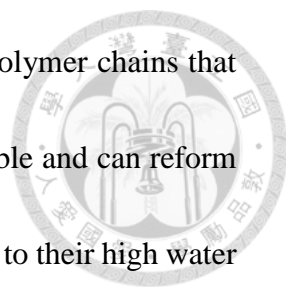


In conclusion, hydrogels have great potential to incorporate other materials into their structure and benefit from their unique properties and augment some of the glaring weaknesses of hydrogels.

### **1.1.1.3 Self-healing Hydrogels**

Autonomous self-healing hydrogels are highly sought after due to their potential to prolong their lifetime and maintain their original properties. Hydrogels exhibit a broad range of tunable structure, mechanical and rheological properties which can mimic many living systems and therefore an increase in their durability and reliability may increase their market value as suitable replacements.<sup>15</sup> Some hydrogels intrinsically have a large amount of reversible cross-links that facilitate self-healing. Dynamic covalent bonds, hydrogen bonds, ionic bonds, hydrophobic interactions and supramolecular host-guest interactions are all examples of reversible cross-links employed by hydrogels to self-heal.<sup>15</sup>

Hydrogen bonding (H-bonds) as a mechanism for self-healing can be both robust

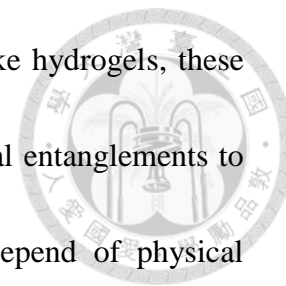


and rapid due to reversible cross-links forming between different polymer chains that contain hydrogen donor and acceptor moieties. H-bonds are reversible and can reform with enough chain mobility which hydrogels are able to provide due to their high water content. Researches have created a self-healing hydrogels using the multivalent hydrogen bonds interaction of 2-ureido-4-pyrimidone (UP<sub>y</sub>) units as end groups. The UP<sub>y</sub>-based monomers were able to form self-complementary H-bonds in the aqueous environment of hydrogels and, as a result, rapidly self-heal incisions made in the gel within two minutes at 20 °C.<sup>16</sup> Varghese et al. were able to design an acryloyl-6-aminocaproic acid (A6ACA) hydrogel that contained hydrophobic and hydrophilic moieties with h-bond mediating side chains.<sup>17</sup> These dangling hydrocarbon side chains containing polar functional groups, seen in Figure 1-3, were able to achieve efficient and robust healing, so much so that the rupture of healed hydrogels were not located at the healed interface.

### **1.1.2 Organogels**

Organogels are a viable alternative to hydrogels as stretchable electro-active material that can endure harsh mechanical deformations. Organogels are semi-solid systems that contain liquid solvent immobilized by a three-dimensional network of gelator fibers.<sup>18, 19</sup> Organogels can be divided into two main classes based on their

gelators: polymeric or low molecular weight (LMW) gelators. Like hydrogels, these polymeric gelators form a network of either cross-links or physical entanglements to immobilize bulk flow of their solvent. LMW organogelators depend of physical interactions to self-assemble into aggregates and induce gelation.<sup>18, 20-22</sup>



Organogels are a solution to two major, intrinsic disadvantages of hydrogels in the field of conductive, stretchable electronics. Hydrogels suffer in the field of stretchable electronics due to their high water content which causes: mixed conduction due to mobile ions dispersed in water and long term environmental, and thus, mechanical instability due to water evaporation from the gel.<sup>19</sup> Organogels that use high boiling point solvents undergo far less solvent loss over time. Joo et al. were able to design a strain-insensitive, stretchable, conductive PEDOT:PSS (poly(3,4-ethylene-dioxythiophene):polystyrene sulfonate)/Acrylamide organogel.<sup>19</sup> Using PEDOT:PSS and polyacrylamide (PAAm) as polymeric gelators in an ethylene glycol (EG) solvent, the researchers were able to design a gel that were only electrically conductive due to the PEDOT:PSS without ion conduction or migration. The PEDOT:PSS-PAAm organogel was able to withstand over 400% strain without mechanical rupture and 150% strain without electrical rupture. The conductivity of the organogel was also strain insensitive up until 100% strain. The use of EG as a solvent prevented solvent evaporation, and the organogels were even able to maintain over 60% of their original

EG after 22 hours under vacuum which can be seen in Figure 1-4.



Organogels, like hydrogels, also have the ability to self-heal due to similar large amounts of reversible bonds within their structure. Low molecular weight organogels (LMOGs) can utilize self-assembly to undergo self-regeneration via weak intermolecular forces such as pi-stacking, H-bonding and van der Waals interactions.<sup>22</sup> Extremely efficient gelators (super-gelators) can also respond to stimuli and trigger gel assembly or disassembly.<sup>22</sup> This allows for some organogels to recover even after extremely large stresses are placed on them, making them one of the most promising self-healing materials.

### 1.1.3 Biodegradable “Green” Substrates

Biodegradable substrates facilitate the shift towards flexible and stretchable electronics while also offering eco-friendly disposal pathways.<sup>3, 24</sup> One of the oldest and well-studied biodegradable substrates is paper. Recently, a high-performance organic field effect transistor with a mobility as high as  $0.56 \text{ cm}^2 \text{ V}^{-1} \text{ s}^{-1}$  was fabricated on top of simple printer paper. However, the large roughness of the paper required a smoothing dielectric of parylene-C to be deposited afterwards.<sup>25</sup> Other well-known biodegradable polymers, such as poly(L-lactide-co-glycolide) (PLGA) by Bao et al. and

deoxyribonucleic acid (DNA) by Chen et al., have recently been used as biodegradable substrates for high performance biocompatible organic devices.<sup>26,27</sup> These devices were flexible and had large potential to be even bioresorbable.<sup>26</sup> This is a growing interest in the biomedical field where devices would need to be safe for *in vivo* use. However, paper, PLGA, and DNA substrates, which can be seen in Figure 1-5 (a-c), are all non-stretchable substrates.

Elastomeric, fully biodegradable, and biocompatible substrates are extremely rare and have recently received much interest as an alternative to traditional stretchable substrates like PDMS and NBR which are very hard to dispose of in an environmentally friendly manner. Kaplan et al. were able to generate elastic hydrogels with tunable properties from covalently cross-linking tyrosine residues in silk proteins<sup>28</sup>. Their gels were able to withstand over 70% compressive strains, tunable stiffnesses between 200-10,000 Pa, and supported cell survival and proliferation when implanted *in vivo*. Langer et al. were able to synthesize a fully biodegradable elastomer referred to as poly(glycerol-sebacate) (PGS), from the polycondensation of glycerol and sebacic acid that could easily be degraded due to the large amount of hydrolyzable cross-links in its gel structure.<sup>29</sup> Their *in vitro* and *in vivo* testing showed that the polymer had good biocompatibility and could be completely resorbed within 60 days of its implantation. In conclusion, a fully biocompatible/biodegradable and stretchable device is difficult to

synthesize but has great future promise in the field of eco-friendly wearable electronics.

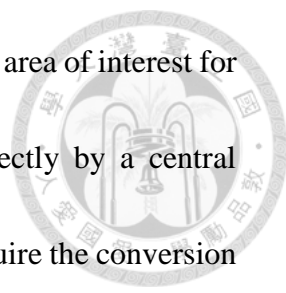


## 1.2 Introduction to Polymer Memory

Polymer-based resistive memories are a promising alternative to traditional inorganic semiconductor-based memory technology for large capacity data storage due to their good scalability, flexibility/stretchability, low cost, and ease of processability. Polymer resistive memory devices have attracted a significant scientific research because conventional silicon based technologies are approaching theoretical and physical limitations in downscaling.

Resistive-type memory devices benefit from a facile fabrication for high data storage density through 2D or 3D (stacking) crossbar arrays since they are not confined by a specific cell structure.<sup>30, 31</sup> Resistive memory defines two states of electrical bistability of high and low conductivity as “1” (ON) or “0” (OFF) in an applied electric field. Areas of interest in the performance of resistive memory devices include large ON-OFF current ratios, low operation voltage, long retention times and high stability. Polymer memory layers and device structures are chosen with great care to improve performance in these areas. Polymer memory layers have various mechanisms, which include: metal-filament growth, space charge limited current, charge transfer, and conformational change.<sup>32</sup>



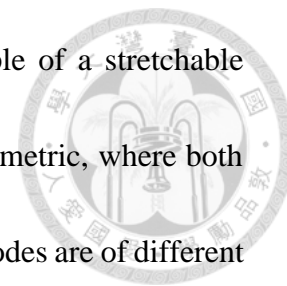


Polymer-based resistive-type memory devices are an important area of interest for modern computers and electronics because they can be read directly by a central processing unit. Other types of storage, like mechanical storage, require the conversion of optical, magnetic or physical signals to electrical signals.<sup>33-35</sup> Polymer-based resistive-type memory is a promising candidate because of their flexible and, sometimes even, stretchable nature.<sup>1-4</sup> In conclusion, polymer resistive memory devices are an attractive alternative or supplementary technology to conventional Si-based electronic memory.

### **1.2.1 Resistor-type Polymer Memory Device Structure and Fabrication**

Most polymer resistor-type memory devices have very simple structures consisting of a polymer memory layer sandwiched between a bottom and top electrode. Figure 1-6 shows the typical structures of resistor memory devices. Polymer memory layers can be deposited with low fabrication costs through solution processing techniques due to the excellent film-forming ability of polymers. These techniques include spin-coating, spray-coating, dip-coating and ink-jet printing. The electrode materials of polymer resistive memory devices are usually Al, Au, Cu, indium tin oxide (ITO) and p- or n-doped Si.<sup>36-38</sup> Recently, stretchable and organic electrodes like silver nano-wires<sup>27</sup>, carbon nano-tubes<sup>39</sup>, and PEDOT:PSS<sup>19</sup> have been used in the fabrication

of flexible resistor memory devices. Figure 1-7 shows an example of a stretchable memory device. The configuration of electrodes can be either symmetric, where both electrodes are of the same material, or asymmetric, where the electrodes are of different materials.



### 1.2.2 Resistor-type Memory Classifications

Resistive memory devices use a writing operation by applying a voltage bias which causes the switching between the memory layers high-resistance (OFF) and low-resistance (ON) state. Polymer materials not only have intrinsic electrical bistability (ON and OFF states) due to properties like charge trapping, charge transfer, phase change and conformation change but also can tune their memory behavior by dopants, conformational changes, changing the electron donor (D) or acceptor (A), different film thicknesses or morphological change.<sup>40-42</sup> Resistive-type memory devices can be classified as either volatile or non-volatile. Volatile memory requires a power source to maintain its ON state and volatile memory effects can be divided into dynamic random access memory (DRAM) and static random access memory (SRAM). Non-volatile memory devices can maintain their ON state after the applied voltage bias has been removed. They can be divided into write-once read-many times (WORM) memory and rewritable (Flash) memory. Flash memory requires applying an appropriate voltage to

switch the ON state back to and OFF state. A summary of resistor-type memory classifications can be seen in Figure 1-8.



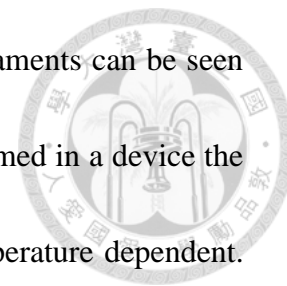
### **1.2.3 Operating Mechanism of Polymer Resistor-type Memory**

The major mechanism behind polymer resistive-type memory is the switching of conductivity in the active polymer material at different electric fields. The most widely used switching mechanisms include: filamentary conduction, charge transfer, charge trapping-detrapping, and conformational changes.<sup>31, 43-50</sup>

#### **1.2.3.1 Filamentary Conduction Mechanism**

Filamentary conduction is the flow of current through a highly localized fraction of the device area.<sup>51,52</sup> Two types of filaments, carbon-rich and metallic, can be observed under an optical or scanning electron microscope.<sup>53-55</sup> Carbon-rich filaments are caused by local degradation of the polymer memory film while metal filaments are caused by migration of the electrode particles through the polymer film.<sup>53</sup> Filamentary conduction can occur to polymers that have both pi-conjugation and coordinating atoms that can bond to metal ions and may be the reason why polymers like polystyrene (PS), polyethylene (PE), polymethylmethacrylate (PMMA), and many more exhibit memory

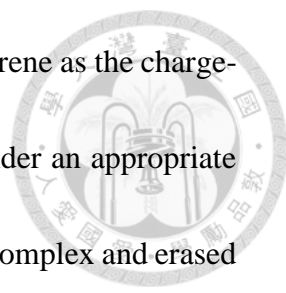
behavior.<sup>43,56</sup> Schematics of carbon-rich filaments and metallic filaments can be seen in Figure 1-9 (a) and (b), respectively. If metallic filaments are formed in a device the ON state will exhibit metallic I-V characteristics and will be temperature dependent.



Devices with filamentary conduction are difficult to control and reproduce because their memory occurrence depends on electrode thickness, film thickness and how the filaments are formed. However, devices that use filamentary conduction as a memory mechanism have been shown to demonstrate consistent non-volatile behavior. A device composed of ITO/6F-BAHP-PC PI/Ag was even able to show flash memory behavior with the ability to rupture filaments after a certain voltage bias was exceeded.<sup>57</sup>

### 1.2.3.2 Charge Transfer (CT) Mechanism

Charge transfer (CT) is a process where the conductivity of an electron donor-acceptor system is increased through a partial transfer of electronic charge from the donor to the acceptor moiety when an appropriate voltage is applied.<sup>58</sup> CT occurs more frequently in polymers that have a donor-acceptor (D-A) structure.<sup>42, 59, 60</sup> Different memory behaviors can be obtained by tuning the electron-donating, or -accepting properties of D-A polymers.<sup>61</sup> A strong dipole moment can sustain a conductive CT state which leads to non-volatile memory behavior. If the dipole moment is not strong enough the removal of an electric field will destabilize the conductive CT state and

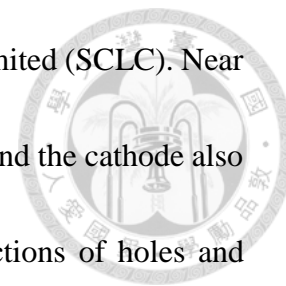


volatile memory behavior will be observed. A device using polyfluorene as the charge-donor and Ir as the charge-acceptor was able to form a CT state under an appropriate applied field.<sup>59</sup> A reverse bias resulted in the dissociation of the CT complex and erased the device back to its OFF state with Flash memory behavior observed. Interestingly, by change the charge-acceptor to and Eu complex, the CT complex remained unerasable and WORM memory was observed.<sup>62</sup>

### 1.2.3.3 Charge Trapping-Detrapping Mechanism

An accumulation of carriers near the electrode builds up a space charge if the electrode-polymer contact is ohmic and the polymer is trap-free. Individual charges have mutual repulsion between them which restricts the total charge injected into the sample. The resulting current is defined as space charge-limited current (SCLC).<sup>43, 63</sup> These space charges can come from: ionized dopants in interfacial depletion regions, accumulation of mobile ions at electrode interfaces, and electrode injection of electrons and/or holes. If traps are present in an insulating material, the magnitude of SCLC will decrease by several orders. If traps are present in the bulk of materials, carrier mobility will be reduced.<sup>64</sup> Traps present at the material interfaces affects the charge injection into the material. Hole injection occurs near the anode when the applied voltage exceed the Schottky barrier. This causes an accumulation of space charges and a redistribution

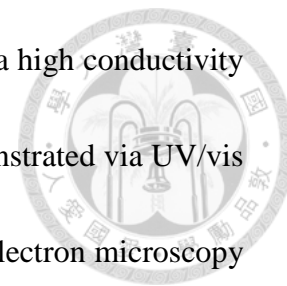
of the electric field and thus the resulting current is space charge-limited (SCLC). Near the threshold voltage, the generated carriers fill some charge traps and the cathode also becomes an electron-injecting contact. This leads to double injections of holes and electrons and, as a result, increased carrier concentration and mobility which causes a rapid increase in current and a switch to the ON state. Figure 1-10 shows the typical mechanisms of electric field-induced charge transfer.



#### 1.2.3.4 Conformational Change

Excellent resistive memory performance can be observed through deliberate modification of polymer structures and tuning of conformational changes. Conformational changes are a mechanism through which non-conjugated polymers can exhibit memory behavior through conformational changes from a regiorandom structure to a regioregular structure. Poly(N-vinylcarbazole) (PVK) derivatives often have carbazole groups that form face-to-face conformations in the ground state which results in a high conductivity state when charge carriers (holes) can be shared and hop through the regioregular carbazole groups.<sup>32, 65</sup> When a flexible spacer is added (O=C-O-C-C) for bridging between carbazole (Cz) groups and the backbone is added, seen in Figure 1-11, a regiorandom structure is formed at the ground state and carriers have a hard time hopping through Cz groups.<sup>32</sup> However, once a field is applied, a face-to-face

regioregular conformation is formed and the device is switched to a high conductivity (ON) state. The conformational changes of a polymer can be demonstrated via UV/vis absorption spectra, X-ray diffraction (XRD) patterns, transmission electron microscopy (TEM), and much more.<sup>32, 65, 66</sup>

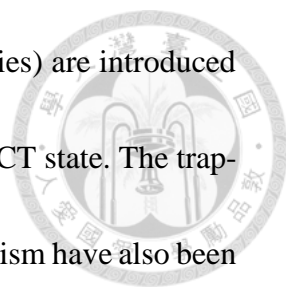


#### **1.2.4 Polymer Materials for Resistor-type Memory**

Many polymers have been investigated for their memory effects. Polyimides, conjugated polymers, and “green” biocompatible polymers have been used due to their inherent electronic bistable switching characteristics that are usually the result of charge transfer or trapping and de-trapping mechanisms. Polymer blends or polymer composites acquire their memory characteristics from homogeneously dispersed nanoparticles inside their polymer matrices. Polymer materials reviewed can be categorized as polyimides, conjugated polymers, “green” polymers, and polymer composites. Their chemical structures can be seen in Table 1-1.

##### **1.2.4.1 Polyimides**

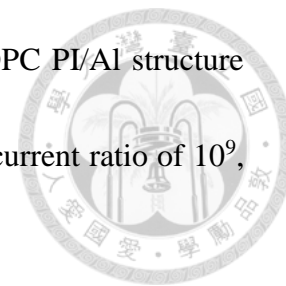
Polyimides (PIs) have excellent mechanical, dielectric, thermal, chemical, and facile functionalization properties. The phthalimide in PIs act as strong electron



acceptors. When electron donor (triphenylamine or carbazole moieties) are introduced into PIs to form a D-A structure, and thus, an electric field-induced CT state. The trap-limited space charge mechanism and filamentary conduction mechanism have also been observed in PI memory behavior to a lesser extent. Polyimides containing triphenylamine (TPA) groups as electron donors in a ITO/6F-HTPA PI/Al structure were reported by Ree et al. to exhibit WORM memory behavior from trap-limited SCLC and filament conduction with high ON/OFF ratios of up to  $10^6$ , long retention times, low power consumption, and high thermal stability up to 150 °C.<sup>67</sup> Polyimides containing carbazole groups as electron donors were also reported to exhibit WORM memory using a D-A structure. Devices in a Al/ PI(CzBD-BTFBPDA)/ITO structure that were fabricated by Shen et al. had high ON/OFF ratios of  $10^6$ , long retention times of  $10^4$  and low turn-on threshold voltages of  $\pm 2.7$  V.<sup>68</sup> Polyimides containing trifluorobiphenyl groups as electron donors in an Al/PI(BTFBPD-BTFBPDA)/ITO structure also exhibited WORM behavior with an ON/OFF current ratio of  $10^4$  and a low turn-on voltage of -1.7V.<sup>69</sup> Polyimide derivative based memory devices can also show rewritable memory behavior. Using anthracene as a hole-transporting and electron-donating moiety on polyimide side chains in an Al/ 6F-HAB-AM PI/Al structure resulted in ambient-stable, nonvolatile, and rewritable bipolar and unipolar switching behavior over a voltage range of  $\pm 2$  V with a high ON/OFF voltage of  $10^7$ .<sup>36</sup> PI



derivatives containing deiphenylcarbamyloxy in an Al/6F-HAB-DPC PI/Al structure exhibited rewritable memory characteristics with a high ON/OFF current ratio of  $10^9$ , long retention times, and low power consumption.<sup>70</sup>



#### 1.2.4.2 $\pi$ -Conjugated Polymers

$\pi$ -conjugated polymers have good electronic properties and some of their derivatives are good candidates for volatile memory. Fluorene-based donor-acceptor copolymer containing electron-donor (fluorene) and -acceptor (1,3,4-oxadiazole) groups in a ITO/PFOxPy/Al structure exhibited DRAM.<sup>22</sup> The volatile memory characteristics can be attributed to the 1,3,4-oxadiazole electron-acceptor moieties. The device exhibited low reading, writing, and erasing voltages and a high ON/OFF ratio of  $10^6$ . Thiophene-based all-conjugated block copolymers (P3HT<sub>52</sub>-B-P3PT<sub>39</sub>) in an ITO/ P3HT<sub>52</sub>-B-P3PT<sub>39</sub>/Al structure exhibited a DRAM characteristic with a high ON/OFF ratio of  $10^6$ .<sup>64</sup> This is thought to happen due to the existence of trapping sites in the P3PT domains since P3HT only showed semiconductor characteristics. Ree et al. reported the use of poly(diethyl dipropargylmalonate) in a ITO/pDEDPM/Al structure to exhibit WORM memory characteristics with a high ON/OFF ratio of  $10^6$ .<sup>41</sup>

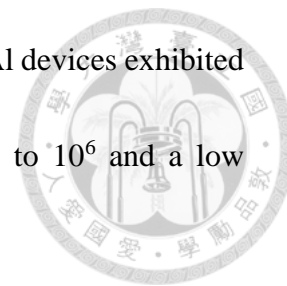
### 1.2.4.3 “Green” and Biocompatible Polymers



Recently, our lab has had success in the production of stretchable resistive memory device based on novel nanostructure-controlled carbohydrate-block-polyisoprene (MH-b-PI) block copolymers.<sup>72</sup> This work marked the first use of carbohydrate-based polymers for resistive memory applications. Oligosaccharides are an interesting hydrophilic biopolymer because they are abundant, renewable, biodegradable and biocompatible. In this study, WORM, flash, and DRAM resistive memory-type could be significantly tuned depending on the nanostructure of the MH-b-PI block copolymers. The maltoheptaose (MH) blocks provided charge trapping and the flexible PI blocks served as stretchable matrices. A highly stretchable memory device using a PDMS/CNTs/MH-b-P<sub>12.6k</sub>/Al structure exhibited excellent ON/OFF current ratios over 10<sup>6</sup> with stable  $V_{\text{set}}$  around -2 V under 0-100% strain. These memory characteristics were maintained over 1000 40% strain cycles. This was one of the first stretchable memory devices made using a biocompatible memory layer and showed great potential applications for high-performance stretchable and wearable electronic devices.

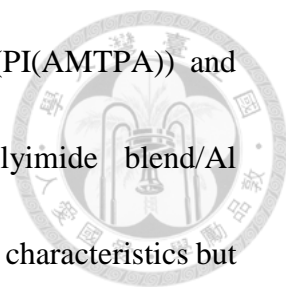
Interestingly, new high performance digital memory devices has recently been fabricated from salmon testes DNA (St-DNA) and DNA-mimics.<sup>73</sup> DNA is a bio-macromolecule which carries genetic information through selective hydrogen-bond nucleobase pairs. They determined the memory properties stemmed from charge

trapping and hopping in the nucleobase moieties. The Al/St-DNA/Al devices exhibited WORM memory behavior with a high ON/OFF current ratio up to  $10^6$  and a low threshold voltage of 2.3V.



#### 1.2.4.4 Polymer Composites

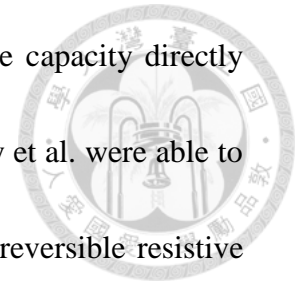
Memory effect in doped or mixed polymer systems is an attractive option in resistive-type memory due to their greatly tunable memory properties. Polymer composites may also impart advantageous mechanical properties to the blend, making flexible and stretchable memory devices possible. Polymer composites that have shown non-volatile WORM behavior include polymer/organic compounds, polymer/ $C_{60}$  derivatives, polymer/carbon nanotubes (CNTs), and polymer/graphene composites. Polymer composites that have shown rewritable behavior include polymer/Au or Ag nanomaterials, polymer/quantum dots, polymer/metal oxide nanomaterials, polymer/carbon nanomaterials, and polymer/ionic liquids. Lai and Chen et al. both demonstrated a composite of poly(methyl methacrylate) (PMMA) and poly(3-butylthiophene) (P3BT) as the memory active layer in a PET/Al/PMMA-P3BT/Al structure which exhibited resistive switching and WORM memory effect under both flat and bending conditions.<sup>74</sup> Yu and Chen et al. were able to fabricate a memory device using a polyimide blend prepared from different blends of poly(4,4'-diamino-




4'-methyltriphenylamine-hexafluoroisopropylidenedipthalimide) (PI(AMTPA)) and polycyclic aromatic compounds (coronene) in a PEN/Al/polyimide blend/Al structure.<sup>75</sup> Devices with just PI(AMTPA) exhibited volatile DRAM characteristics but adding in 3% coronene with respect to PI(AMTPA) resulted in flash-type memory. Increasing the percentage of coronene to 15% resulted in WORM memory characteristics.

Kang et al. were able to fabricate a resistive memory device using poly(N-vinyl carbazole) and carbon nanotube (CNT) composite thin films.<sup>76</sup> By varying the CNT content in the composites, they observed insulator behavior, WORM memory effects, rewritable memory effects and conductive behavior. Graphene composites also showed similar results with augmentations to thermal, mechanical and electrical properties. Shang et al. used a PVK-graphene composite which could also be used to tune memory effects.<sup>77</sup> A 2 wt% graphene composite showed WORM memory effects with a turn-on voltage of -2.1 V and an ON/OFF current of  $8 \times 10^3$ . When the wt% was increased to 4%, rewritable memory effects were observed with a threshold voltage of -1.7 V, erasing voltage of 3.4 V and an ON/OFF current of  $10^3$ . They attributed their memory effects to electron trapping in the graphene nanosheets within the PVK matrix. Son and Choi et al. reported gold nanoparticles combined with nonconjugated PVK to form a flexible non-volatile memory.<sup>78</sup> Increasing the concentrations of Au NPs the ON/OFF

current ratio also increased which signified an increase in storage capacity directly related to increase the concentration of Au NPs. White and Weiney et al. were able to combine silver nanowires (AgNWs) with polystyrene for form a reversible resistive switching device.<sup>79</sup> They deduced that the mechanism behind this behavior was field-induced silver filament formation between adjacent nanowires and nanowires clusters.



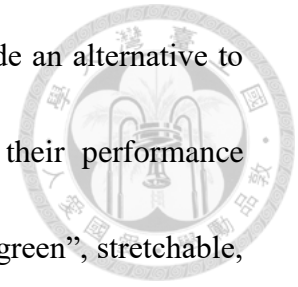
### 1.3 Research Objectives



The goal of this thesis was to facilely fabricate a “green”, low-cost, biodegradable, stretchable, and mechanically robust substrate that addressed and resolved some of the major weaknesses of other popular biodegradable/stretchable substrates commonly used in polymer electronic research. The substrate aimed to focus on some of the main intrinsic disadvantages of biodegradable/stretchable substrates which include: water evaporation in hydrogels, solvent biocompatibility in organogels, lack of biodegradability, recyclability, self-healing in elastomers, and lack of stretchability in biodegradable elastomers. After a suitable substrate could be manufactured, we aimed to classify and explain its novel/advantageous characteristics. A designation of pseudo-hydrogel seemed to be an appropriate name for this material due to its similarity with double-network hydrogels but lack of some of their major, class-defining characteristics.

The next goal of this thesis was to use this new class of materials as the substrate in a fully stretchable polymer resistive memory device. The memory material and electrodes were chosen as St-DNA and 1:4 PEDOT:PSS : PU blend respectively due to their biodegradable/biocompatible and stretchable properties. Great care was taken to ensure that each component could be easily broken down in DI water. The device should also be facilely fabricated and have good performance.

The major goal of “green” electronics is not only to provide an alternative to inorganic materials but also match and even surpass some of their performance characteristics. The goal of this thesis is to fabricate a substrate a “green”, stretchable, and biodegradable substrate that can rival, and even surpass in some areas, traditional stretchable electronic substrates like polydimethylsiloxane (PDMS). By doing so, more research may be done to further grow and improve the field of eco-friendly, recyclable, and environmentally-conscious electronic design. As proof of this concept, a fully stretchable, organic, biodegradable, and high-performance resistor memory device was fabricated using this substrate in order to reinforce these principles.




## 1.4 References



1. M. Irimia-Vladu, *Chem. Soc. Rev.* 2014, 43, 588;
2. M. Irimia-Vladu, E. D. Głowacki, G. Voss, S. Bauer, N. S. Sariciftci, *Mater. Today* 2012, 15, 340;
3. S. W. Hwang, J. K. Song, X. Huang, H. Cheng, S. K. Kang, B. H. Kim, J. H. Kim, S. Yu, Y. Huang, J. A. Rogers, *Adv. Mater.* 2014, 26, 3905;
4. J. A. Rogers, T. Someya, Y. Huang, *Science* 2010, 327, 1603;
5. H. Yuk, T. Zhang, G. A. Parada, X. Liu, X. Zhao, *Nat. Commun.* 2016, 7;
6. A. B. Imran, K. Esaki, H. Gotoh, T. Seki, K. Ito, Y. Sakai, Y. Takeoka, *Nat. Commun.* 2014, 5;
7. J.-Y. Sun, X. Zhao, W. R. Illeperuma, O. Chaudhuri, K. H. Oh, D. J. Mooney, J. J. Vlassak, Z. Suo, *Nature* 2012, 489, 133;
8. F. Ullah, M. B. H. Othman, F. Javed, Z. Ahmad, H. M. Akil, *Mater. Sci. Eng. C.* 2015, 57, 414;
9. J. Maitra, V. K. Shukla, *Am. J. Polym. Sci.* 2014, 4, 25;
10. W. Sun, B. Xue, Y. Li, M. Qin, J. Wu, K. Lu, J. Wu, Y. Cao, Q. Jiang, W. Wang, *Adv. Funct. Mater.* 2016, 26, 9044;
11. T. Nakajima, *Polym. J.* 2017;
12. J. P. Gong, Y. Katsuyama, T. Kurokawa, Y. Osada, *Adv. Mater.* 2003, 15, 1155;




- 
13. G. Cai, J. Wang, K. Qian, J. Chen, S. Li, P. S. Lee, *Adv. Sci.* 2016;
14. S. Lin, C. Cao, Q. Wang, M. Gonzalez, J. E. Dolbow, X. Zhao, *Soft Matter* 2014, 10, 7519;
15. D. L. Taylor, *Adv. Mater.* 2016;
16. J. Cui, A. del Campo, *Chem. Commun.* 2012, 48, 9302;
17. A. Phadke, C. Zhang, B. Arman, C.-C. Hsu, R. A. Mashelkar, A. K. Lele, M. J. Tauber, G. Arya, S. Varghese, *Proc. Natl. Acad. Sci. U.S.A.* 2012, 109, 4383;
18. A. Vintiloiu, J.-C. Leroux, *J. Control. Release* 2008, 125, 179;
19. Y. Y. Lee, H. Y. Kang, S. H. Gwon, G. M. Choi, S. M. Lim, J. Y. Sun, Y. C. Joo, *Adv. Mater.* 2016, 28, 1636;
20. J. Puigmartí-Luis, V. Laukhin, Á. Pérez del Pino, J. Vidal-Gancedo, C. Rovira, E. Laukhina, D. B. Amabilino, *Angew. Chem. Int. Ed.* 2007, 46, 238;
21. S. S. Babu, S. Prasanthkumar, A. Ajayaghosh, *Angew. Chem. Int. Ed.* 2012, 51, 1766;
22. A. R. Hirst, B. Escuder, J. F. Miravet, D. K. Smith, *Angew. Chem. Int. Ed.* 2008, 47, 8002;
23. Z. Wei, J. H. Yang, J. Zhou, F. Xu, M. Zrínyi, P. H. Dussault, Y. Osada, Y. M. Chen, *Chem. Soc. Rev.* 2014, 43, 8114;
24. H. Zhu, Z. Xiao, D. Liu, Y. Li, N. J. Weadock, Z. Fang, J. Huang, L. Hu, *Energy*

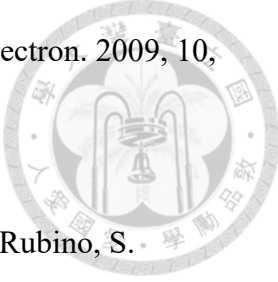
Environ. Sci. 2013, 6, 2105;


25. B. Peng, X. Ren, Z. Wang, X. Wang, R. C. Roberts, P. K. Chan, *Sci. Rep.* 2014, 4, 6430;
26. C. J. Bettinger, Z. Bao, *Adv. Mater.* 2010, 22, 651;
27. C.-C. Shih, C.-Y. Chung, J.-Y. Lam, H.-C. Wu, Y. Morimitsu, H. Matsuno, K. Tanaka, W.-C. Chen, *Chem. Commun.* 2016, 52, 13463;
28. B. P. Partlow, C. W. Hanna, J. Rnjak-Kovacina, J. E. Moreau, M. B. Applegate, K. A. Burke, B. Marelli, A. N. Mitropoulos, F. G. Omenetto, D. L. Kaplan, *Adv. Funct. Mater.* 2014, 24, 4615;
29. Y. Wang, G. A. Ameer, B. J. Sheppard, R. Langer, *Nat. Biotechnol.* 2002, 20, 602;
30. P. Heremans, G. H. Gelinck, R. Muller, K.-J. Baeg, D.-Y. Kim, Y.-Y. Noh, *Chem. Mater.* 2010, 23, 341;
31. N.-H. You, C.-C. Chueh, C.-L. Liu, M. Ueda, W.-C. Chen, *Macromolecules* 2009, 42, 4456;
32. E. Teo, Q. Ling, Y. Song, Y. Tan, W. Wang, E. Kang, D. Chan, C. Zhu, *Org. Electron.* 2006, 7, 173;
33. S. H. Jo, W. Lu, *Nano Lett.* 2008, 8, 392;
34. Y. Yang, J. Ouyang, L. Ma, R. H. Tseng, C. W. Chu, *Adv. Funct. Mater.* 2006, 16,

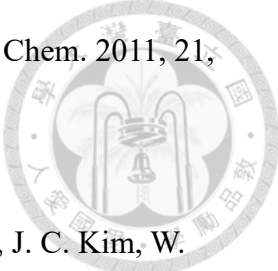


1001;

- 
35. T. W. Kim, Y. Yang, F. Li, W. L. Kwan, *NPG Asia Mater.* 2012, 4, e18;
36. S. Park, K. Kim, D. M. Kim, W. Kwon, J. Choi, M. Ree, *ACS Appl. Mater. Interfaces.* 2011, 3, 765;
37. B. Hu, X. Zhu, X. Chen, L. Pan, S. Peng, Y. Wu, J. Shang, G. Liu, Q. Yan, R.-W. Li, *J. Am. Chem. Soc.* 2012, 134, 17408;
38. G. Tian, S. Qi, F. Chen, L. Shi, W. Hu, D. Wu, *Appl. Phys. Lett.* 2011, 98, 92;
39. C. C. Shih, W. Y. Lee, C. Lu, H. C. Wu, W. C. Chen, *Adv. Electron. Mater.* 2017, 3;
40. C.-L. Liu, T. Kurosawa, A.-D. Yu, T. Higashihara, M. Ueda, W.-C. Chen, *J. Phys. Chem. C* 2011, 115, 5930;
41. T. J. Lee, S. Park, S. G. Hahm, D. M. Kim, K. Kim, J. Kim, W. Kwon, Y. Kim, T. Chang, M. Ree, *J. Phys. Chem. C* 2009, 113, 3855;
42. T. J. Lee, Y.-G. Ko, H.-J. Yen, K. Kim, D. M. Kim, W. Kwon, S. G. Hahm, G.-S. Liou, M. Ree, *Polym. Chem.* 2012, 3, 1276;
43. Q.-D. Ling, D.-J. Liaw, C. Zhu, D. S.-H. Chan, E.-T. Kang, K.-G. Neoh, *Prog. Polym. Sci.* 2008, 33, 917;
44. X. D. Zhuang, Y. Chen, G. Liu, B. Zhang, K. G. Neoh, E. T. Kang, C. X. Zhu, Y. X. Li, L. J. Niu, *Adv. Funct. Mater.* 2010, 20, 2916;

- 
45. B. Cho, T.-W. Kim, M. Choe, G. Wang, S. Song, T. Lee, *Org. Electron.* 2009, 10, 473;
46. D. Attianese, M. Petrosino, P. Vacca, S. Concilio, P. Iannelli, A. Rubino, S. Bellone, *IEEE Electr. Device* 2008, 29, 44;
47. P. Guo, Y.-W. Dong, X. Ji, Y.-X. Lu, W. Xu, *IEEE Electr. Device* 2007, 28, 572;
48. W. Tang, H. Shi, G. Xu, B. S. Ong, Z. D. Popovic, J. Deng, J. Zhao, G. Rao, *Adv. Mater.* 2005, 17, 2307;
49. J. H. Smits, S. C. Meskers, R. A. Janssen, A. W. Marsman, D. M. de Leeuw, *Adv. Mater.* 2005, 17, 1169;
50. F. Verbakel, S. C. Meskers, R. A. Janssen, *Chem. Mater.* 2006, 18, 2707;
51. G. Dearnaley, D. Morgan, A. Stoneham, *J. Non-Cryst. Solids* 1970, 4, 593;
52. G. Dearnaley, A. Stoneham, D. Morgan, *Rep. Prog. Phys.* 1970, 33, 1129;
53. P. Sliva, G. Dir, C. Griffiths, *J. Non-Cryst. Solids* 1970, 2, 316;
54. H. Carchano, R. Lacoste, Y. Segui, *Appl. Phys. Lett.* 1971, 19, 414;
55. L. Pender, R. Fleming, *J. Appl. Phys.* 1975, 46, 3426;
56. W.-J. Joo, T.-L. Choi, J. Lee, S. K. Lee, M.-S. Jung, N. Kim, J. M. Kim, *J. Phys. Chem. B* 2006, 110, 23812;
57. B. Hu, F. Zhuge, X. Zhu, S. Peng, X. Chen, L. Pan, Q. Yan, R.-W. Li, *J. Mater. Chem.* 2012, 22, 520;

- 
58. C. W. Chu, J. Ouyang, J. H. Tseng, Y. Yang, *Adv. Mater.* 2005, 17, 1440;
59. S. J. Liu, Z. H. Lin, Q. Zhao, Y. Ma, H. F. Shi, M. D. Yi, Q. D. Ling, Q. L. Fan,  
C. X. Zhu, E. T. Kang, *Adv. Funct. Mater.* 2011, 21, 979;
60. B. Zhang, G. Liu, Y. Chen, C. Wang, K. G. Neoh, T. Bai, E. T. Kang,  
*ChemPlusChem* 2012, 77, 74;
61. C.-L. Liu, W.-C. Chen, *Polym. Chem.* 2011, 2, 2169;
62. Q.-D. Ling, Y. Song, E. Y. H. Teo, S.-L. Lim, C. Zhu, D. S. H. Chan, D.-L.  
Kwong, E.-T. Kang, K.-G. Neoh, *Electrochem. Solid State Lett.* 2006, 9, G268;
63. B. Cho, S. Song, Y. Ji, T. W. Kim, T. Lee, *Adv. Funct. Mater.* 2011, 21, 2806;
64. Y.-C. Lai, K. Ohshimizu, W.-Y. Lee, J.-C. Hsu, T. Higashihara, M. Ueda, W.-C.  
Chen, *J. Mater. Chem.* 2011, 21, 14502;
65. S. L. Lim, Q. Ling, E. Y. H. Teo, C. X. Zhu, D. S. H. Chan, E.-T. Kang, K. G.  
Neoh, *Chem. Mater.* 2007, 19, 5148;
66. S. J. Liu, P. Wang, Q. Zhao, H. Y. Yang, J. Wong, H. B. Sun, X. C. Dong, W. P.  
Lin, W. Huang, *Adv. Mater.* 2012, 24, 2901;
67. D. M. Kim, S. Park, T. J. Lee, S. G. Hahm, K. Kim, J. C. Kim, W. Kwon, M. Ree,  
*Langmuir* 2009, 25, 11713;
68. Y.-Q. Li, R.-C. Fang, A.-M. Zheng, Y.-Y. Chu, X. Tao, H.-H. Xu, S.-J. Ding, Y.-Z.  
Shen, *J. Mater. Chem.* 2011, 21, 15643;

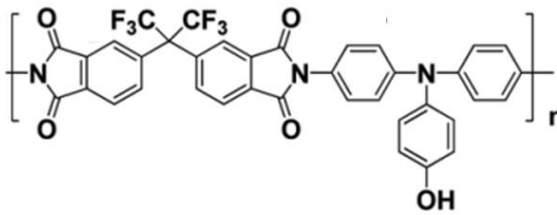
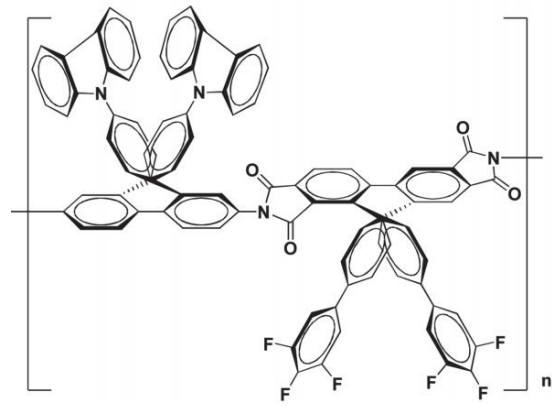
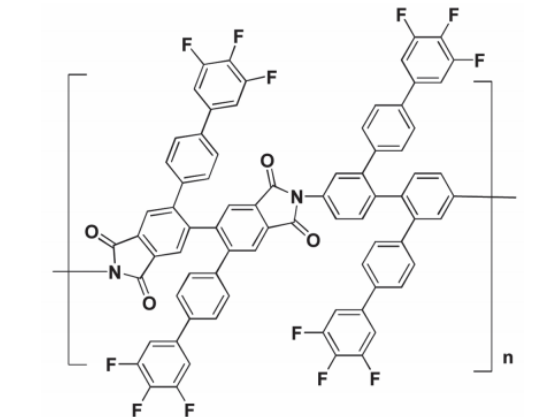
- 
69. Y. Li, H. Xu, X. Tao, K. Qian, S. Fu, Y. Shen, S. Ding, *J. Mater. Chem.* 2011, 21, 1810;
70. S. G. Hahm, S. Choi, S.-H. Hong, T. J. Lee, S. Park, D. M. Kim, J. C. Kim, W. Kwon, K. Kim, M.-J. Kim, *J. Mater. Chem.* 2009, 19, 2207;
71. Q. D. Ling, Y. Song, S. L. Lim, E. Y. H. Teo, Y. P. Tan, C. Zhu, D. S. H. Chan, D. L. Kwong, E. T. Kang, K. G. Neoh, *Angew. Chem.* 2006, 118, 3013;
72. C. C. Hung, Y. C. Chiu, H. C. Wu, C. Lu, C. Bouilhac, I. Otsuka, S. Halila, R. Borsali, S. H. Tung, W. C. Chen, *Adv. Funct. Mater.* 2017, 27;
73. J. Lee, Y. Kim, C. Kim, M. Ree, *Mater. Horiz.* 2017, 4, 423;
74. Y. C. Lai, F. C. Hsu, J. Y. Chen, H. He Jr, T. C. Chang, Y. P. Hsieh, T. Y. Lin, Y. J. Yang, Y. F. Chen, *Adv. Mater.* 2013, 25, 2733;
75. A.-D. Yu, T. Kurosawa, Y.-H. Chou, K. Aoyagi, Y. Shoji, T. Higashihara, M. Ueda, C.-L. Liu, W.-C. Chen, *ACS Appl. Mater. Interfaces.* 2013, 5, 4921;
76. G. Liu, Q.-D. Ling, E. Y. H. Teo, C.-X. Zhu, D. S.-H. Chan, K.-G. Neoh, E.-T. Kang, *ACS Nano* 2009, 3, 1929;
77. Q. Zhang, J. Pan, X. Yi, L. Li, S. Shang, *Org. Electron.* 2012, 13, 1289;
78. D. I. Son, D. H. Park, J. B. Kim, J.-W. Choi, T. W. Kim, B. Angadi, Y. Yi, W. K. Choi, *J. Phys. Chem. C* 2010, 115, 2341;
79. S. I. White, P. M. Vora, J. M. Kikkawa, K. I. Winey, *Adv. Funct. Mater.* 2011, 21,

233.

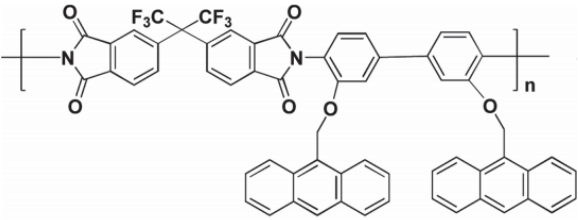

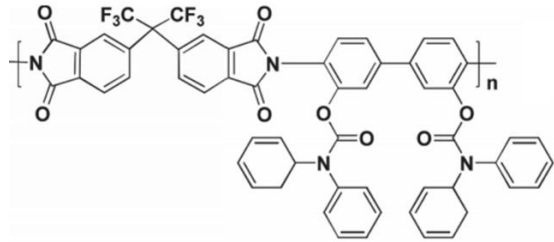


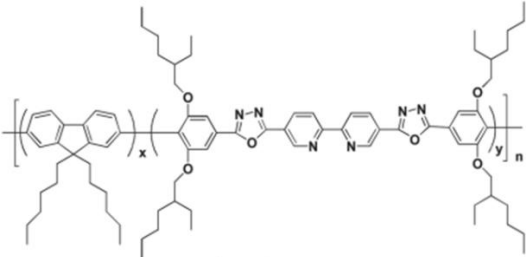
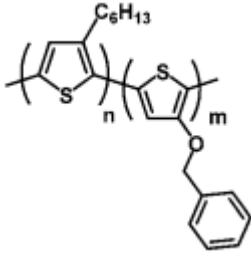
## Tables

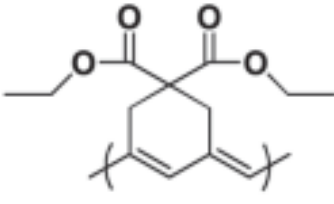

**Table 1-1.** Chemical structures of electroactive layers and their memory characteristics

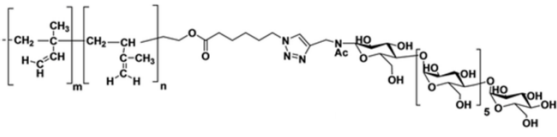
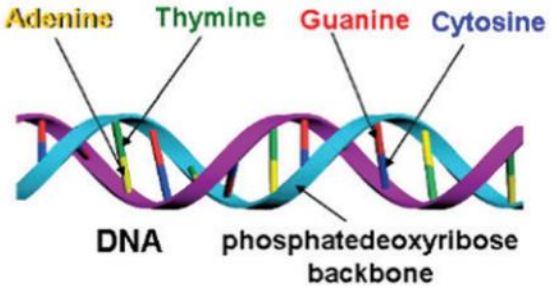
Polyimides		
Electroactive layer	Memory performance and structure	Reference
 <p style="text-align: center;">ITO/6F-HTPA PI/Al</p>	WORM	67
 <p style="text-align: center;">Al/ PI(CzBD-BTFBPDA)/ITO</p>	WORM	68
 <p style="text-align: center;">Al/PI(BTFBPD-BTFBPDA)/ITO</p>	WORM	69



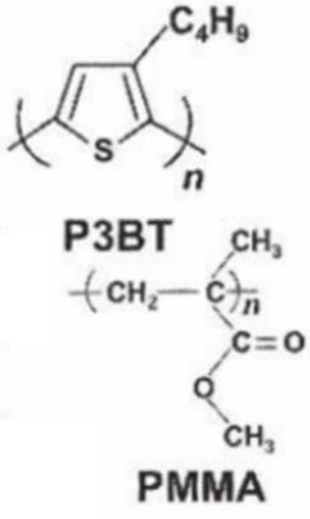

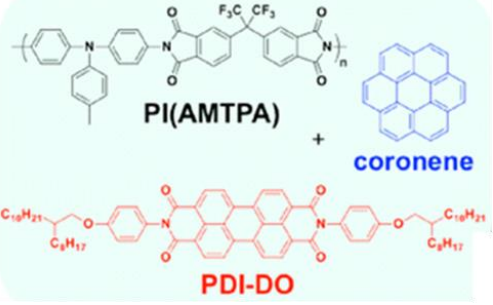
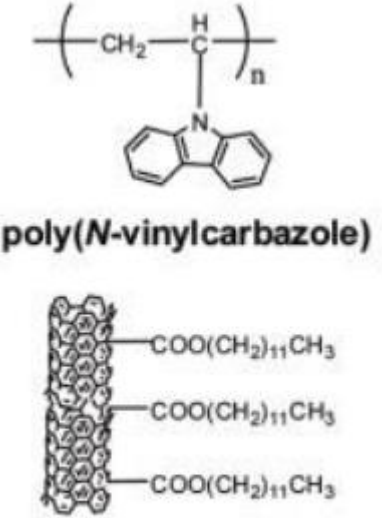
 <p style="text-align: center;">Al/ 6F-HAB-AM PI/AI</p>	Flash	
 <p style="text-align: center;">Al/6F-HAB-DPC PI/AI</p>	Flash	70

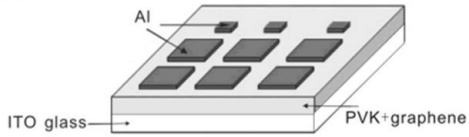

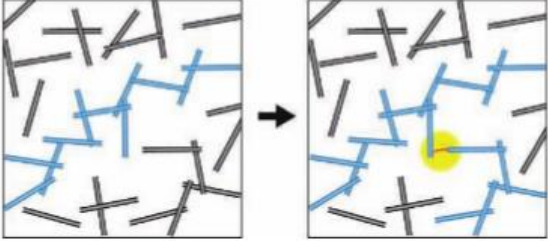
$\pi$ -Conjugated Polymers		
Electroactive layer	Memory performance and structure	Reference
 <p style="text-align: center;">ITO/PFO<sub>x</sub>Py/AI</p>	DRAM	71
 <p style="text-align: center;">ITO/ P3HT<sub>52</sub>-B-P3PT<sub>39</sub>/AI</p>	DRAM	64

 <p style="text-align: center;">ITO/pDEDPM/Al</p>	WORM	
--	------	---

“Green” and Biocompatible Polymers		
Electroactive layer	Memory performance and structure	Reference
 <p style="text-align: center;">PDMS/CNTs/MH-b-P12.6k/Al</p>	WORM, DRAM, and Flash	72
 <p style="text-align: center;">Al/St-DNA/Al</p>	WORM	73

Polymer Composites		
Electroactive layer	Memory performance and structure	Reference

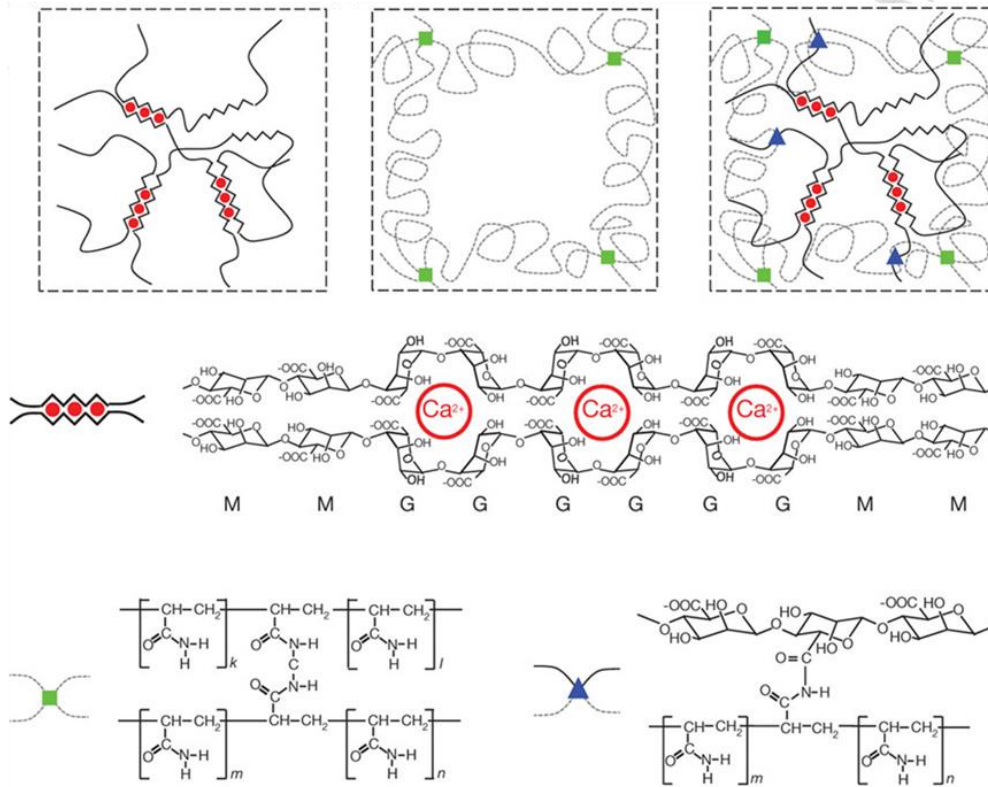
 <p>PET/Al/PMMA-P3BT/Al</p>	<p>WORM</p>	
 <p>PEN/Al/polyimide blend/Al</p>	<p>DRAM and Flash</p>	<p>75</p>
 <p>ITO/CNT blend/Al</p>	<p>WORM</p>	<p>76</p>

 <p>ITO/Graphene blend/Al</p>	<p>WORM and Flash</p>	
 <p>Silver Nanowire Nanocomposite</p>	<p>Reversible resistive switching behavior</p>	<p>79</p>

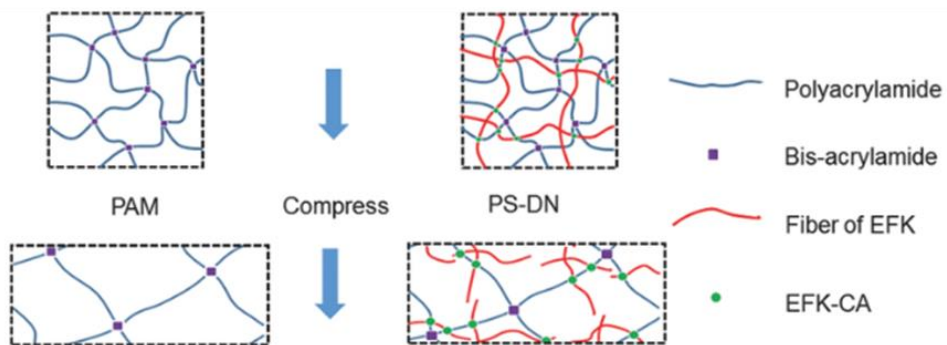
Figures



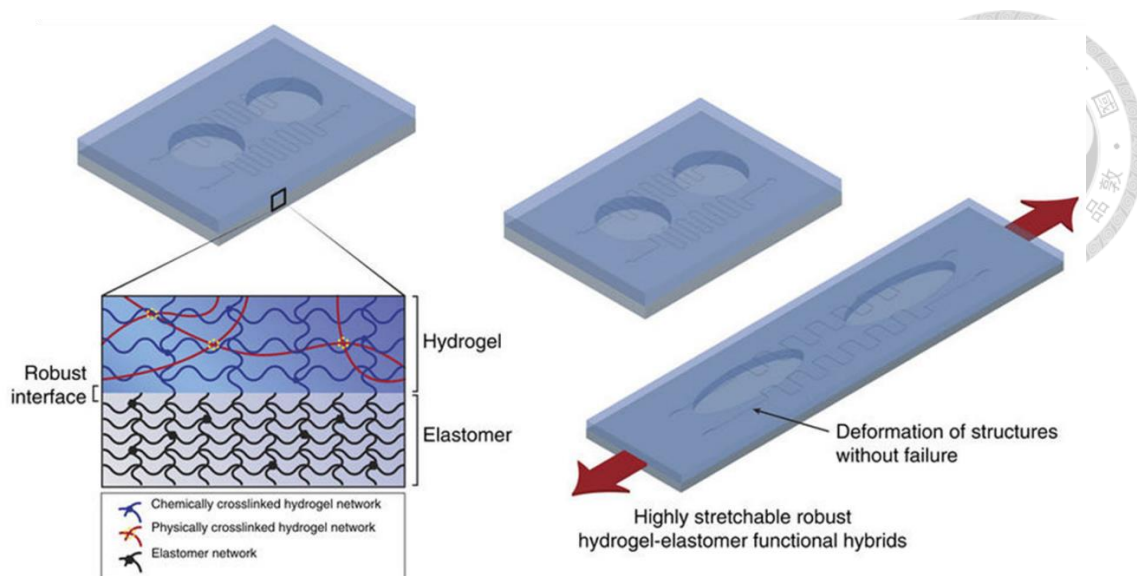
(a)



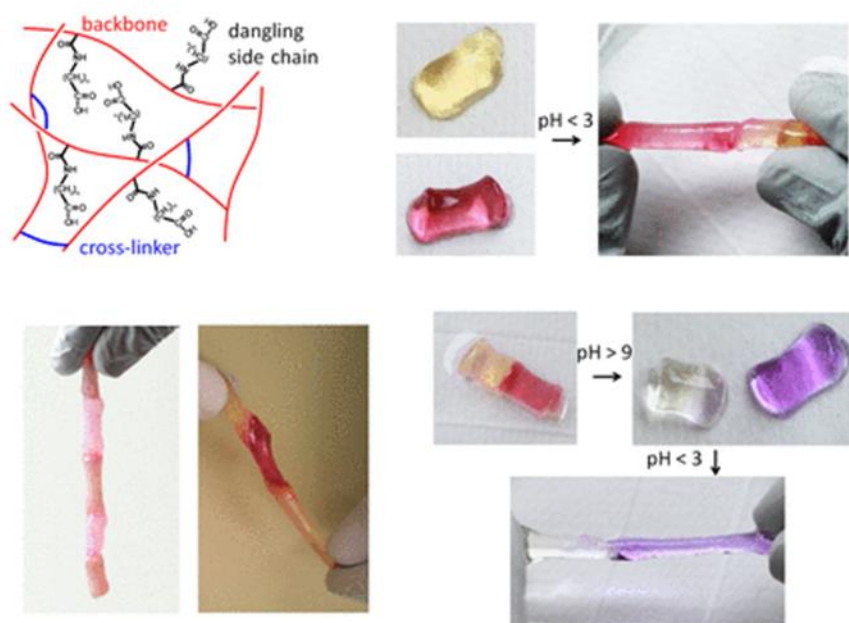
(b)



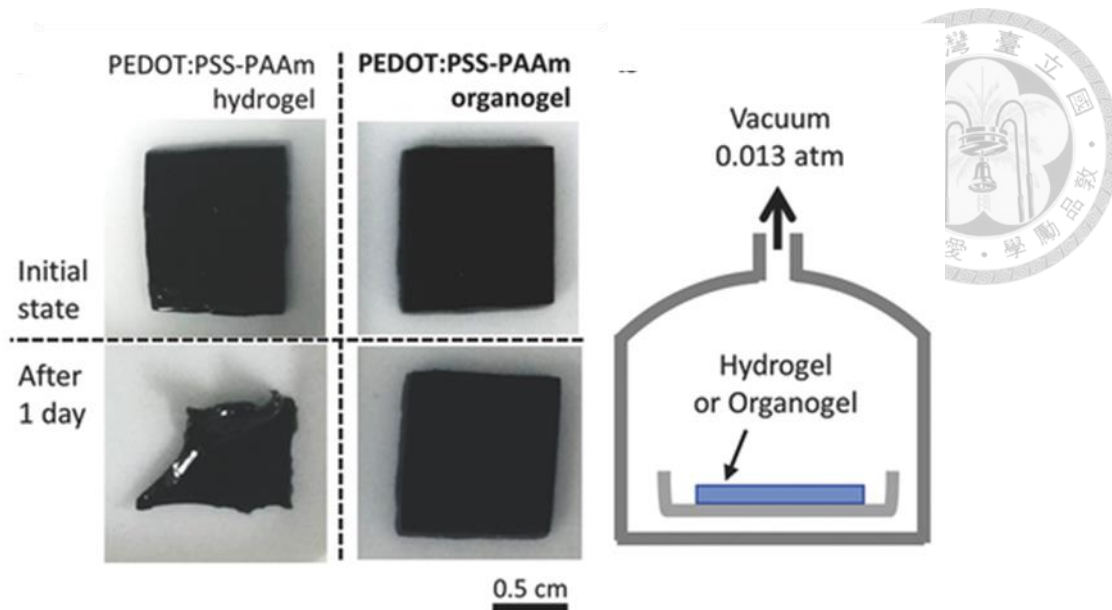
**Figure 1-1.** Double-network hydrogel diagrams in an (a) alginate–polyacrylamide double-network gel<sup>7</sup> and (b) polymer-supramolecular polymer double-network gel.<sup>10</sup>



**Figure 1-2.** Stretchable and dehydration resistant hydrogel-elastomer hybrid.<sup>5</sup>

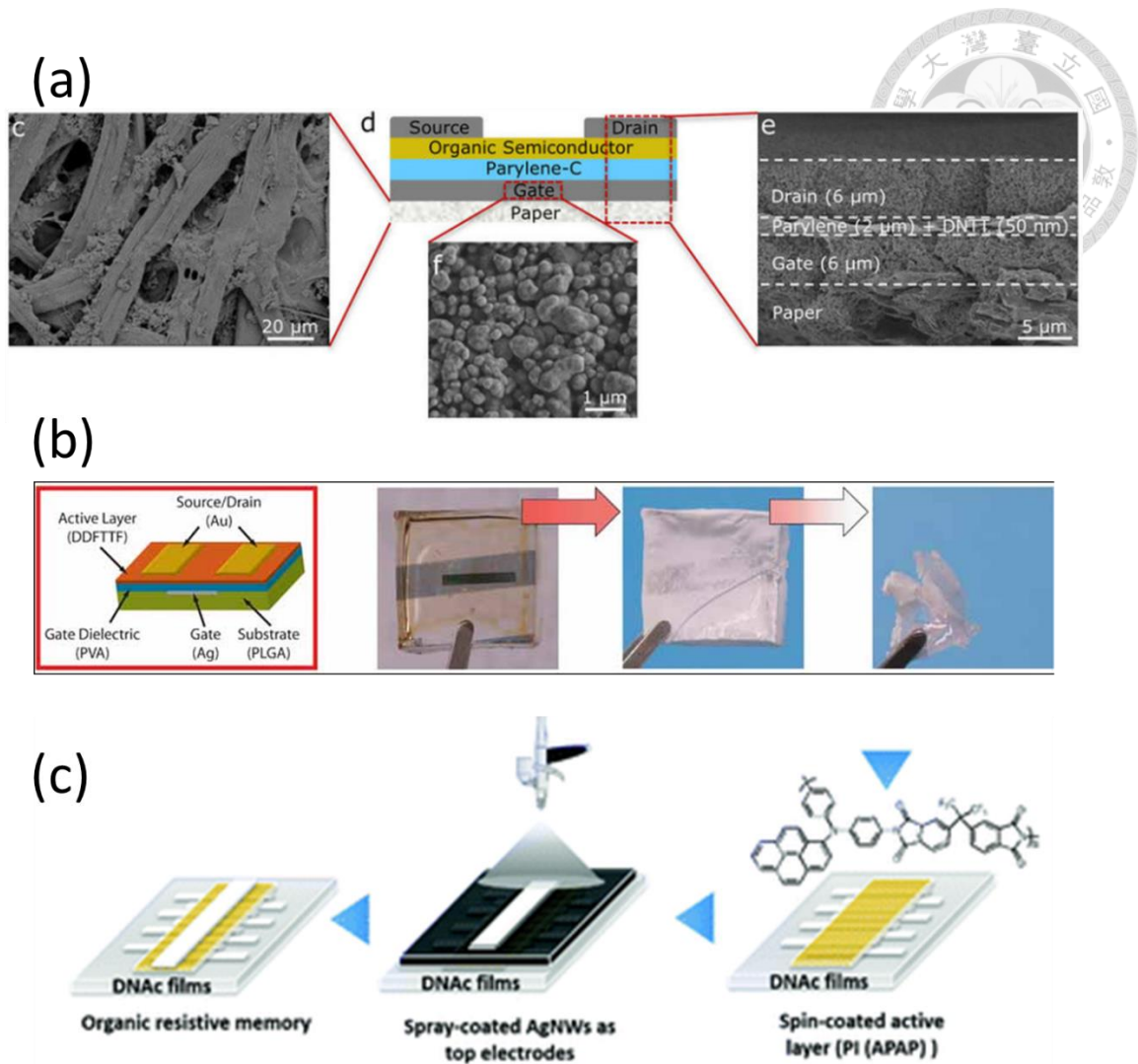


**Figure 1-3.** Self-healing A6ACA hydrogels containing dangling side chains with carboxyl groups.<sup>17</sup>



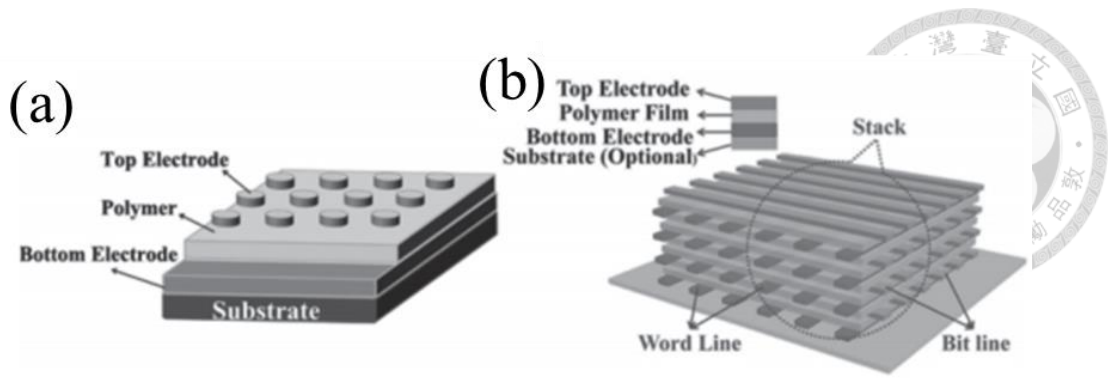
**Figure 1-4.** Environmentally stable PEDOT:PSS-PAAm organogels before and after being stored in a vacuum for 22 hours.<sup>19</sup>



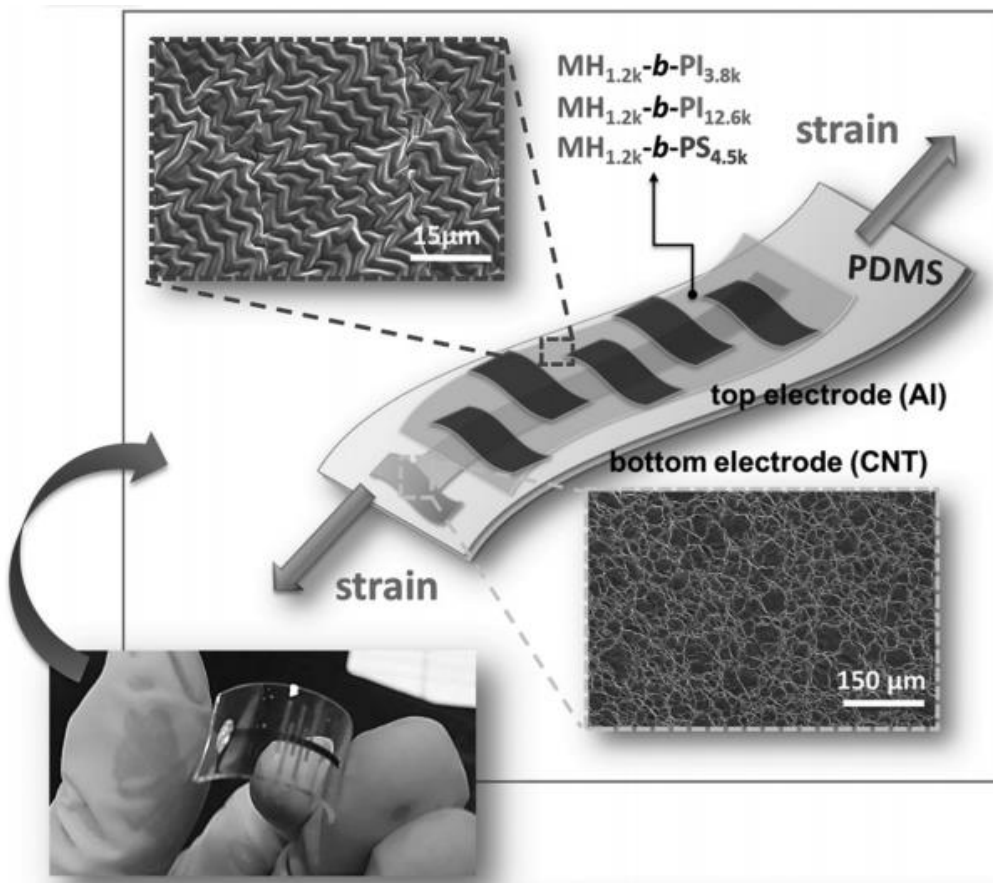


**Figure 1-5.** Examples of biodegradable substrates used to make electronic devices which include: (a) organic transistor active-matrix driver on a paper substrate<sup>25</sup>, (b) organic thin film transistor fabricated on resorbable PLGA<sup>26</sup>, (c) Organic resistive memory fabricated on DNAC substrate.<sup>27</sup>

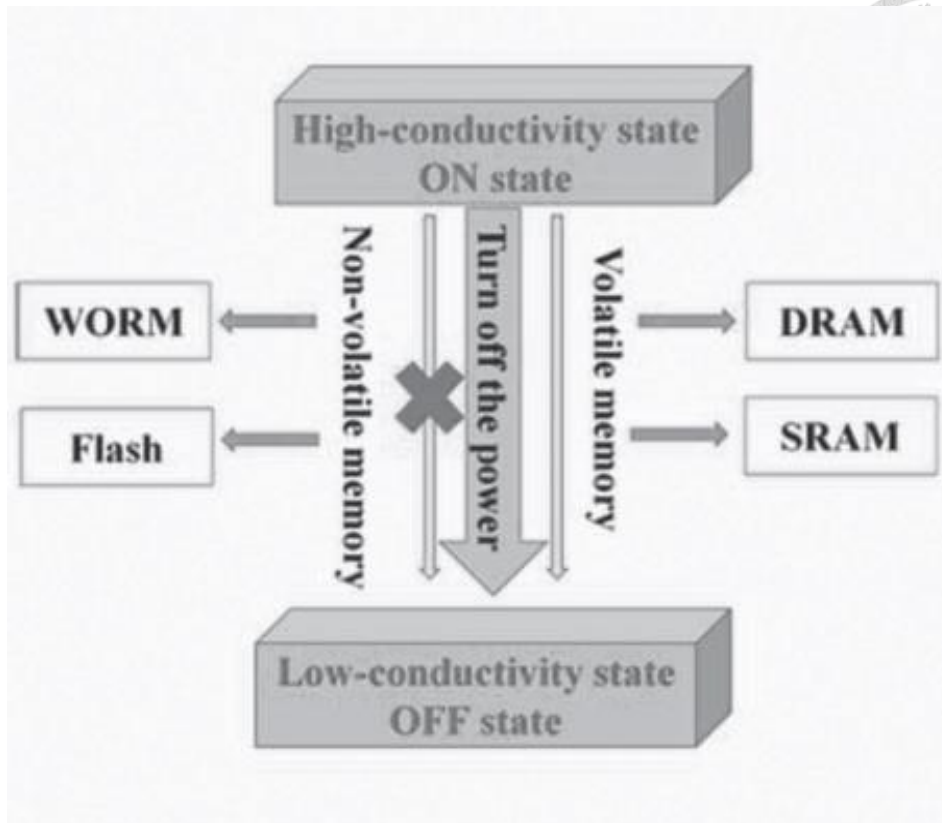




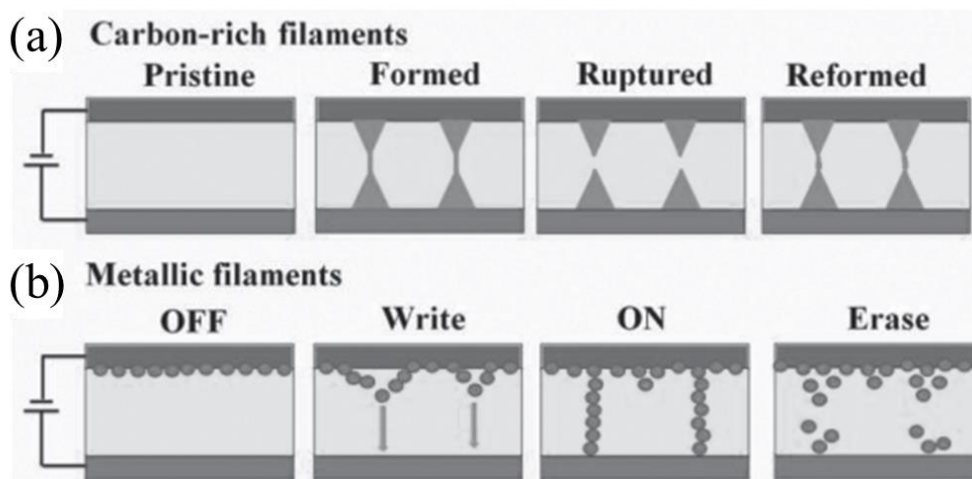
**Figure 1-6.** Device structure of resistor-type memory: (a) MIM test cell and (b) cross-point array



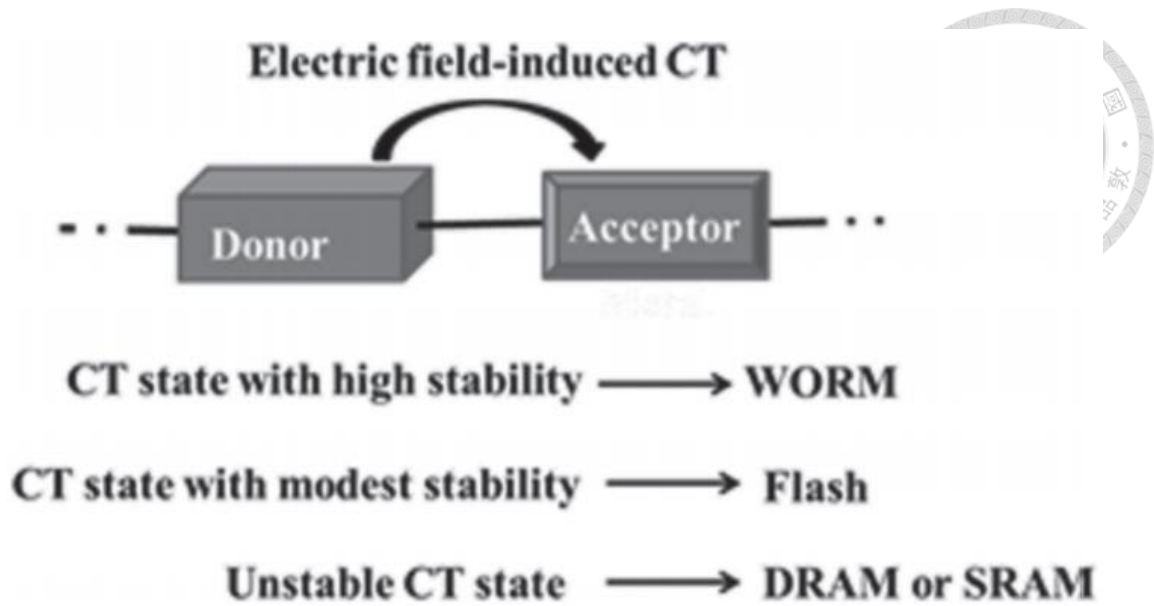
**Figure 1-7.** Device structure of stretchable memory device with a structure of PDMS/CNTs/MH-b-P<sub>12.6k</sub>/Al.<sup>72</sup>



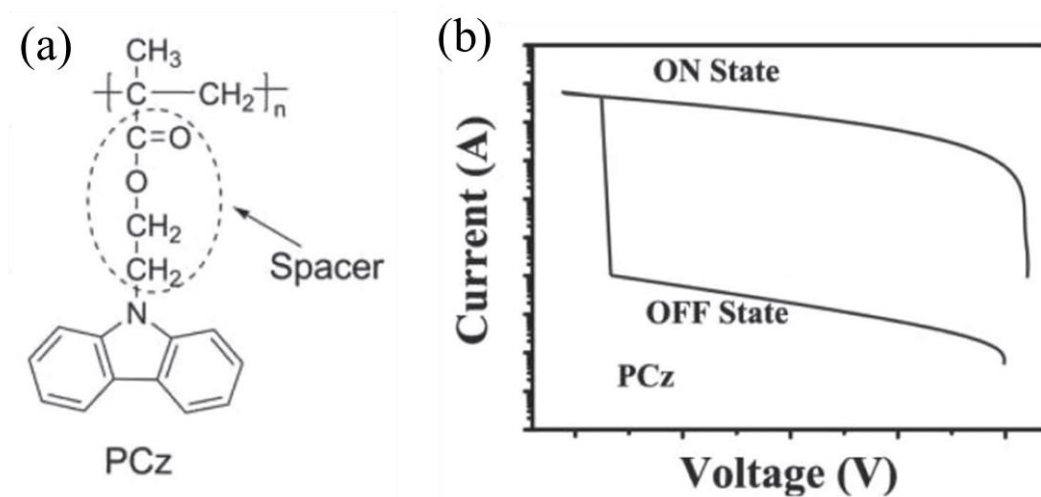
**Figure 1-8.** Class archetypes of polymer resistive memories



**Figure 1-9.** Schematics of the switching effects of (a) carbon-rich filaments and (b) metallic filaments

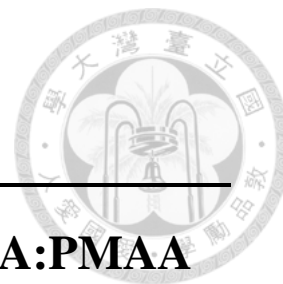


**Figure 1-10.** Mechanisms of electric field-induced charge transfer



**Figure 1-11.** Example of conformational change memory behavior using the (a) chemical structure of PCz and (b) current voltage characteristics

# Chapter 2



---

## Fabrication and Characterization of PVA:PMAA Pseudo-Hydrogels for Biocompatible and Stretchable Electronic Substrates

### 2.1 Introduction to PVA:PMAA Pseudo-Hydrogel

In this chapter, we focus on fabricating a stretchable, biocompatible, non-toxic, biocompatible pseudo-hydrogel material that overcomes the intrinsic weaknesses of hydrogels and while having similar or superior properties to traditional stretchable electronic substrates. Hydrogels are a viable “green” alternative to traditional stretchable electronic substrates like polydimethylsiloxane (PDMS) and nitrile-butadiene rubber (NBR) but lack a direct integration pathway into electronic devices because of intrinsic properties like solvent evaporation, high water content, and poor mechanical characteristics.<sup>1-</sup>

<sup>13</sup> Using hydrophilic polymers like poly(vinyl alcohol) (PVA) and poly(methacrylic acid) (PMAA) and hygroscopic plasticizers like EG can help retain the water content of the gel.<sup>14-20</sup> Techniques like using a double-network of polymers, which include a network of sacrificial and reversible bonds, can help

improve the mechanical properties of the gel.<sup>6-8</sup> Under the direction of these concepts, our pseudo-hydrogel is fabricated and characterized.



## **2.2 Experimental**

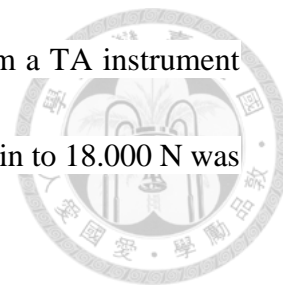
### **2.2.1 Materials**

Poly(vinyl alcohol) (PVA) (87-90% hydrolyzed and 30,000-70,000 average molecular weight) was purchased from Sigma-Aldrich. Poly(methacrylic acid) (PMAA) was purchased from Scientific Polymer Products. Ethylene glycol (EG) (99.8% anhydrous) was purchased from Sigma-Aldrich. All materials were used without any further purification.

### **2.2.2 Characterization**

Thermogravimetric analysis (TGA) was conducted with a TA Instruments Q50. 9-12 mg of the substrates were heated under nitrogen flow (flow rate of 40 ml/min) at a heating rate of 10 °C from 100 to 600 °C. Differential scanning calorimetry (DSC) curves were obtained using a TA Instruments Q100 at a heating rate of 5 °C from 0 to 250 °C. X-ray diffraction (XRD) analysis (XRD) was done using X'Pert from PANalytical at a  $2\theta$  range of 10-60. Infrared spectroscopy (FT-IR) was done using a Spectrum Two IR Spectrometer from PerkinElmer at a wavenumber range of 4000 to 450  $\text{cm}^{-1}$ . Stress-

strain, stress-relaxation, and load-unload curves were obtained from a TA instrument DMA Q800. For the stress-strain curves, a ramp force of 0.200 N/min to 18.000 N was chosen.



### **2.2.3 Fabrication of Pseudo-Hydrogels**

PVA and PMAA were dissolved at a 1:0, 2:1, 1:1, 1:2, and 0:1 PVA:PMAA mass ratio in ethylene glycol (EG) at a concentration of 200mg total solute/mL EG solvent. These solution mixtures were stirred and heated at 60 °C overnight to fully disperse. Three mL of the mixed solution was poured into a cleaned bare silicon wafer lined 3x3x1.5cm Teflon molds and heated at 200 °C for three hours to evaporate out the EG and form the pseudo-hydrogel substrates. The bare Si wafer was cleaned by ultrasonication with acetone, toluene, and IPA purchased from Sigma-Aldrich for 15 minutes each. Solution amounts, temperatures, and heating times were later varied to analyze their effects later on. The substrates were removed from the molds and allowed to rest in ambient conditions for 12 hours before testing. All reagents and solvents were used without further purification. A schematic of the fabrication process can be seen in Figure 2-1.

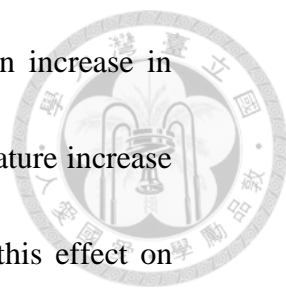
## **2.3 Results and Discussion**



### 2.3.1 Pseudo-hydrogel Analysis

#### 2.3.1.1 Thermogravimetric Analysis (TGA)

TGA experiments were carried out on the blended pseudo-hydrogels as well as their pure constituents. The goal was to gain a better understanding on the effect that casting the polymers/polymer blends at 200 °C in EG had on their thermal stability and decomposition. Figure 2-2 (a) and (b) shows the TGA and DTG thermograms, respectively, of PVA casted in EG and DI water. PVA casted in EG exhibited a smaller –DTG peak at 296 °C compared to 314 °C if PVA casted in water. The change in –DTG peaks for PVA casted in EG may come from the change in crystallinity that arises from casting in a different solvent. Further proof of this idea can be seen in Figure 2-2 (c) and (d), which shows the TGA curves of PMAA. PMAA is an amorphous polymer and there seems to be little to no change in the thermograms of PMAA casted either EG or DI water. Figure 2-2 (e) and (f) shows the TGA and DTG, curves, respectively, for the PVA:PMAA pseudo-hydrogel blends and their constituents. The DTG thermogram showed a PVA peak shift from 296 °C to 327 °C plus a decrease in intensity as the amount of PMAA increase in the blends. Furthermore, the PMAA peak at 425 °C increased in intensity as ratio of it increased in the blend. From these results we can see that casting the PVA and PMAA may have induced a slight degree of

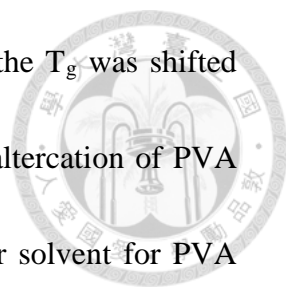


crosslinking/structural change in the PVA matrix which caused an increase in thermal stability. This can be seen by the PVA degradation temperature increase as well as the decrease in intensity. Similar studies have shown this effect on thermal stability in PVA/methylcellulose hydrogel blends<sup>15</sup>, and PVA/starch films with citric acid (CA) additives.<sup>21</sup> The addition of CA into PVA during high temperature molding resulted in an esterification reaction that resulted in chemical crosslinking in the blended PVA system. Excess CA also formed strong hydrogen bonding between the hydroxyl groups of PVA and the carbonyl groups of CA which also enhanced thermal stability. This system is very similar to our pseudo-hydrogel systems and suggest that casting PVA and PMAA in EG at 200 °C results in an effectively blended gel structure.

### **2.3.1.2 Differential Scanning Calorimetry (DSC)**

To investigate both the effects of the different solvents on the crystallinity of PVA and effects of PVA and PMAA on the crystallinity of the pseudo-hydrogels, DSC testing was done at a range of 0-250 °C at a heating and cooling rate of 10 °C. As seen in Figure 2-3 (a), PVA casted in distilled water at 80 °C showed a  $T_g$  of 64 °C and a  $T_c$  of 181 °C while PVA casted in EG at 200 °C showed a  $T_g$  of 79 °C and a  $T_c$  of 183 °C. This shows that by changing the solvent from water to EG,





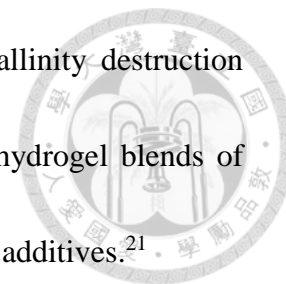
the crystalline structure of PVA was affected in such a way that the  $T_g$  was shifted upwards around 15 °C. A different  $T_g$  seems to signify a slight alteration of PVA crystal structure. This might be due to EG being a relatively poor solvent for PVA compared to water which affects the crystallite formation.<sup>22, 23</sup> A thermogram of PVA and PMAA at a concentration of 200 mg/mL EG casted at 200 °C and their 2:1, 1:1, and 1:2 PVA:PMAA pseudo-hydrogel blends are shown in Figure 2-3 (b). Only pure PVA casted in EG shows a  $T_g$  and  $T_c$ . The 1:1 pseudo-hydrogel was run at a range from -40 °C to 250 °C and showed no peaks either as further proof. This lack of a melting endothermic peak is most likely due to the amorphous structures of PMAA, 2:1, 1:1, and 1:2 pseudo-hydrogels. Since PMAA is known to be an amorphous structure, this suggests that PMAA dispersed and integrated via hydrogen bond cross-links into PVA well enough to destroy its crystalline structure after being casted. This phenomena has also been noted with PVA/cellulose hydrogel blends<sup>14</sup>, PVA/methylcellulose hydrogel blends<sup>15</sup>, starch/gelatin blend films<sup>24</sup>, and cellulose/thermoplastic polyurethane blend films<sup>25</sup>, where the introduction of a second amorphous component through cross-linking breaks the crystalline structure of the first component, increasing the overall miscibility of the two components, and resulting in an overall amorphous structure. This is important because the addition of cross-links and restructuring of a polymer blend gel can change its respective mechanical properties.



### 2.3.1.3 X-ray Diffraction (XRD)

Wide angle x-ray diffraction (WAXD) was used to help determine the crystalline nature of the pure constituents and the pseudo-hydrogel blends. PVA casted in water and EG were again compared to see the effect of EG on the crystalline structure of PVA. As seen in Figure 2-4 (a), a clear decrease in PVA crystalline structure is seen at a peak angle of  $2\theta = 20$ . This may be due to the plasticizing effect of EG on the packed structure which leads to a destruction of crystalline domains. In Figure 2-4 (b), the WAXD patterns of PVA, PMAA, and the pseudo-hydrogel blends casted in EG are shown. PMAA is an amorphous polymer and exhibits no crystalline peaks. As the PMAA content increases in the pseudo-hydrogels, a clear decrease in PVA peak intensity at  $2\theta = 20$  is seen. The decrease in crystallinity may be due to hydrogen-bond cross-linking between the hydroxyl group of PVA and the carboxyl group of PMAA as well as covalent crosslinking between the two component disrupting the crystallization of PVA which leads to peak disappearance and a decrease in degree of crystallinity. These results are in good agreement with the DSC thermograms which also show no noticeable crystalline peaks in the pseudo-hydrogel blends. This disarrangement of PVA chain packing may lead to and enhancement of immovability of

macromolecules and hydrophilicity. Similar cases in PVA crystallinity destruction through the addition of amorphous polymers have been seen in hydrogel blends of PVA/cellulose<sup>14</sup>, PVA/methylcellulose<sup>15</sup>, and PVA/starch with CA additives.<sup>21</sup>



#### 2.3.1.4 Infrared Spectroscopy (FTIR)

FTIR analysis was used to help determine the effect different solvents had on the chemical makeup of the gels as well as give insight to the degree of cross-linking. PVA (87-90% hydrolyzed) casted in water showed a similar spectra to literature findings of a typical FTIR spectra of PVA (85-88% hydrolyzed).<sup>26</sup> Both exhibited an intense peak at  $1731\text{ cm}^{-1}$  due to the existence of C=O bonds due to vinyl acetate groups that are present due to the incomplete hydrolysis of PVA. When PVA is casted in EG at  $200\text{ }^{\circ}\text{C}$ , we notice a disappearance of this C=O peak which may be due to a polymerization reaction between the vinyl acetate groups and the OH group of EG. We used further testing by casting PVA in DMSO at  $200\text{mg/mL}$  solvent and noticed no change in the C=O peak in the spectra which suggests that ethylene glycol has an effect in decreasing the amount of vinyl acetate groups present in PVA. These results can be seen in Figure 2-5 (a) and (b). We also noticed a change in the PVA crystallinity peak of  $1141\text{ cm}^{-1}$  when casting in different solvents. This has been noted in literature and has been attributed to a change in chain packing which results in a different crystal structure.<sup>27</sup>

The effect of EG as a solvent has also been noted in the TGA and DSC thermograms.

As seen in Figure 2-5 (c), instead of a steep slope at  $1141\text{ cm}^{-1}$ , which is typical for PVA casted in water, two peaks are present which can be attributed to a heterogeneous crystal structure of PVA. PMAA casted in EG showed a more intense O-H band intensity compared to PMAA casted in water. This we believe can be attributed to the trapped water or EG in the system which seems to leave the system upon increasing the casting duration which can be seen in Figure 2-6 (a) and (b).

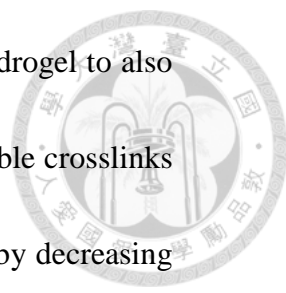
The effect of blending ratios can be seen in Figure 2-7. Foremost, we believe the pseudo-gel structure is mostly composed of strong hydrogen bonds at crosslinking times less than 3 hours at  $200\text{ }^{\circ}\text{C}$ . This is because the 1:1 gels fabricated under these conditions are easily dissolved in water which suggests a negligible amount of permanent crosslinks. Figure 2-7 (a) and (b) shows the FTIR spectra of the pseudo-hydrogel blends as well as their pure constituents. The spectra suggest that the gels are a well-blended structure since they follow a distinct pattern where the pseudo-hydrogels that possess more PVA in their system have a lower C=O peak (from the carboxyl group of PMAA) and a larger O-H peak (from the alcohol group in PVA). If crosslinking in the form of ester linkages were the dominant force in the gels, we would expect the 2:1 PVA:PMAA pseudo-hydrogel to have the largest C=O peak since it has the closest equimolar ratio between PVA and PMAA to form cross-links. However, this is the

opposite where the 2:1 pseudo-hydrogel actually has the least intense C=O peak at 1750-1735  $\text{cm}^{-1}$ . Therefore we can assume that ester crosslinks between the carboxyl and OH groups of PMAA and PVA, respectively are not present in a high amount in the pseudo-hydrogels that have been cross-linked at 200 °C for 3 hours.

The effect of crosslinking times on the IR spectra of a 1:1 pseudo-hydrogel can be seen in Figure 2-8 (a). As the cross-linking temperature or time increases, we can observe an increase in the C=O peak intensity as well as a decrease in the OH band intensity. When the ratio of the intensity of the C=O peak ( $A_{1710}$ ) and O-H peak ( $A_{3320}$ ) are compared to the C-H peak from alkyl groups ( $A_{2930}$ ), which remains almost constant, we clearly see the decrease of in the  $A_{3320}/A_{2930}$  ratio and increase in the  $A_{1710}/A_{2930}$  ratio as the cross-linking time and temperature increases. This can be seen in Figure 2-8 (b). It should be noted that cross-linking parameters under 200 °C and 3 hours most likely result in a gel blend that is held together by a vast majority of strong hydrogen bonds rather than covalent ester linkages since these gels are able to dissolve in water easily.

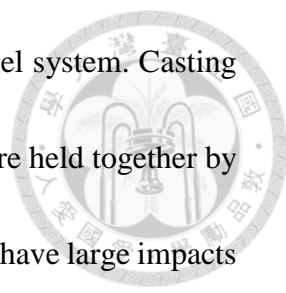
### 2.3.1.5 Self-healing Properties

Self-healing is an important property that many pseudo-hydrogels exhibit due to their multitude of reversible bonds.<sup>9, 11-13</sup> Due to the large number of strong hydrogen-



bonds in the pseudo-hydrogel network, we expected the pseudo-hydrogel to also exhibit self-healing. Following this principle, the amount of reversible crosslinks was increased by lowering the casting temperature to 150 °C thereby decreasing the amount of covalent ester crosslinks between the polymers and promote self-healing. Self-healing was tested by cutting through the pseudo-hydrogels while they were still inside the Teflon molds using a scalpel and testing the cut-point under strain. A 1:1 mass ratio PVA:PMAA pseudo-hydrogel was shown to exhibit self-healing properties in ambient conditions. However, the healing time required was over four days which is very long. The resulting healed pseudo-hydrogel can be seen in in Figure 2.9. This may be due to the lack of water inside the pseudo-hydrogels, which is only around 25%. Compared to traditional hydrogels, whose water contents can reach an excess of 200%, the chain mobility of pseudo-hydrogels is limited.<sup>3, 8</sup> Using this hypothesis, the pseudo-hydrogel was tested for self-healing under a temperature of 60 °C and under high humidity from a nearby water capsule. The results were not only an extremely quick healing time of one, two, and five minutes but also a return back to pristine elongation lengths and a similar Young's modulus. This can be seen in Figure 2-10.

### **2.3.2 Water and Pseudo-hydrogel interactions**



Water is used as an important plasticizer in the pseudo-hydrogel system. Casting PVA and PMAA in EG at 200 °C forms a three-dimensional structure held together by covalent and strong hydrogen bond cross-links. PMAA and EG both have large impacts in destroying the crystalline domains of PVA chain packing to remove rigidity but it was found that without water, the system remained fairly rigid. Water incorporation in a three-dimensional system can increase molecular mobility by acting as lubricants for polymer chains, allowing fibers to slide over one another. Water molecules may also disjoin the hydrogen bonds between PVA-PMAA, PVA-PVA, and PMAA-PMAA, for more favorable water-PVA/PMAA hydrogen bonds, which reorganizes the polymer network and increases polymer chain mobility.<sup>16, 28, 29</sup> The plasticizing effect of water molecules on polymer chains has also been seen in edible films<sup>30-32</sup>, biodegradable polymers<sup>33</sup>, and hydrophilic polymers.<sup>34, 35</sup> In conclusion, the absorption and retention of water in the pseudo-hydrogels are paramount in retaining their good mechanical properties.

### **2.3.2.1 Water Vapor Absorption and Equilibrium**

Water retention and absorption are two extremely important topics in the hydrogel and organogel systems.<sup>1, 36, 37</sup> This is because solvents play a large part in the polymer chain mobility, and hence, mechanical properties of gel systems. The mechanical

properties of pseudo-hydrogels are no exception to this solvent dependence.

However, one of the biggest advantages of pseudo-hydrogels compared to

hydrogel is water absorption and retention. These unique properties may include:

the hygroscopicity of EG, hydrophilicity/hygroscopicity of PVA, and increased

vapor permeability of disrupted PVA chains.

Casting the pseudo-hydrogels in EG at 200 °C results trace amounts of EG

remaining in the polymer network. EG is a polyol, which are highly hygroscopic

molecules that act as plasticizers but, more importantly, significantly increase the

amount of water absorbed which have a large effect on increasing chain mobility.

EG, as well as PMAA, may disrupt the double polymer network enough to increase

the diffusion of water molecules into the matrix. Similar effects are seen when EG

is added into gelatin films<sup>38</sup>, polyethylene glycol 400 (PEG400) is added into

methylcellulose films<sup>39</sup>, and glycerol, another polyol, is added into iota-

carrageenan edible films.<sup>16</sup> However it can be noted that the extent to which

mechanical properties, like elongation, are enhanced is much lower than the

pseudo-hydrogel system.

PVA films have been shown to possess high water-vapor permeability and

hygroscopicity. PVA forms strong hydrogen bonds with water through its

hydroxyl group. Their hygroscopic nature has been documented in PVA films<sup>40</sup>,



relative humidity detection<sup>17</sup>, and as part of PVA-PAA interpenetrating network (IPN) hydrogels.<sup>18</sup> Hygroscopicity of PVA chains allows for water to be absorbed and held while the high vapor permeability increases the depth in which adsorbed water molecules can penetrate in the polymer network system.

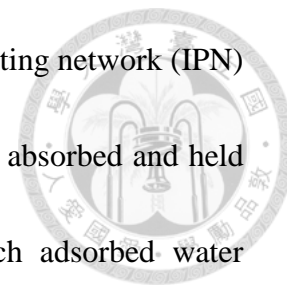
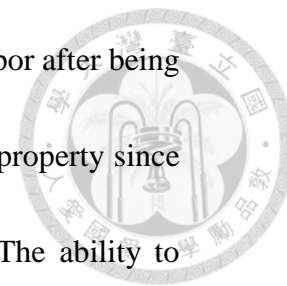


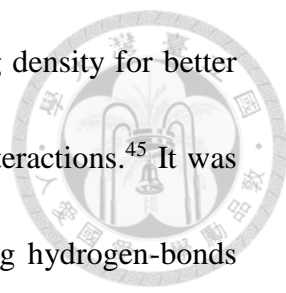
Figure 2-11 shows the weight percent of water absorbed by the pseudo-hydrogels and their pure constituents after vacuuming the substrates for 24 hours under a pressure of 75 cmHg. PVA casted in EG and the three pseudo-hydrogel blends were able to absorb around 25 wt% of their dry weight in water vapor after 24 hours. PMAA casted in EG was only able to absorb around 15 wt% of its dry weight after this time period. This may be due to the more hydrophilic nature of PVA which allows for more water vapor to be absorbed from the environment. It should also be noted that the pseudo-hydrogels require a much lower amount of water content compared to conventional hydrogels for high chain mobility, and thus, good mechanical properties. The pseudo-hydrogel were able to maintain an equilibrium with the absorbed water vapor which may be due to the hydrophilic polymer chains and strong hydrogen bonds formed between PVA/PMAA-water. This can be seen in Figure 2-12, where the mass of the pseudo-hydrogel remains fairly constant with no large decrease in weight over 30 days. It is important to note that the water content in the pseudo-hydrogels is dependent on the water moisture in the air and thus will oscillate a small amount due to humidity

deviations. The ability for the pseudo-hydrogels to absorb water vapor after being vacuumed and retain this water content is an extremely important property since water is the main plasticizer in the PVA-PMAA chain system. The ability to absorb and retain water is one of the biggest intrinsic obstacles in hydrogel systems since they possess a large amount of water which is almost impossible to maintain an equilibrium with.



### **2.3.2.2 Recycling and Biodegradable Potential**

PVA is a non-toxic, water-soluble, biocompatible, and biodegradable polymer.<sup>19, 42</sup> PMAA is a non-toxic, water-soluble, and biocompatible polymer with biodegradable potential.<sup>20, 41, 42</sup> Cross-linked and isotactic PMAA have been shown to have biodegradable properties.<sup>43, 44</sup> The 1:1 PVA:PMAA pseudo-hydrogel was able to dissolve fully in water and be recycled and recasted into another stretchable 1:1 PVA:PMAA substrate as seen in Figure 2-13. The ability for the pseudo-hydrogel to dissolve in water is another unique property as most hydrogels structures remain stable within water solutions. This phenomena closely follows the work of Professor Robert Langer on biodegradable elastomers. Dr. Langer developed a criteria for a biodegradable elastomer with good mechanical properties that included: (i) hydrolysis as a degradation mechanism; (ii) ester



crosslinks as a hydrolyzable chemical bond; (iii) low cross-linking density for better mechanical properties; (iv) a large degree of hydrogen-bonding interactions.<sup>45</sup> It was also shown that PVA and PMAA prefer to form extremely strong hydrogen-bonds between each other when forming a 3-dimensional structure, which satisfies the (iv) requirement.<sup>28,29</sup> Therefore the dissolution of the pseudo-hydrogel in can be attributed to the large amount of hydrogen bonds, which in an excess of water molecules will cause to reform. Dissolution in water is a unique advantage over elastomers because it allows for a pathway for recycling. In the dispersed aqueous phase, the polymers can be separated and reused which is not possible for many cross-linked double-network hydrogels, elastomers and hydrogel-elastomer substrates.

### **2.3.2.3 Effect of Vapor Content of the Mechanical Properties of a Pseudo-hydrogel**

The effect of absorbed vapor content on the mechanical properties of a 1:1 pseudo-hydrogel can be seen in Figure 2-14. Since water is the main chain plasticizer in the pseudo-hydrogel system, a decrease in water content leads to a sharp increase in the stiffness of the pseudo-hydrogels. Table 2-1 shows the Young's modulus as the water content increases. The water content and the Young's modulus of the pseudo-hydrogel systems seems to be inversely proportional, with an increase in water content leading to a decrease in Young's modulus. This suggests that water is a very effective plasticizer

in the pseudo-hydrogel, since an increase of ~20% water in the system would lead to a two order decrease in Young's modulus in the 1:1 pseudo-hydrogel.



### **2.3.3 Mechanical Properties**

The mechanical properties of the pseudo-hydrogels come from the plasticizing mechanism of water, random chain coil formation during casting, and a 3D gel structure made up of a large density of strong, reversible hydrogen bonds and a small amount of covalent cross-links. Together, these factors result in a suitable, stretchable, electronic substrate with high elongation rates, tunable mechanical properties, and fast response times.

#### **2.3.3.1 Stress-Strain Curves and Relaxation Times of Pseudo-hydrogel Blends**

Figure 2-15 displays the stress strain curves for PVA, PMAA, and the three blended hydrogels casted in EG. As seen in Table 2-2, the Young's modulus increases as the amount of PVA increases in the blend. This is expected due to the crystalline nature of PVA in EG as seen in the DSC thermograms and XRD. However, it should also be noted that in the 2:1 PVA:PMAA blended pseudo-hydrogel is almost two orders smaller than PVA casted in EG. This is also supported by the DSC and XRD data, in which the degree of crystallinity is found

to be very small and the overall nature of the system is concluded to be amorphous.

One important property of a well-blended systems independent of polymer ratios is the ability to finely tune mechanical properties. The pseudo-hydrogels exhibited tunable

Young's moduli based on the amount of PVA, a crystalline polymer, added. The 2:1,

1:1, and 1:2 pseudo-hydrogels showed large elongations, with 1:1 and 2:1 blends

capable of over 500% elongation. The mechanism behind this may be due to the 3-D

structure made up of mostly strong hydrogen bonds with a small amount of covalent

cross-links since it has often been noted that double-network gels have mechanical

properties exceeding their pure constituents.<sup>3, 45</sup> It should also be The 1:1 PVA:PMAA

pseudo-hydrogel had the best overall qualities, with a sizable elongation and large linear

region. The strain-relaxation time from 25% strain is of the pseudo-hydrogels blends

can be seen in Figure 2-16. Table 2-3 shows their 80% recovery time, 90% recovery

time, and their recovery percentage after 60s. The 2:1 blend had the fastest 80%

recovery time of 1.2s, a slower 90% recovery time of 17.4s, and the worst recovery

percentage after 60s of 92.50%. This may be due to some small amounts of PVA

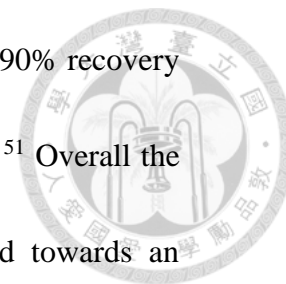
crystalline domains that and a inhibit reformation during strain-relaxation. The 1:2

blend had the slowest 80% and 90% recovery times of 6s and 18s, respectively, but the

best recovery percentage after 60s of 97.15%. This may be due to the amorphous nature

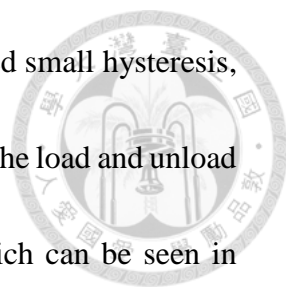
of PMAA which allows for easier chain packing without crystalline domains during

relaxation. The 1:1 blend had the best overall performance with a 90% recovery time of 9.6s which is close to other highly-responsive hydrogels.<sup>6, 51</sup> Overall the data agrees with the TGA, DSC, and XRD data which pointed towards an amorphous well-blended double-polymer network.



### **2.3.3.2 Relaxation Times and Load-Unload Cycles**

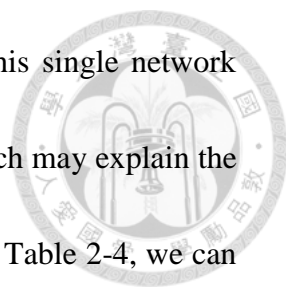
Fast recovery from strain is an important mechanical property for gels that desire to mimic articular cartilage.<sup>6</sup> Gels that aim to mimic skin should also have extremely fast recovery speeds to restore themselves from quick movements like running, jumping, and bending. Stress-relaxation in gels normally arises through the breaking and reforming of reversible cross-links within the system.<sup>47, 48</sup> In the case of pseudo-hydrogels, these reversible cross-links may come from strong hydrogen bonds between polymer chains and water which are easily reformed and have good bond energy. One reason for the quick a recovery/relaxation times may come from the non-covalent interactions of the pseudo-hydrogel, which is mostly made up of strong hydrogen bonds which are easy to reform and restructure back into random coil alignments during recovery. Further investigate mechanical and self-healing properties of the 1:1 pseudo-hydrogel are done due to its fast relaxation times. The 1:1 pseudo-hydrogel was subjected to 10 load-unload cycles,



with a relaxation period of 1 minute.. The pseudo-hydrogel exhibited small hysteresis, which can be seen in Figure 2-17 (a), with a noticeable area between the load and unload curves which accounts for energy dissipated per unit volume, which can be seen in Figure 2-17 (b). Again, this may be due to the 3D structure of the PVA:PMAA pseudo-hydrogel which has a network of strong hydrogen bonds that can dissipate energy by breaking and reforming before the small amount of covalent cross-links formed during casting are destroyed.<sup>6-8</sup>

### **2.3.3.3 Effect of Different Cross-linking Times and Temperatures**

Increasing the cross-linking time while maintaining the temperature at 200 °C results in a larger Young's modulus as well as a decrease in elongation. This may be due to the change in the density of ester cross-links between PVA and PMAA chains which has been suggested using FTIR analysis. With an increase in cross-link density, it seems that the elongation is also affected and the pseudo-hydrogel system becomes less stretchable. This can be seen in Figure 2-18. This may be due to the breaking of the covalent network earlier since the amount of reversible hydrogen bonds is relatively lower than before. Lowering the cross-linking temperature from 200 °C to 150 °C results in a lower Young's modulus as well as a smaller elongation. This is probably due to the lack of covalent cross-links in this system which means that the pseudo-



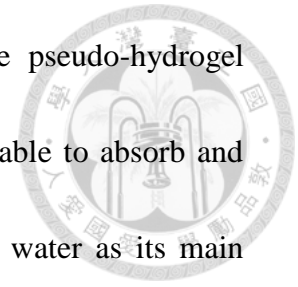
hydrogel system is almost fully composed of hydrogen bonds. This single network system is less mechanically robust as a double-network system which may explain the soft nature of this pseudo-hydrogel. From this cross-linking data in Table 2-4, we can surmise that the best network structure for the pseudo-hydrogel is one that has a large amount of strong hydrogen bonds and a small, but not negligible, amount of covalent crosslinks to form a 3D gel network. The 25% strain recovery of the pseudo-hydrogel at different crosslink times show that the gels recover quickly despite changes in cross-linking density. This may be because water is the main plasticizer of the chains and thus, the recovery is more dependent on the water content of the pseudo-hydrogels than the cross-linking density. It should be noted that the 1:1 pseudo-hydrogel casted at 150 °C for 6hrs had a slower recovery time which may be due to the lack of a significant amount of cross-links between PVA and PMAA. The recovery times can be seen in Figure 2-19 and Table 2-5.

## **2.4 Conclusion**

In conclusion, a biocompatible, non-toxic, self-healing, mechanically tough, vapor absorbing and retaining, and recyclable PVA:PMAA pseudo-hydrogel is facilely fabricated. TGA, DSC, XRD, FTIR and self-healing testing were used to confirm that the full blending of PVA and PMAA polymers as well as give insight




on the strong hydrogen cross-link bonding between them. The pseudo-hydrogel interactions with water were especially important as the gel was able to absorb and retain water vapor which is a novel property. The gel relied on water as its main plasticizer and strong hydrogen bonds as the major network inside the gel. The gel was also able to dissolve fully in water which is important for recycling and biodegradable pathways. Stress-strain curves, relaxation times, loading and unloading mechanical testing revealed the high elongation, fast recovery, and tunable mechanical properties which helped confirm the double-network nature of the pseudo-hydrogel structure.





## 2.5 References

1. H. Yuk, T. Zhang, G. A. Parada, X. Liu, X. Zhao, *Nat. Commun.* 2016, 7;
2. A. B. Imran, K. Esaki, H. Gotoh, T. Seki, K. Ito, Y. Sakai, Y. Takeoka, *Nat. Commun.* 2014, 5;
3. J.-Y. Sun, X. Zhao, W. R. Illeperuma, O. Chaudhuri, K. H. Oh, D. J. Mooney, J. J. Vlassak, Z. Suo, *Nature* 2012, 489, 133;
4. F. Ullah, M. B. H. Othman, F. Javed, Z. Ahmad, H. M. Akil, *Mater. Sci. Eng. C.* 2015, 57, 414;
5. J. Maitra, V. K. Shukla, *Am. J. Polym. Sci.* 2014, 4, 25;
6. W. Sun, B. Xue, Y. Li, M. Qin, J. Wu, K. Lu, J. Wu, Y. Cao, Q. Jiang, W. Wang, *Adv. Funct. Mater.* 2016, 26, 9044;
7. T. Nakajima, *Polym. J.* 2017;
8. J. P. Gong, Y. Katsuyama, T. Kurokawa, Y. Osada, *Adv. Mater.* 2003, 15, 1155;
9. G. Cai, J. Wang, K. Qian, J. Chen, S. Li, P. S. Lee, *Adv. Sci.* 2016;
10. S. Lin, C. Cao, Q. Wang, M. Gonzalez, J. E. Dolbow, X. Zhao, *Soft Matter* 2014, 10, 7519;
11. D. L. Taylor, *Adv. Mater.* 2016;

- 
12. J. Cui, A. del Campo, *Chem. Commun.* 2012, 48, 9302;
13. A. Phadke, C. Zhang, B. Arman, C.-C. Hsu, R. A. Mashelkar, A. K. Lele, M. J. Tauber, G. Arya, S. Varghese, *Proc. Natl. Acad. Sci. U.S.A.* 2012, 109, 4383;
14. C. Chang, A. Lue, L. Zhang, *Macromol. Chem. Phys.* 2008, 209, 1266;
15. J.-S. Park, J.-W. Park, E. Ruckenstein, *Polymer* 2001, 42, 4271;
16. T. Karbowiak, H. Hervet, L. Léger, D. Champion, F. Debeaufort, A. Voilley, *Biomacromolecules.* 2006, 7, 2011;
17. H. Liang, L. Zheng, S. Liao, *Int. J. Hydrogen Energy* 2012, 37, 12860;
18. G. Silva, P. Sobral, R. Carvalho, P. Bergo, O. Mendieta-Taboada, A. Habitante, J. *Polym. Environ.* 2008, 16, 276;
19. R. A. Gross, B. Kalra, *Science* 2002, 297, 803;
20. P. Yang, D. Li, S. Jin, J. Ding, J. Guo, W. Shi, C. Wang, *Biomaterials.* 2014, 35, 2079;
21. R. Shi, J. Bi, Z. Zhang, A. Zhu, D. Chen, X. Zhou, L. Zhang, W. Tian, *Carbohydr. Polym.* 2008, 74, 763;
22. N. A. Peppas, E. W. Merrill, *J. Appl. Polym. Sci.* 1976, 20, 1457;
23. K. Yamaura, H. Kitahara, T. Tanigami, *J. Appl. Polym. Sci.* 1997, 64, 1283;
24. E. A. Soliman, M. Furuta, *Food Nutr. Sci.* 2014, 2014;
25. X. Zhang, J. Zhu, X. Liu, J. Feng, *Cellulose.* 2012, 19, 121;

26. H. Mansur, C. Sadahira, A. Souza, A. Mansur, *Mater. Sci. Eng. C*, 2008, 28, 539
27. P. Hong, J. Chen, H. Wu, *J. Appl. Polym. Sci.* 1998, 69, 2477
28. I. Okhrimenko, E. D'yakonova, *Polym. Sci. (USSR)* 1964, 6, 2095;
29. G. Distler, E. D'yakonova, I. Yefremov, Y. I. Kortukova, I. Okhrimenko, P. Sotnikov, *Polym. Sci. (USSR)* 1966, 8, 1917;
30. Y. ROOS, M. KAREL, *J. Food Sci.* 1991, 56, 38;
31. S. Mali, L. Sakanaka, F. Yamashita, M. Grossmann, *Carbohydr. Polym.* 2005, 60, 283;
32. N. Gontard, S. Guilbert, J. L. CUQ, *J. Food Sci.* 1993, 58, 206;
33. P. Blasi, S. S. D'Souza, F. Selmin, P. P. DeLuca, *J. Control. Release* 2005, 108, 1;
34. Z. Ping, Q. Nguyen, S. Chen, J. Zhou, Y. Ding, *Polymer* 2001, 42, 8461;
35. H. Bair, G. Johnson, E. Anderson, S. Matsuoka, *Polym. Eng. Sci.* 1981, 21, 930;
36. T.-Y. Liu, S.-Y. Chen, Y.-L. Lin, D.-M. Liu, *Langmuir* 2006, 22, 9740;
37. Y. Y. Lee, H. Y. Kang, S. H. Gwon, G. M. Choi, S. M. Lim, J. Y. Sun, Y. C. Joo, *Adv. Mater.* 2016, 28, 1636;
38. N. Cao, X. Yang, Y. Fu, *Food Hydrocoll.* 2009, 23, 729;
39. F. Debeaufort, A. Voilley, *J. Agric. Food Chem.* 1997, 45, 685;
40. Y. Xianda, W. Anlai, C. Suqin, *Desalination* 1987, 62, 293;
41. W. Amass, A. Amass, B. Tighe, *Polym. Int.* 1998, 47, 89;



42. G. Saunders, B. MacCreath, Application Compendium. Agilent Technologies  
2010;
43. C. De Vasconcelos, d. P. Bezerril, D. Dos Santos, d. T. Dantas, M. Pereira, J.  
Fonseca, Biomacromolecules. 2006, 7, 1245;
44. R. Larson, E. Bookland, R. Williams, K. Yocom, D. Saucy, M. Freeman, G.  
Swift, J. Environ. Polym. Degrad. 1997, 5, 41;
45. Y. Wang, G. A. Ameer, B. J. Sheppard, R. Langer, Nat. Biotechnol. 2002, 20,  
602;
46. K. Kumeta, I. Nagashima, J. Appl. Polym. Sci. 2003, 90, 2420;
47. O. Chaudhuri, L. Gu, D. Klumpers, M. Darnell, S. A. Bencherif, J. C. Weaver, N.  
Huebsch, H.-p. Lee, E. Lippens, G. N. Duda, Nat. Mater. 2015;
48. X. Zhao, N. Huebsch, D. J. Mooney, Z. Suo, J. Appl. Phys. 2010, 107, 063509.



## Tables



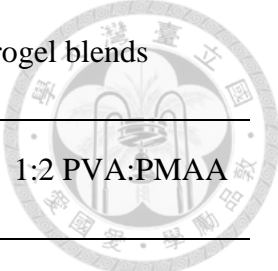
**Table 2-1.** Effect of vapor content on the Young's modulus of a 1:1 pseudo-hydrogel

Water Content (%)	Young's Modulus (MPa)
1.90	1.6026
8.40	0.1278
11.89	0.0218
22.10	0.0126

**Table 2-2.** Stress-strain curve data for PVA, PMAA, and pseudo-hydrogel blends

casted in EG.

	PVA	2:1	1:1	1:2	PMAA
Young's Modulus (MPa)	2.22	0.0168	0.0075	0.0048	0.0018
Linear Region (%)	~8.00	~30.00	~42.00	~22.00	~15.00
Elongation (%)	36.38	250.70	>567.60	>553.10	321.9

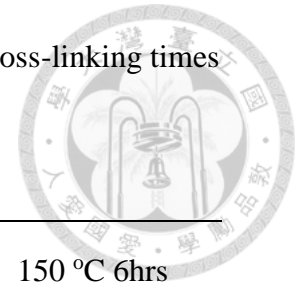
**Table 2-3.** Strain-relaxation curves from 25% strain for pseudo-hydrogel blends

	2:1 PVA:PMAA	1:1 PVA:PMAA	1:2 PVA:PMAA
80% Recovery Time (s)	1.20	1.80	6.00
90% Recovery Time (s)	17.40	9.60	18.00
Recovery after 60s (%)	92.50	95.84	97.15

**Table 2-4.** Stress-strain curve data for different cross-linking times of a 1:1 pseudo-hydrogel blend

	200 °C 5hrs	200 °C 4hrs	200 °C hrs	150 °C 6hrs
Young's Modulus (MPa)	0.1580	0.0224	0.0075	0.0018
Elongation (%)	346.80	403.80	>567.60	256.80

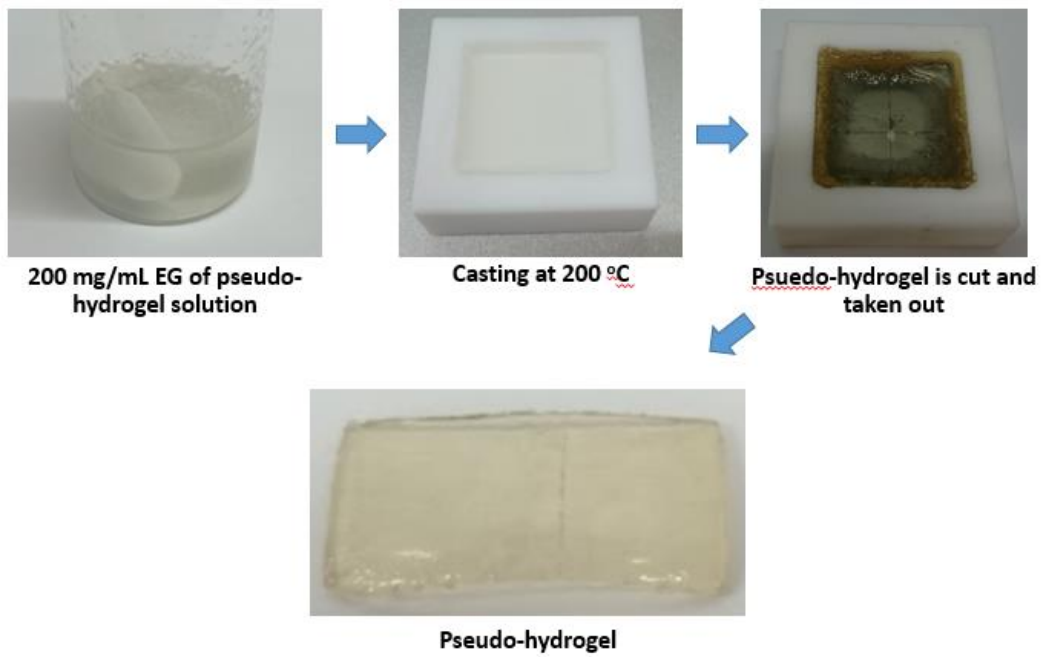
**Table 2-5.** Strain-relaxation curves from 25% strain for different cross-linking times of a 1:1 pseudo-hydrogel blend



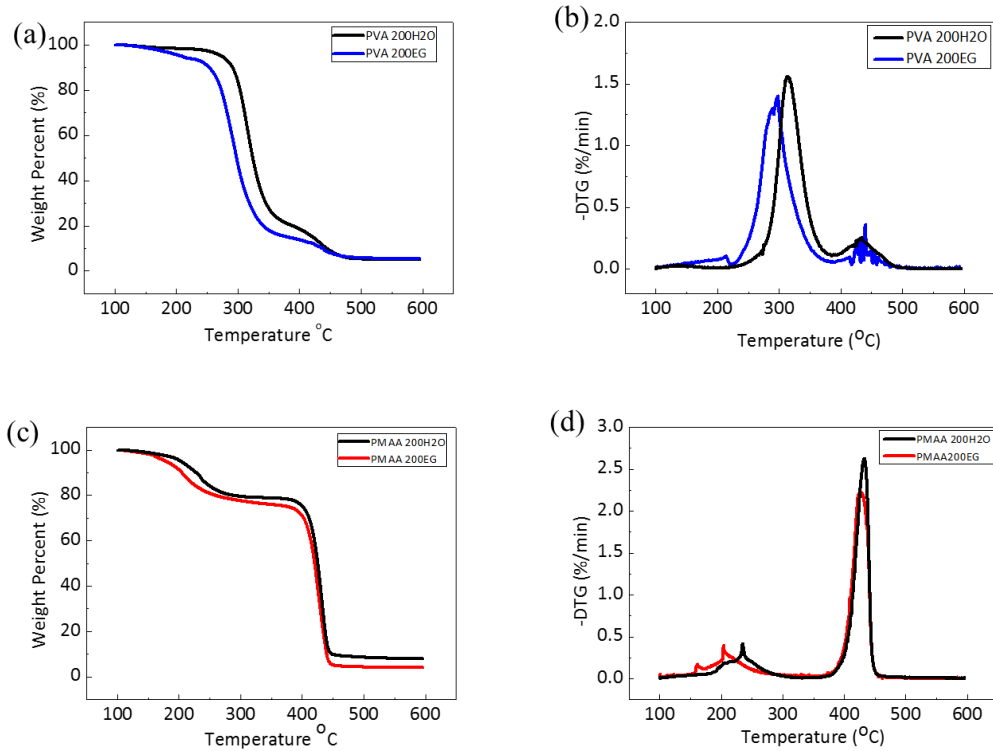
	200 °C 5hrs	200 °C 3hrs	150 °C 6hrs
80% Recovery Time (s)	1.80	1.80	5.40
90% Recovery Time (s)	7.80	9.60	13.80
Recovery after 60s (%)	95.21	95.84	97.63

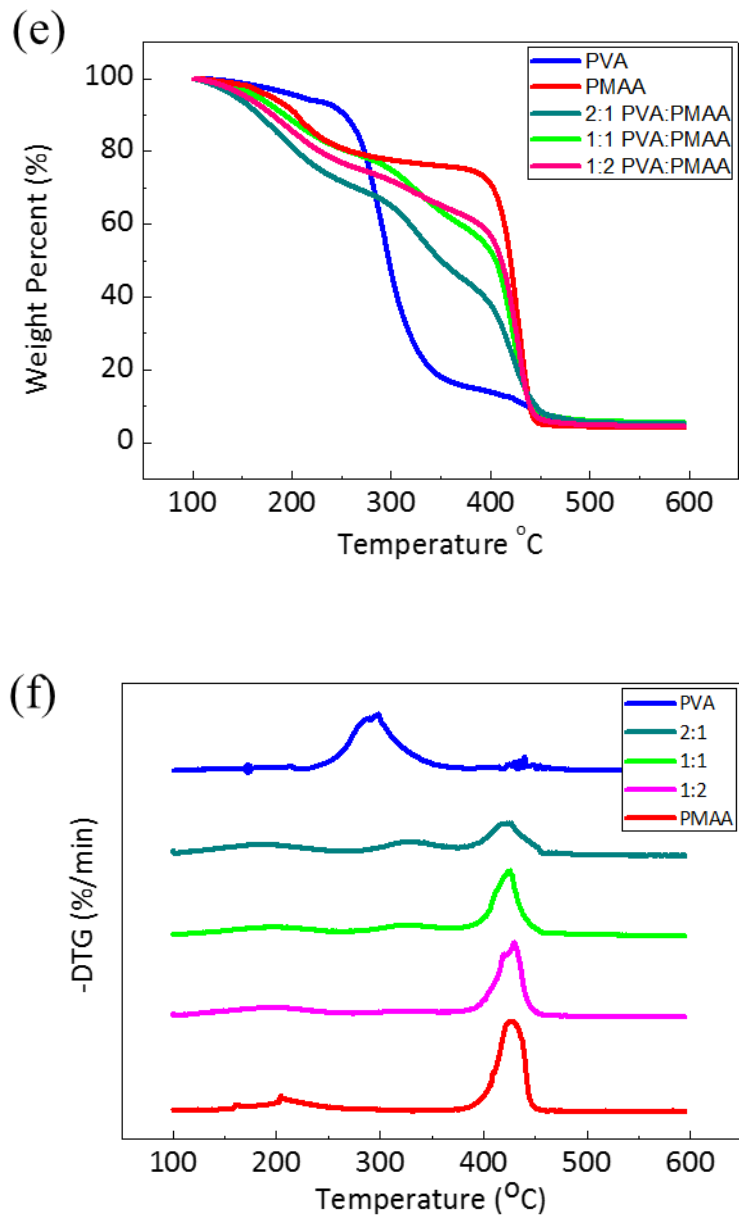


## Figures

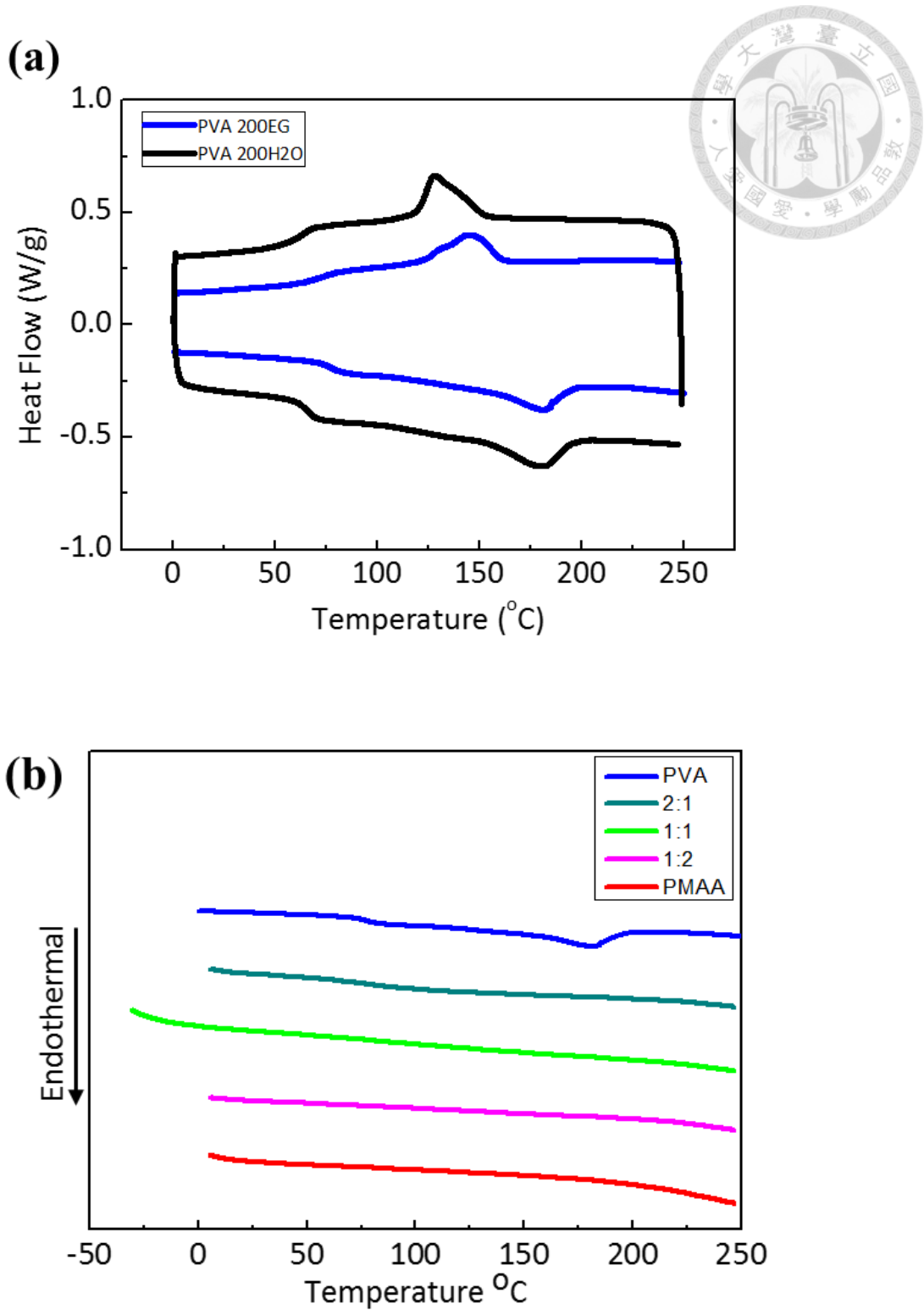


**Figure 2-1.** Facile fabrication of PVA:PMAA pseudo-hydrogel.

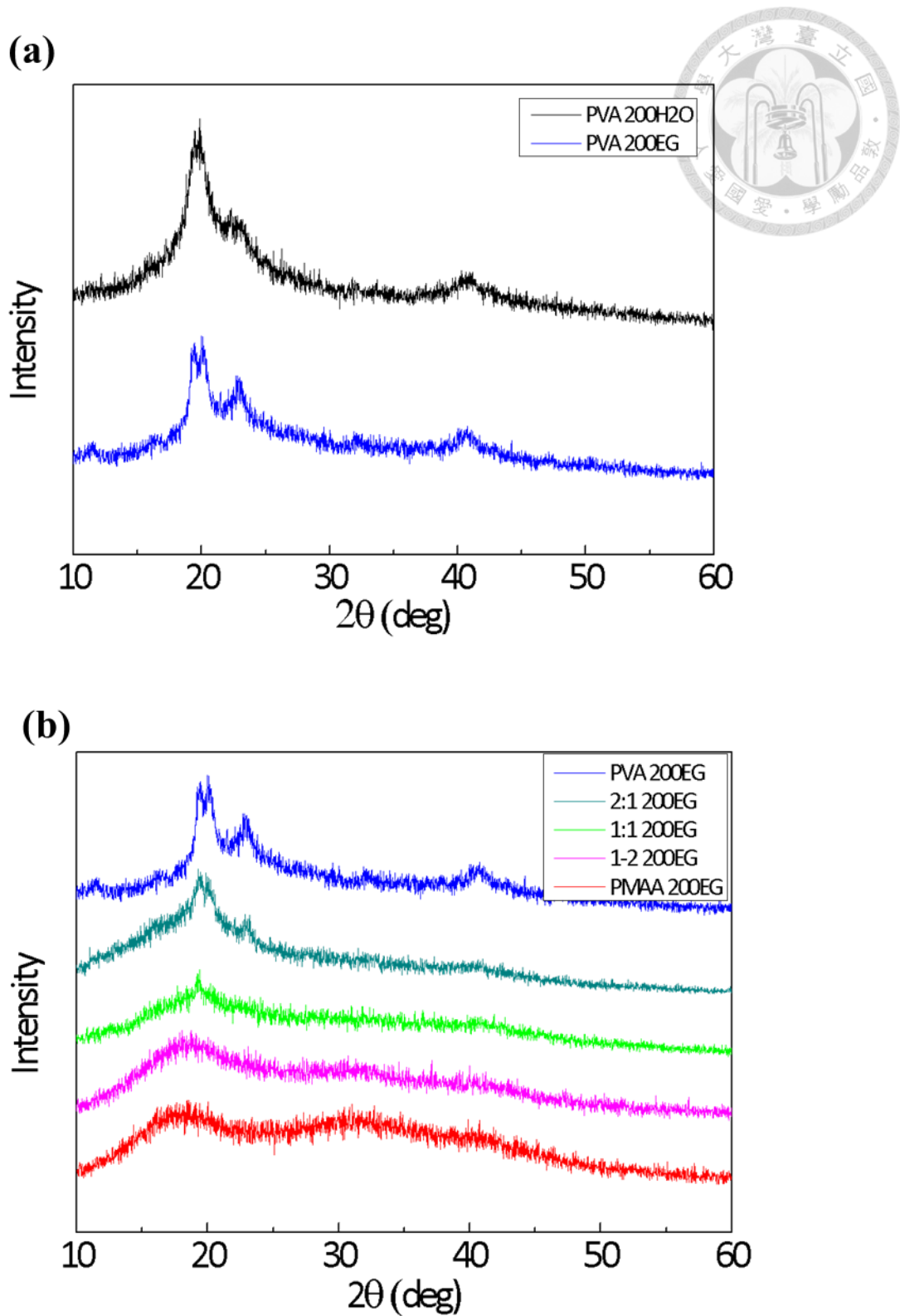




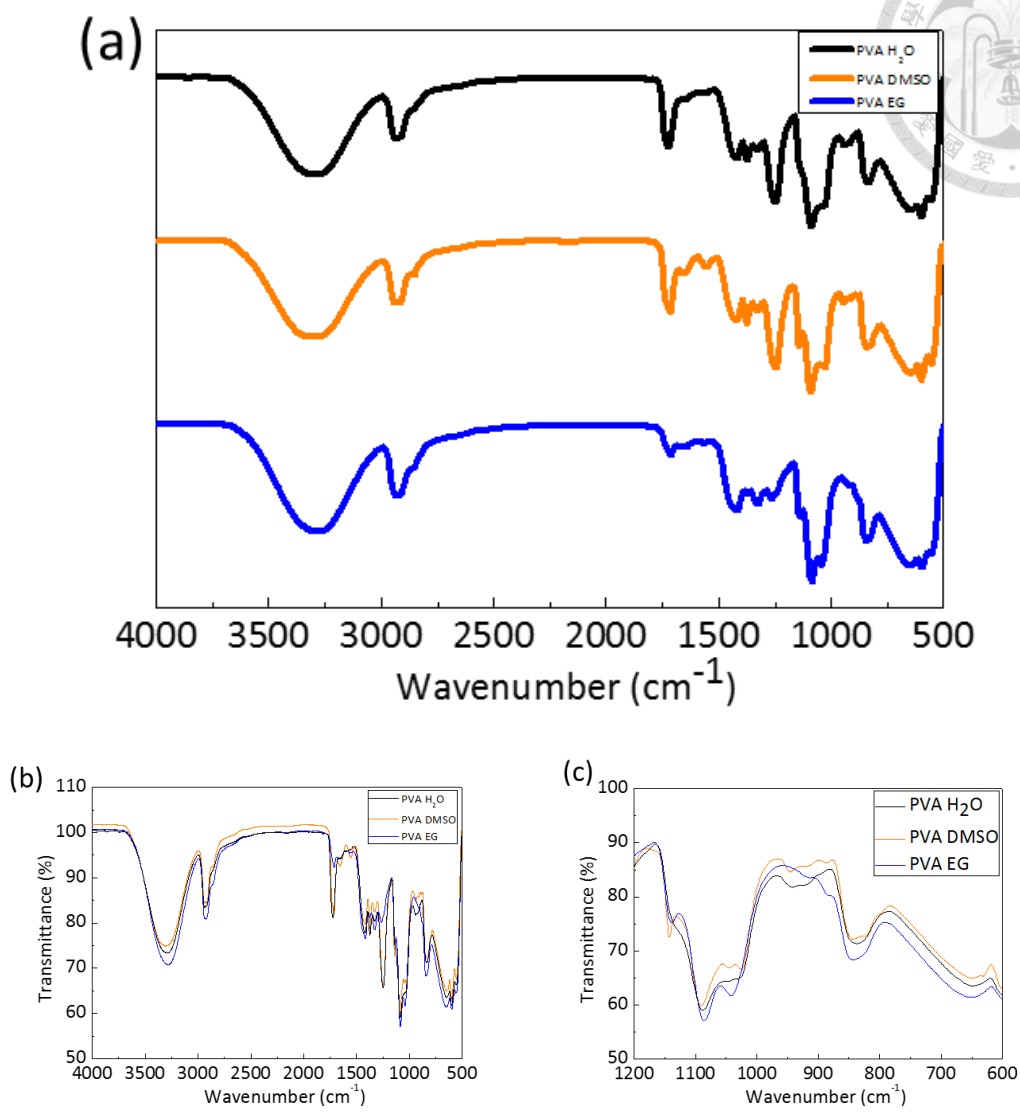
**Figure 2-2.** Plotted (a) TGA and (b) DTG thermogram of PVA casted in EG and Water. (c) TGA and (d) DTG of PMAA casted in EG and Water. (e) TGA and (f) DTG of PVA, PMAA, and pseudo-hydrogel blends casted in EG.



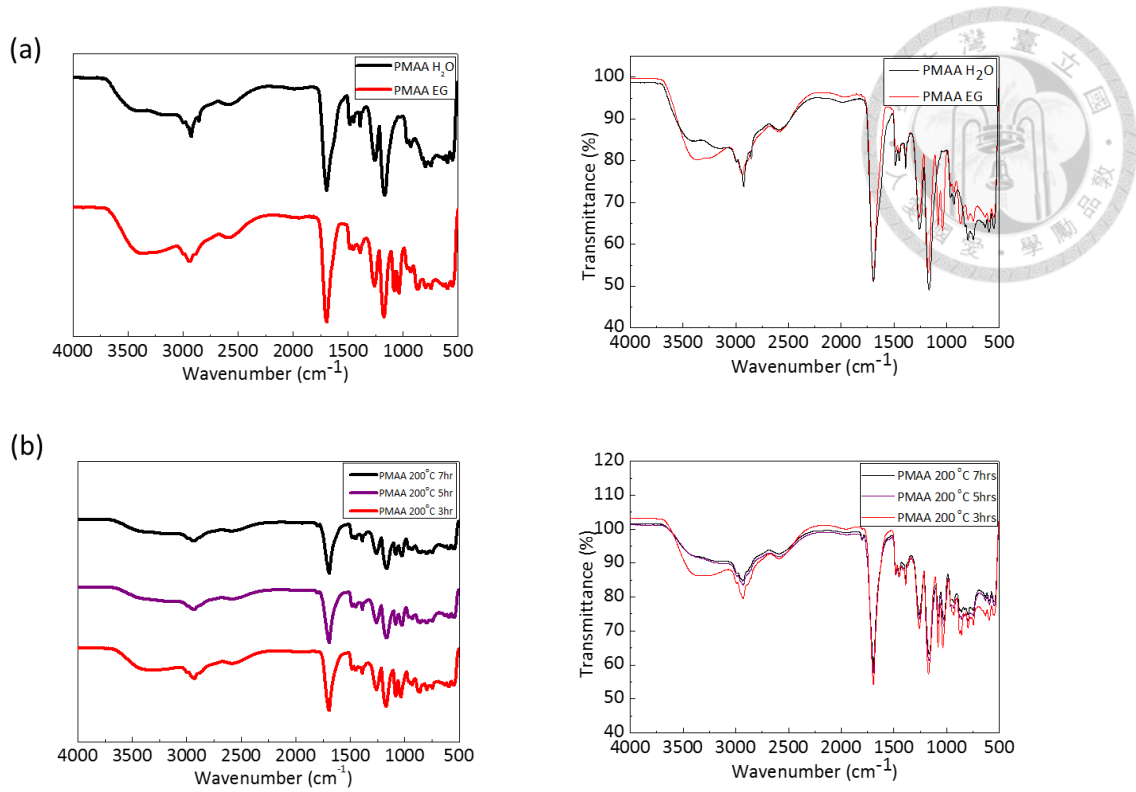
**Figure 2-3.** DSC thermograms of (a) PVA casted in EG and Water (b) PVA, PMAA, and pseudo-hydrogel blends casted in EG



**Figure 2-4.** XRD diagrams of (a) PVA casted in EG and Water (b) PVA, PMAA, and pseudo-hydrogel blends casted in EG

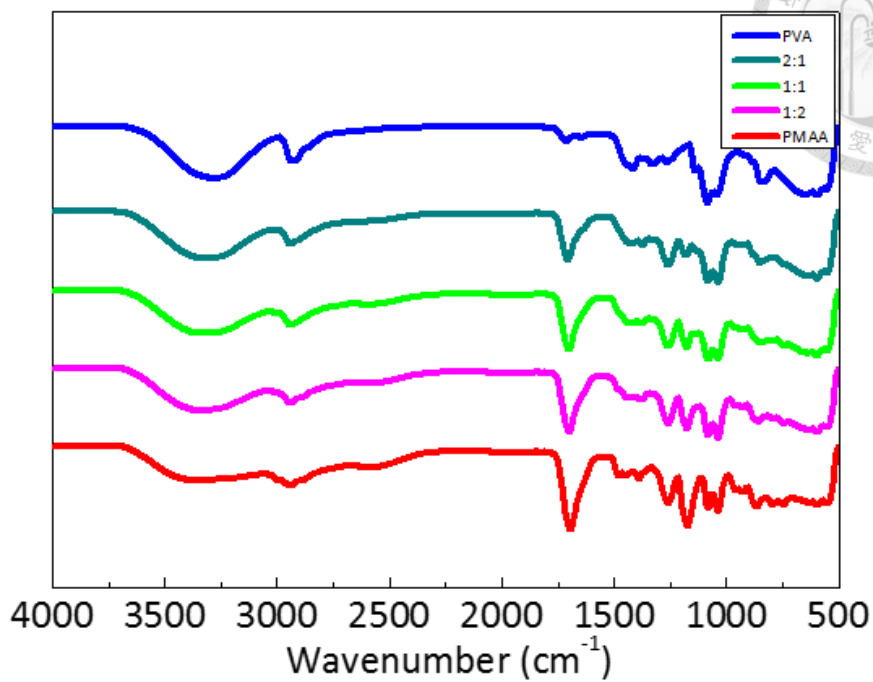


**Figure 2-5.** FTIR spectra of PVA casted in water, DMSO, and EG in (a) overlay, (b) offsets, and (c) close-up of 1200 to 600 cm<sup>-1</sup>.

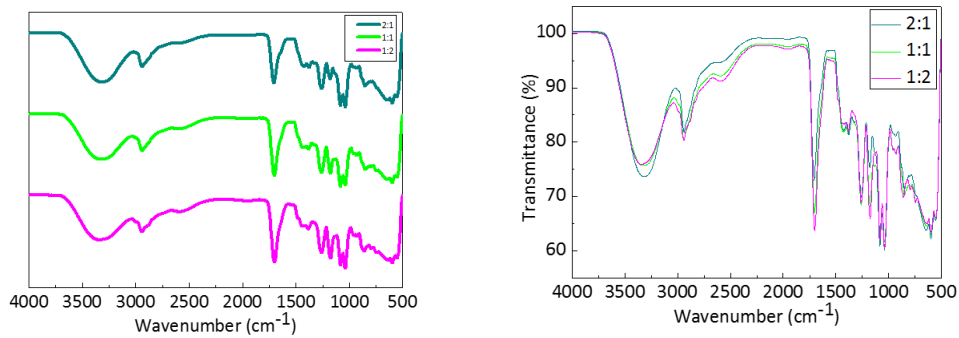


**Figure 2-6.** FTIR spectra of (a) PMAA casted in water and DMSO and (b) PMAA casted under different durations at 200 °C in EG.

(a)

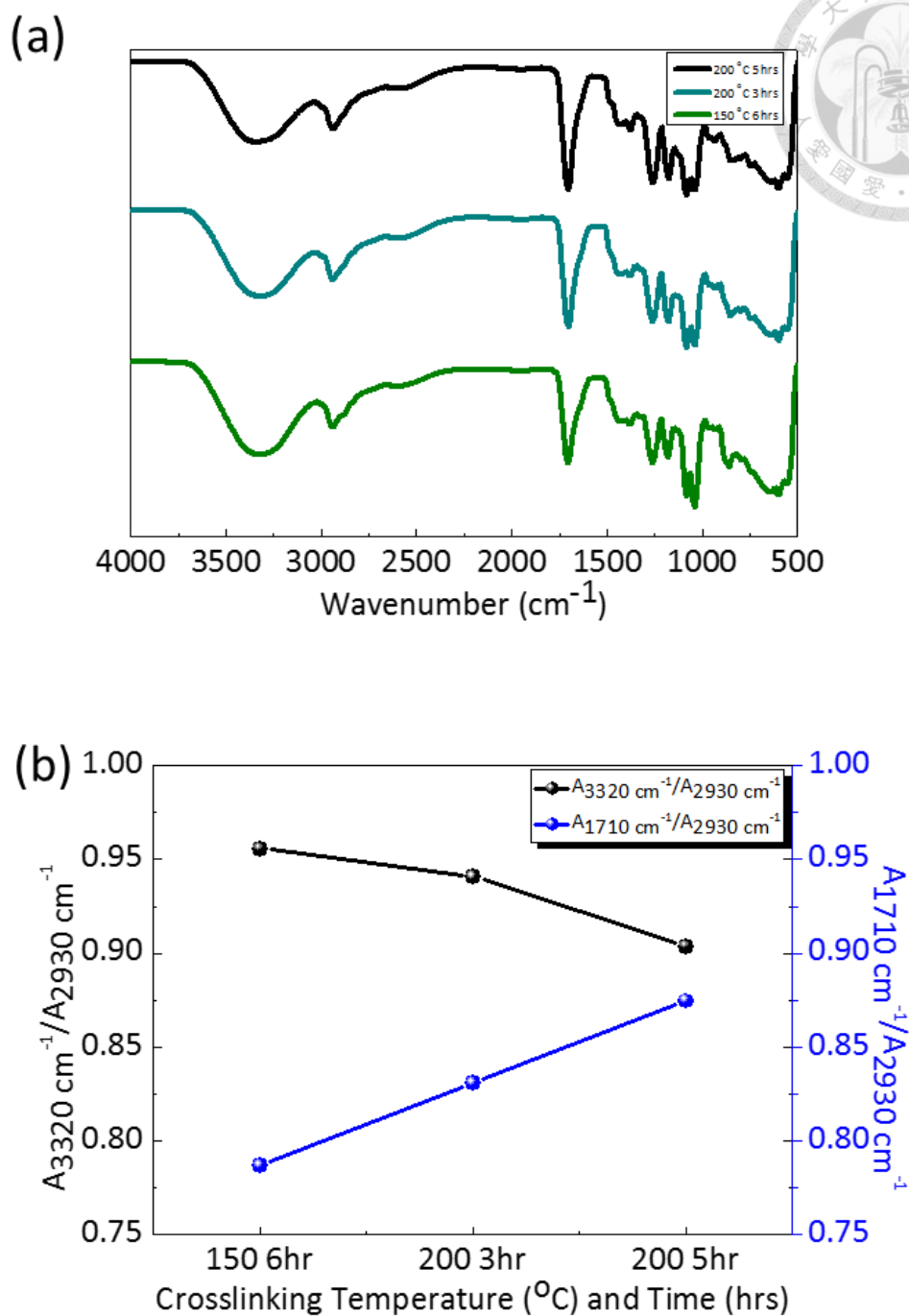


(b)



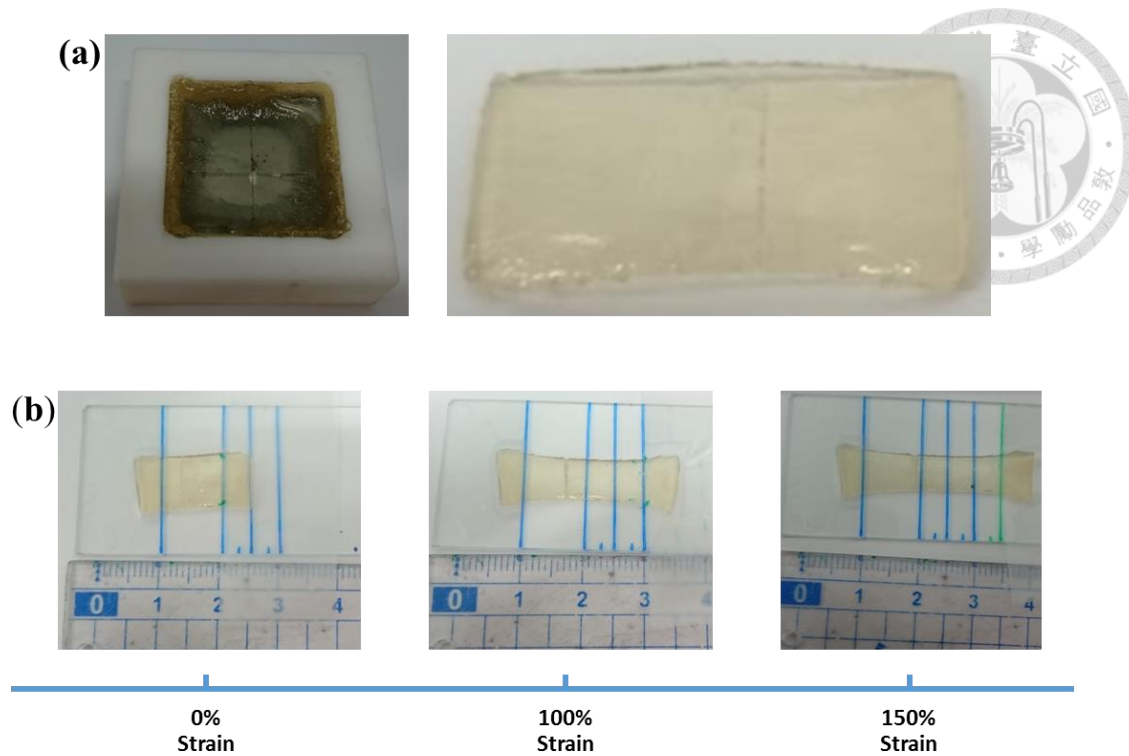
**Figure 2-7.** FTIR spectra of (a) pseudo-hydrogels and their pure constituents and (b)

close-up of the pseudo-hydrogel blends.

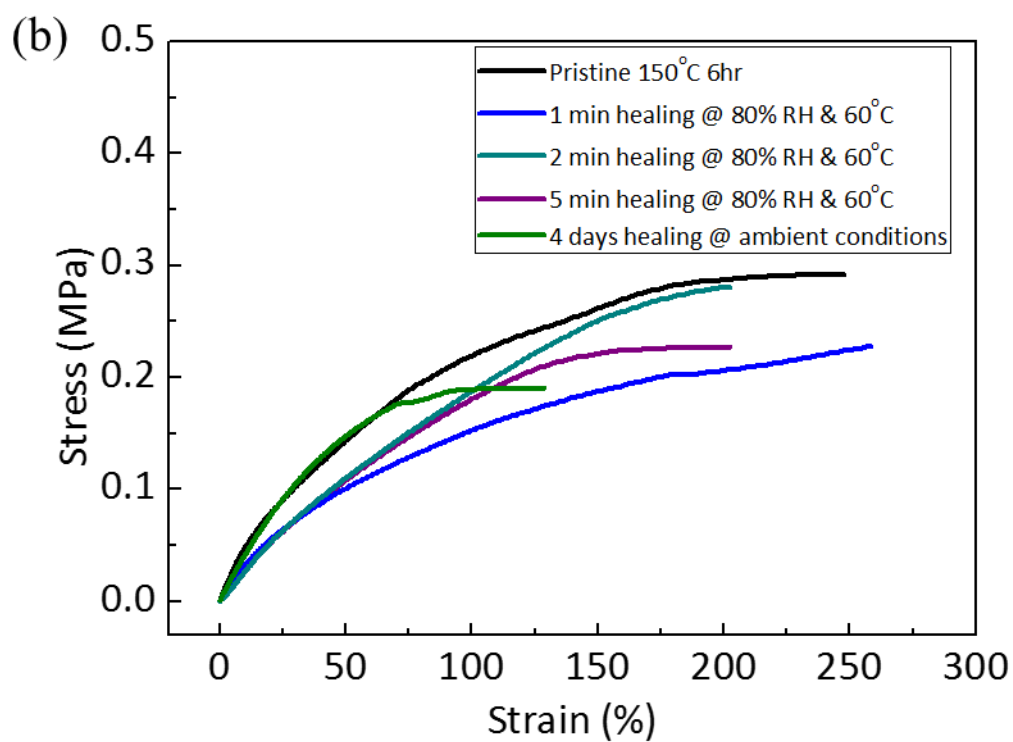
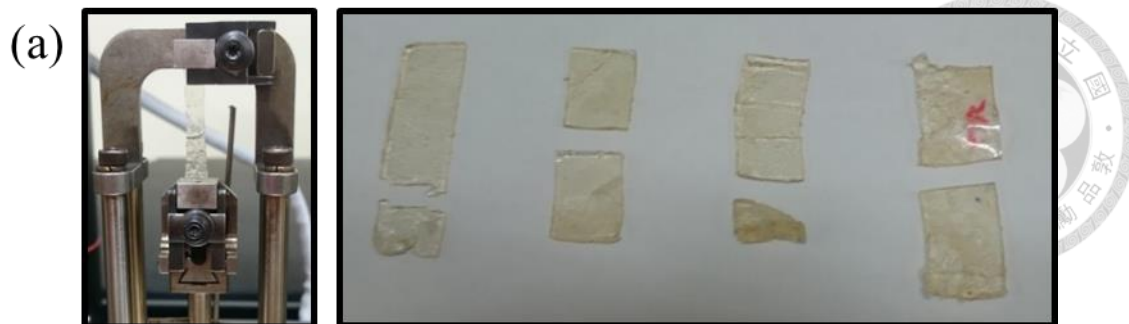


**Figure 2-8.** FTIR spectra of (a) 1:1 PVA:PMAA pseudo-hydrogel and (b) the change in  $A_{3320}/A_{2930}$  ratio and  $A_{1710}/A_{2930}$  as a function of cross-linking temperature and duration.

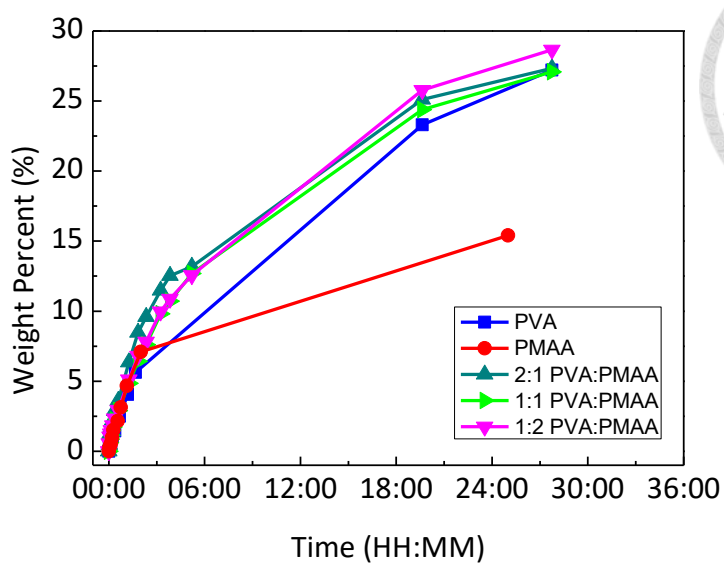




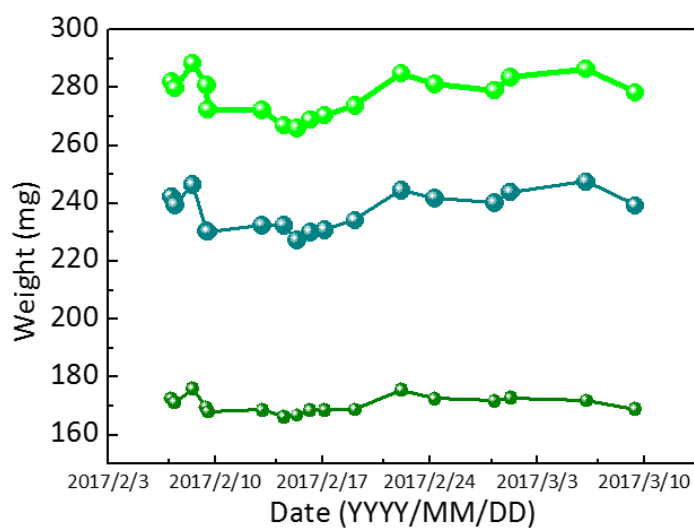
**Figure 2-9.** Picture of (a) cut and self-healed under ambient condition pseudo-hydrogel casted at 200 °C with (b) strain testing.



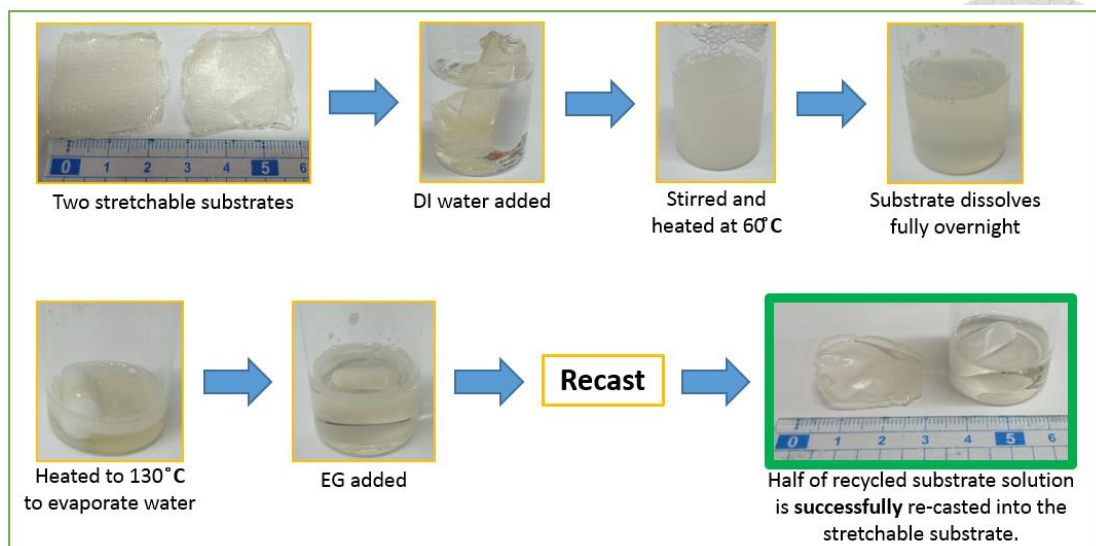
**Figure 2-10.** Picture of (a) cut and self-healed under 60 °C and high humidity pseudo-hydrogel casted at 150 °C and its corresponding (b) stress-strain curve.



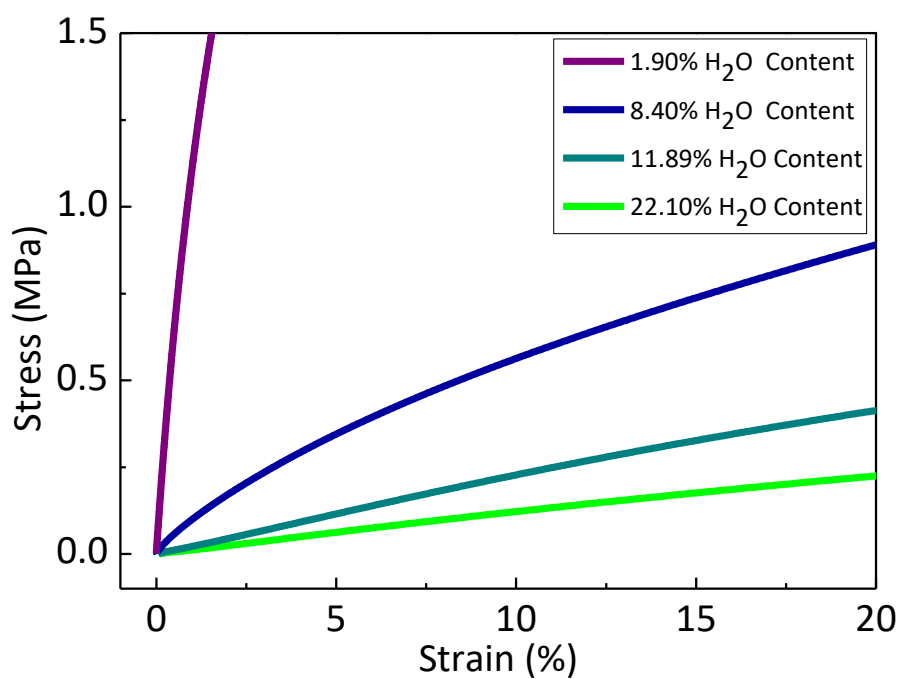
**Figure 2-11.** Water vapor absorption of PVA, PMAA, and pseudo-hydrogel blends casted in EG



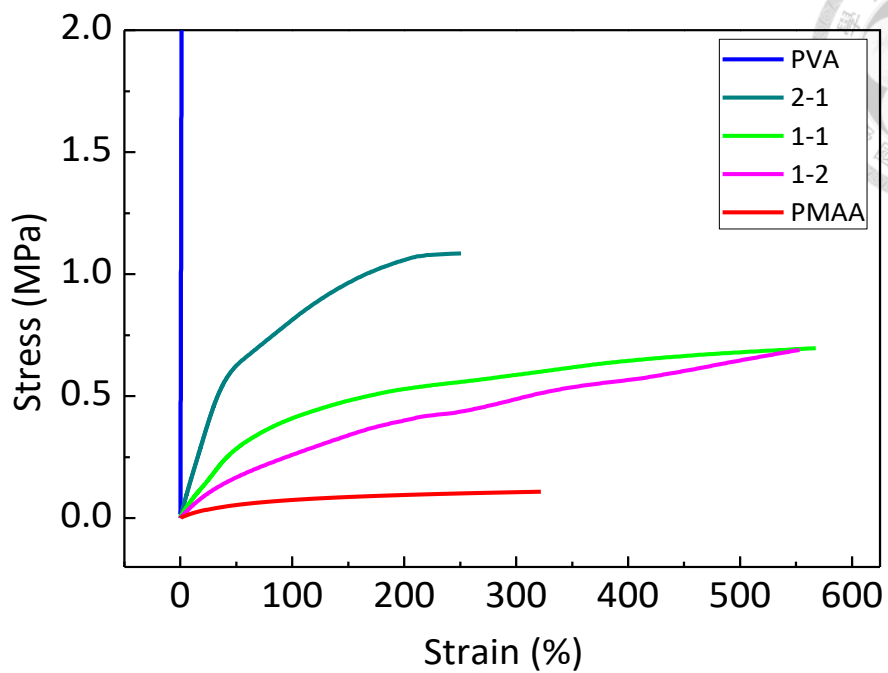
**Figure 2-12.** Water vapor retention of three 1:1 pseudo-hydrogel samples.



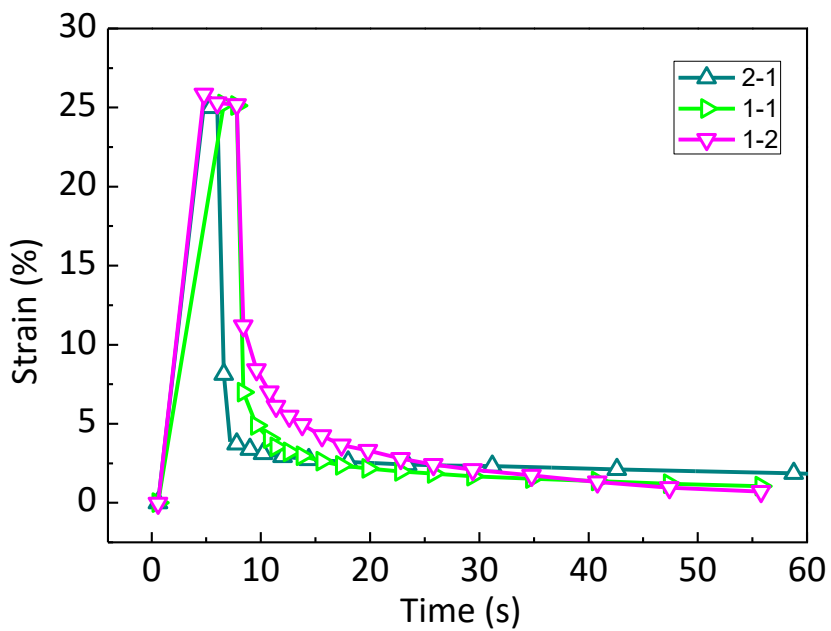
**Figure 2-13.** Recycling through dissolution in DI water of 1:1 pseudo-hydrogel.



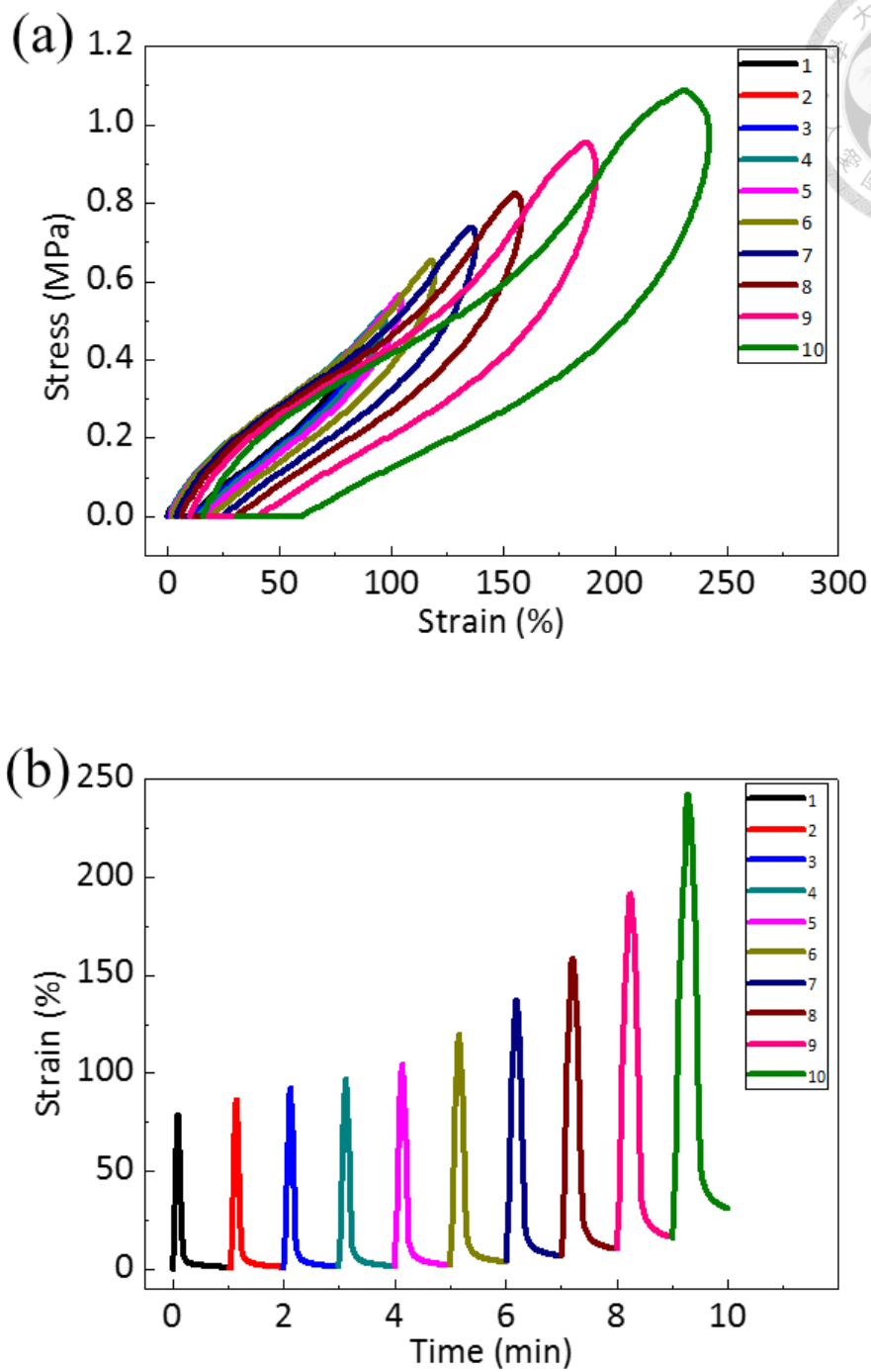
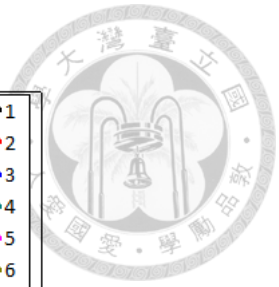
**Figure 2-14.** Effect of vapor content on the Stress-strain curve of a 1:1 pseudo-hydrogel



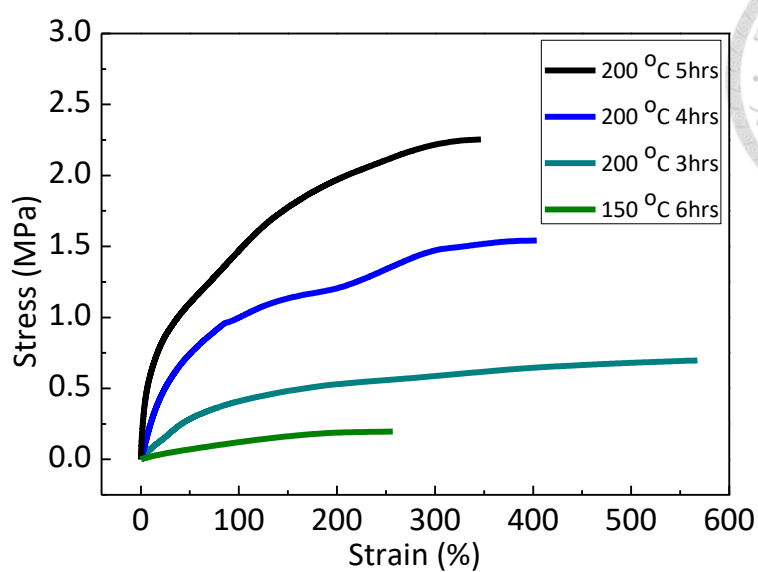
**Figure 2-15.** Stress-strain curves of PVA, PMAA, and pseudo-hydrogel blends casted in EG.



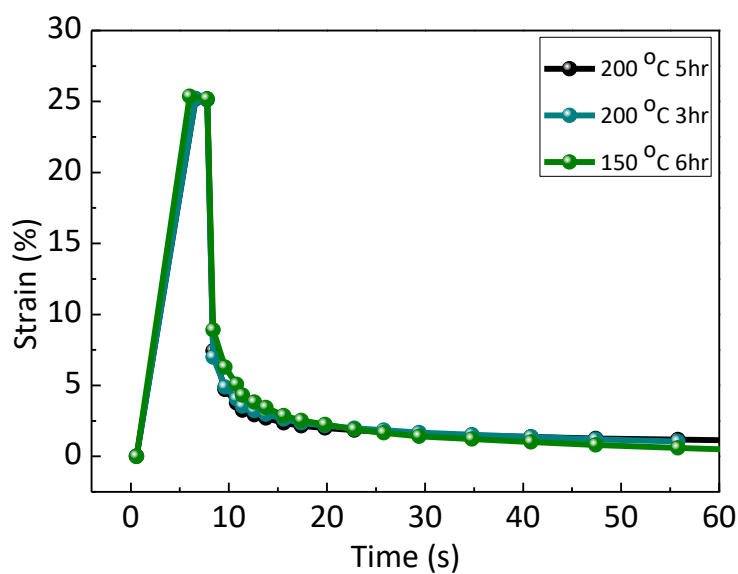
**Figure 2-16.** Strain-recovery curves at 25% strain of pseudo-hydrogel blends



**Figure 2-17.** (a) Load-unload cycles of 1:1 pseudo-hydrogel and (b) stress relaxation curves for 1:1 pseudo-hydrogel.

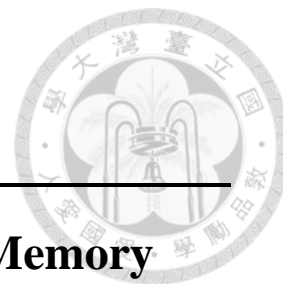


**Figure 2-18.** Stress-strain curves of a 1:1 pseudo-hydrogel at different cross-linking temperatures and times.



**Figure 2-19.** Strain-recovery curves at 25% strain of a 1:1 pseudo-hydrogel at different cross-linking temperatures and times.

# Chapter 3



---

## **Biocompatible and Stretchable DNA Memory fabricated on a PVA:PMAA Pseudo Hydrogel**

### **3.1 Introduction to Biocompatible Memory Devices**

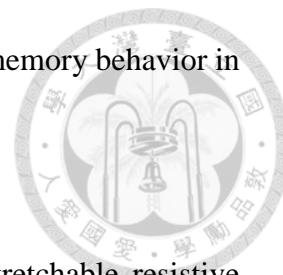
Polymer-based resistive memories are a promising alternative to traditional inorganic semiconductor-based memory technology for large capacity data storage due to their good scalability, flexibility/stretchability, low cost, and ease of processability.<sup>1-</sup>

<sup>5</sup> Polymer resistive memory devices have attracted a significant scientific research because conventional silicon based technologies are approaching theoretical and physical limitations in downscaling.

Resistive-type memory devices benefit from a facile fabrication for high data storage density since they are not confined by a specific cell structure.<sup>6, 7</sup> Resistive memory defines two states of electrical bistability of high and low conductivity as “1” (ON) or “0” (OFF) in an applied electric field. Areas of interest in the performance of resistive memory devices include large ON-OFF current ratios, low operation voltage, long retention times, high stability, and more recently, biocompatibility, intrinsic flexibility/stretchability, and performance retention under flex/strain. Polymer memory



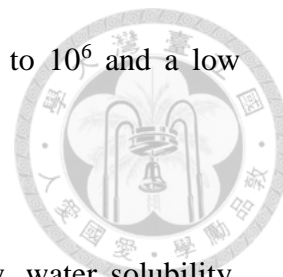
layers and device structures are chosen with great care to improve memory behavior in these areas.<sup>9-11</sup>



Recently, our lab has had success in the production of stretchable resistive memory device based on novel nanostructure-controlled carbohydrate-block-polyisoprene (MH-b-PI) block copolymers.<sup>1</sup> Oligosaccharides are an interesting hydrophilic biopolymer because they are abundant, renewable, biodegradable and biocompatible. In this study, WORM, flash, and DRAM resistive memory-type could be significantly tuned depending on the nanostructure of the MH-b-PI block copolymers. A highly stretchable memory device using a PDMS/CNTs/MH-b-PI2.6k/Al structure exhibited excellent ON/OFF current ratios over  $10^6$  with stable  $V_{set}$  around -2 V under 0-100% strain. These memory characteristics were maintained over 500 30% strain cycles. This was one of the first stretchable memory devices made using a biocompatible memory layer and showed great potential applications for high-performance stretchable and wearable electronic devices.

Interestingly, new high performance digital memory devices has recently been fabricated from salmon testes DNA (St-DNA) and DNA-mimics.<sup>4</sup> DNA is a bio-macromolecule which carries genetic information through selective hydrogen-bond nucleobase pairs. They determined the memory properties stemmed from charge trapping and hopping in the nucleobase moieties. The Al/St-DNA/Al devices exhibited

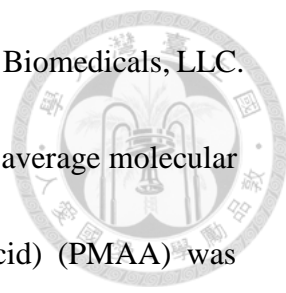
WORM memory behavior with a high ON/OFF current ratio up to  $10^6$  and a low threshold voltage of 2.3 V.



In this study, we continue the themes of biocompatibility, water solubility, stretchability, and high performance in fabricating a fully stretchable, air-stable resistor-type memory device on top of the 1:1 PVA:PMAA pseudo-hydrogel. The stretchable bottom and top electrodes were composed of a polymer blend between PEDOT:PSS and polyurethane (PU) at a 1:4 ratio (1:4 PEDOT:PU) to ensure strain independent current flow at strains up to 50%. The memory layer consisted of St-DNA inspired from<sup>2, 4</sup>. The memory effects were obtained by the I-V characteristics using a device structure of 1:1 pseudo-hydrogel/1:4 PEDOT:PU/St-DNA/1:4 PEDOT:PU. The device succeeded in obtaining similar WORM memory behaviors to the literature values even under 10%, 30%, 50% strain, and cycling tests. The device was also a proof of concept for a fully stretchable “green” electronic device in which the 1:1 PVA:PMAA pseudo-hydrogel proved a viable alternative to PDMS due to its smooth surface and hydrophilic nature.

## **3.2 Experimental**

### **3.2.1 Materials**



Deoxyribonucleic Acid Sodium Salt was purchased from MP Biomedicals, LLC. Poly(vinyl alcohol) (PVA) (87-90% hydrolyzed and 30,000-70,000 average molecular weight) was purchased from Sigma-Aldrich. Poly(methacrylic acid) (PMAA) was purchased from Scientific Polymer Products. Ethylene glycol (EG) (99.8% anhydrous), was purchased from Sigma-Aldrich. Methyl alcohol (methanol, anhydrous, >99.5%), acetone (>99.5%), toluene (>99.5%), and isopropyl alcohol (IPA, >99.5%) were purchased from Macron Fine Chemicals. Highly flexible, solvent-free, aliphatic polyester polyurethane (PU) dispersion (Alberdingk® U 3251) was purchased from Alberdingk Boley, Inc. Zonyl FS-300 fluoro-surfactant (Zonyl, ~40% solids in H<sub>2</sub>O) was purchased from Fluka Analytical. Pelco Colloidal Silver Liquid (silver paint) was purchased from, Ted Pella, Inc. PH1000 PEDOT/PSS was purchased from UniRegion Biotech. All materials were used without any further purification.

### **3.2.2 Characterization**

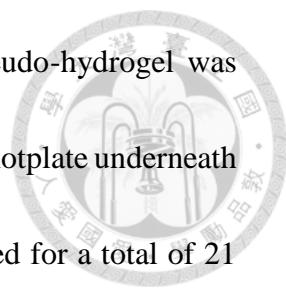
The morphologies of the pseudo-hydrogel substrate were obtained with a Nanoscope 3D Controller Atomic Force Micrograph (AFM, Digital Instruments) operated in tapping mode at room temperature. The electrical characterization of the memory device was performed by a Keithley 4200-SCS semiconductor parameter analyzer in ambient conditions at room temperature with all biasing applied on the top

electrodes.



### 3.3.3 Fabrication and Measurement of Memory Devices

The memory device was fabricated on top of a 1:1 PVA:PMAA pseudo-hydrogel. The 1:1 pseudo-hydrogel was prepared from a 1:1 mass ratio of PVA:PMAA dissolved in EG at a concentration of 200 mg/mL. Two mL of the solution was casted at 200 °C for 2 hours in a 3x3x1.5 cm<sup>3</sup> Teflon mold lined with a cleaned Si wafer at the bottom to produce a smooth substrate upon peeling off. The bare Si wafer was cleaned by ultrasonication with acetone, toluene, and IPA for 15 min each. The top and bottom electrodes were produced from a blend of PEDOT:PSS and PU. The PEDOT was prepared by mixing 20 mL of PH1000 PEDOT:PSS with 2mL of DMSO as a pretreatment to increase the conductivity and 200 µL of Zonyl as a surfactant. The PEDOT solution was stirred overnight at room temperature. The PU solution was prepared by dissolving 2 mL of 400 mg/mL PU in 20 mL of DI water and was stirred overnight also. The two solutions were blended by adding the all of PEDOT solution very slowly into a vigorously stirring PU solution. The 1:4 PEDOT:PU solution was then mixed overnight before spraying. The 1:4 PEDOT:PU solution was filtered through a 0.45 µm pore size PTFE membrane syringe filter into the spray-coating machine capsule. A narrow 0.5 mm bottom gate was patterned on the 1:1 pseudo-

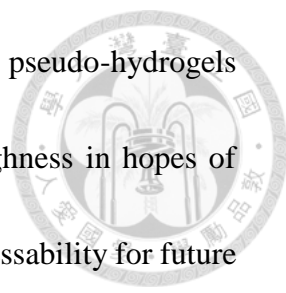


hydrogel using scotch tape as a shadow mask. The patterned pseudo-hydrogel was positioned under the spray nozzle at a spray height of 23 cm and the hotplate underneath the pseudo-hydrogel is set at 50 °C. The bottom electrode is sprayed for a total of 21 seconds at intervals of 1s spraying and 9s drying. The DNA solution is made by dissolving DNA sodium salt in 1 mL of water at a concentration of 27 mg/mL. After stirring for 6 hours, 2 mL of methanol is added to decrease the concentration for 9 mg/mL. The mixed solution is stirred overnight and spin coated onto the 1:4 PEDOT:PU bottom gate at 800rpm for 90s. For the top gate, 1:4 PEDOT:PU is spray-coated onto an OTS treated 300nm silicon oxide wafer using a shadow mask for patterning. The spray parameters are the same as the previously sprayed bottom gate. The top gate is transferred on top the DNA layer by aligning the top and bottom gates to form a cross-section and then applying small pressure on top the OTS wafer at 45 °C. Once the device is fabricated, colloidal silver liquid is painted on-top of the bottom and top electrodes to improve surface contact. A schematic of the DNA resistor memory device can be seen in Figure 3-1.

### **3.3 Results and Discussion**

#### **3.3.1 Pseudo-hydrogel Surface Morphology**

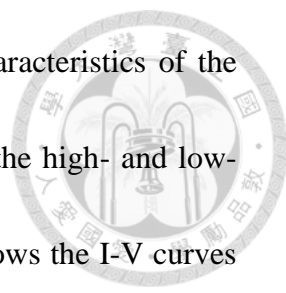
One important factor of suitable organic substrates for electronic devices is the surface roughness of the scaffold.<sup>11, 12</sup> A low substrate surface roughness is paramount



in good electronic performance of subsequent layers. Therefore, the pseudo-hydrogels are casted on top of cleaned silicon wafers with low surface roughness in hopes of manufacturing a biocompatible stretchable scaffold with good processability for future layers. Similar methods are used to lower the surface roughness of common stretchable substrates like PDMS. The AFM profiles can be seen in Figure 3-2 for 25  $\mu\text{m}^2$  and 100  $\mu\text{m}^2$ . The roughness of the 1:1 pseudo-hydrogel is extremely low, being less than 0.370 nm, which signifies an adequately smooth surface. This is comparable to the roughness of silicon wafers and PDMS casted on top of silicon wafers which proves that the pseudo-hydrogels can be an alternative, “green” option for fabrication of stretchable electronics. The AFM images also prove that the pseudo-hydrogel is not porous, which is a common characteristic of some hydrogels and would prove to be a difficult intrinsic property when fabricating bottom-up electronic device structures.

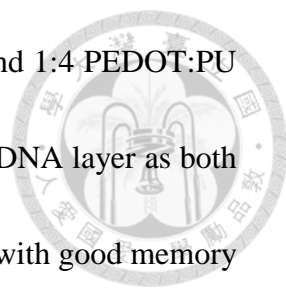
### **3.3.2 Memory Device Characterization**

The performance of a 1:1 pseudo-hydrogel/1:4 PEDOT:PU/St-DNA/1:4 PEDOT:PU device structure resistor-memory device was systematically investigated and compared to literature findings. The memory effects of the DNA-devices fabricated



by Ree et al. were studied based on the current-voltage (I-V) characteristics of the devices and how the DNA memory-devices stored data based on the high- and low-conductivity responses to applied external voltages. Figure 3-3, shows the I-V curves and retention times of the St-DNA (sodium salt) memory devices fabricated on a device structure of 300nm silicon oxide/Al/St-DNA/Al.<sup>4</sup> The St-DNA film is initially at a very low current level (OFF-state) and jump to a high level (ON-state) around 2.3 V, its critical switching-on voltage ( $V_{c,ON}$ ), when a positive voltage sweep is applied with a compliance current of 0.01 A. The ON-state is retained during subsequent forward, reverse, and negative voltage sweeps. The ON-state also remained even after the electrical power was turned off for a duration over 40,000 seconds. The ON/OFF current ratio was estimated to be  $10^5$  at a reading voltage of 1 V.

In comparison, Figure 3-4, shows the I-V curves and retention times of the St-DNA (sodium salt) memory devices in a device structure of 1:1 pseudo-hydrogel/1:4 PEDOT:PU/St-DNA/1:4 PEDOT:PU. The St-DNA film is also initially at a very low current level (OFF-state) and jump to a high level (ON-state) around 2.0 V ( $V_{c,ON}$ ). The ON-state is retained during subsequent forward, reverse, and negative voltage sweeps. The ON-state also remained even after the electrical power was turned off for a duration over 10,000 seconds. The ON/OFF current ratio was estimated to around  $10^4$  at a reading voltage of 1 V. In conclusion, changing the device structure of to an intrinsically

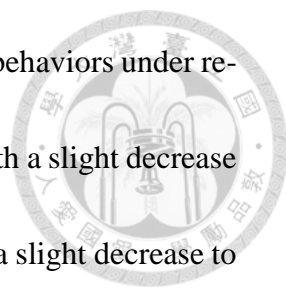


stretchable device using the 1:1 pseudo-hydrogel as the substrate and 1:4 PEDOT:PU as electrodes did not seem to affect the memory behavior of the St-DNA layer as both devices, literature and our work, exhibit WORM memory behavior with good memory retention. The decrease in ON/OFF current may be due to the less insulative property of the 1:1 pseudo-hydrogel compared to 300nm silicon oxide, which was used as the substrate in literature. The slight change in  $V_{c,ON}$  might be due to film thickness changes and the use of different electrodes between literature and this work. However, the values are quite similar and indicative that the St-DNA films show similar memory characteristics despite a change in device structure. Overall, both devices demonstrated excellent unipolar unipolar WORM memory characteristics with high ON/OFF current ratios and low power consumption.

### **3.3.2.1 Memory Device Performance Under Strain**

To evaluate the feasibility of using St-DNA as a stretchable organic memory in stretchable electronic applications, the electrical switching behaviors and retention times from different memory devices were tested under 10, 30, and 50% strains. Their I-V curves and retention times can be seen in Figure 3-5. As shown in Figures 3-6, the





organic memory exhibited similar WORM-type memory switching behaviors under re-stretching from 10 to 50% strain. The  $V_{c,ON}$  remained around 2 V with a slight decrease to 1.9 V at 50% and the ON/OFF current remained around  $10^4$  with a slight decrease to  $10^3$  at 30 and 50% strain. Under various strain conditions, a low-writing voltage under 5 V was retained, demonstrating the advantage of low-power consumption of stretchable memory applications. The distinguishable ON/OFF states at the reading voltage of 1 V were preserved under each stretching condition, which means that there is a low probability of misreading data under different stretching conditions. This is an extremely important factor in the field of wearable electronics where accuracy of measurements under strain are of utmost importance. These results suggest that our device of a 1:1 pseudo-hydrogel/1:4 PEDOT:PU/St-DNA/1:4 PEDOT:PU can operate and be programmed well for digital data even if the organic memory device is being elongated.

The durability of the programmed ON/OFF state under stretching conditions was further investigated. The DNA memory device was subject to a durability test after being programmed to the ON-state. The device was stretched to 30% strain and then relaxed to its 0% strain length for 500 cycles. A cycling strain of 30% was chosen because it is the on the upper end of typical strains wearable electronics might face. As shown in Figure 3-7, the ON state could retain its high-current conductivity and showed

only slight degradation after 500 cycles of being stretched by 30% strain. This suggests that the data retention of the device is quite durable, since it was able to retain its high ON state even under numerous cycles of elongation and relaxation.



### 3.3.2.2 DNA Memory Mechanism

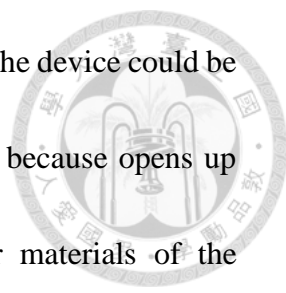
Much testing was done by Ree et al. on the WORM memory mechanism of DNA<sup>4</sup>. The unipolar WORM memory characteristics were understood to be initially controlled by ohmic conduction process in the low voltage region<sup>13</sup>, by trap-limited space charge limited conduction (SCLC) until  $V_{c,ON}$ <sup>14</sup>, and by ohmic conduction after  $V_{c,ON}$ . The DNA polymers also had low energy barriers compared to the Al in the literature device which indicated that the electrical conduction processes were mainly driven by hole injection, which means that the devices are all p-type. Since the memory behavior is similar between the literature device and our stretchable device, we can also assume our device is p-type. These permanent memory behaviors are thought to arise from the nucleobase units of DNA. This was concluded by the fact that the DNA mimicking P4HBA and P9HNA, which contained no nucleobase moieties, exhibited no memory behavior while P4HBA and P9HNA that included nucleobase moieties did exhibit WORM memory. Ree et al. investigated DNA brush copolymers containing purine nucleobase units which were found to have higher  $V_{c,ON}$  values as well as lower

ON-current levels compared to brush copolymers containing pyrimidine nucleobases.<sup>4</sup>

This was explained by the additional imidazole ring that the purine nucleobase had, which allowed for a deeper well to trap charges. It was then suggested that during a voltage sweep, the nucleobase moieties of purine or pyrimidine that were distributed in the polymer film could successfully trap charges and then transport them through the film layer via a hopping process when the purine and pyrimidine wells were filled fully at  $V_{c,ON}$ . Further proof of purine and pyrimidine moiety spacing in thin films attributing to charge trapping and hopping were given by the significant increase in  $V_{c,ON}$  and lowering of the ON-current level upon DNA complexation with cetyltrimethylammonium surfactant which increased the interdistance space between the nucleobase moieties. Thus, the electrical switching mechanism for resistive-memory behavior in DNA devices was attributed to charge trapping and hopping due to these observations.<sup>4</sup> Our device structure of a 1:1 pseudo-hydrogel/1:4 PEDOT:PU/St-DNA/1:4 PEDOT:PU further confirms these findings since the electrodes are comprised of 1:4 PEDOT:PU and therefore no metallic filamentary conduction can occur in the DNA memory layer.

### 3.3.3 Memory Device Dissolution in Water

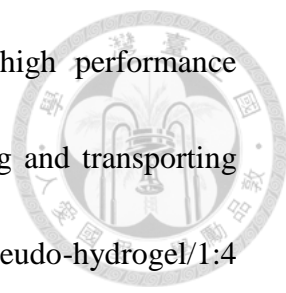
Great care was taken in choosing water-soluble materials to fabricate the



stretchable DNA resistive-memory device which would ensure that the device could be easily degraded in DI water. Dissolution in water is advantageous because opens up many “green” avenues to safely discard a device.<sup>15</sup> The major materials of the stretchable device, which include PVA, PMAA, EG, PU, PEDOT:PSS and DNA, are all water soluble, biodegradable (PVA<sup>16-18</sup> and DNA<sup>2,4</sup>) or biocompatible (PMAA,<sup>19-22</sup> PEDOT:PSS,<sup>23, 24</sup> and PU<sup>25</sup>) polymers, nontoxic, and approved by the FDA for use in medical device . As seen in Figure 3-8, the device could be easily fully dissolved in water at 60°C within 24 hours. Degradation through autocatalytic hydrolysis and bulk erosion begins as early as 10min. Dissolution in water can increase the surface area of biodegradable polymers which can increase the rate of their degradation. Dissolution can also decrease the amount of space a device takes up upon discarding. Water soluble polymers can also be subject to sonication and enzymatic degradation to safely discard them.<sup>26</sup> In conclusion, the DNA devices were fabricated using all biocompatible or biodegradable polymers and have an enormous potential to be easily, quickly, and safely discarded and pose little to no environmental or biological hazard, which is one of the biggest disadvantages of inorganic electronics.

### 3.3.4 Conclusions

In conclusion, we built upon the stretchable, biocompatible, nontoxic, and



water-soluble nature of the pseudo-hydrogel and fabricated a high performance resistive DNA memory device using St-DNA as a charge trapping and transporting layer. The memory device was composed using a structure of 1:1 pseudo-hydrogel/1:4 PEDOT:PU/St-DNA/1:4 PEDOT:PU to preserve the “green” properties of the pseudo-hydrogel. The device exhibited WORM memory characteristics similar to literature findings with a  $V_{c,ON}$  of 2 V, a high ON/OFF current ratio as high as  $10^4$  and a long retention time of  $10^4$ s. The device also retained these memory characteristics under 10, 30, and 50% strain as well as 500 strain cycles at 30% strain. The device could be easily dissolved in DI water which opens up bioresorbability and biodegradability potential.

### 3.4 References

1. C. C. Hung, Y. C. Chiu, H. C. Wu, C. Lu, C. Bouilhac, I. Otsuka, S. Halila, R. Borsali, S. H. Tung, W. C. Chen, *Adv. Funct. Mater.* 2017, 27;
2. C.-C. Shih, C.-Y. Chung, J.-Y. Lam, H.-C. Wu, Y. Morimitsu, H. Matsuno, K. Tanaka, W.-C. Chen, *Chem. Commun.* 2016, 52, 13463;
3. J. Yao, J. Lin, Y. Dai, G. Ruan, Z. Yan, L. Li, L. Zhong, D. Natelson, J. M. Tour, *Nat. Commun.* 2012, 3, 1101;
4. J. Lee, Y. Kim, C. Kim, M. Ree, *Mater. Horiz.* 2017, 4, 423;
5. Y.-C. Lai, Y.-C. Huang, T.-Y. Lin, Y.-X. Wang, C.-Y. Chang, Y. Li, T.-Y. Lin, B.-W. Ye, Y.-P. Hsieh, W.-F. Su, *NPG Asia Mater.* 2014, 6, e87;
6. J. H. Smits, S. C. Meskers, R. A. Janssen, A. W. Marsman, D. M. de Leeuw, *Adv. Mater.* 2005, 17, 1169;
7. F. Verbakel, S. C. Meskers, R. A. Janssen, *Chem. Mater.* 2006, 18, 2707;
8. C. W. Chu, J. Ouyang, J. H. Tseng, Y. Yang, *Adv. Mater.* 2005, 17, 1440;
9. S. L. Lim, Q. Ling, E. Y. H. Teo, C. X. Zhu, D. S. H. Chan, E.-T. Kang, K. G. Neoh, *Chem. Mater.* 2007, 19, 5148;
10. B. Cho, S. Song, Y. Ji, T. W. Kim, T. Lee, *Adv. Funct. Mater.* 2011, 21, 2806;
11. B. Peng, X. Ren, Z. Wang, X. Wang, R. C. Roberts, P. K. Chan, *Sci. Rep.*



- 2014, 4, 6430;
12. C. J. Bettinger, Z. Bao, *Adv. Mater.* 2010, 22, 651;
13. A. Campbell, D. Bradley, D. Lidzey, *J. Appl. Phys.* 1997, 82, 6326;
14. P. Mark, W. Helfrich, *J. Appl. Phys.* 1962, 33, 205;
15. L. Yin, A. B. Farimani, K. Min, N. Vishal, J. Lam, Y. K. Lee, N. R. Aluru,  
J. A. Rogers, *Adv. Mater.* 2015, 27, 1857;
16. G. Silva, P. Sobral, R. Carvalho, P. Bergo, O. Mendieta-Taboada, A.  
Habitante, *J. Polym. Environ.* 2008, 16, 276;
17. R. A. Gross, B. Kalra, *Science* 2002, 297, 803;
18. G. Saunders, B. MacCreath, *Application Compendium. Agilent  
Technologies* 2010;
19. L. Yu, N. Ren, K. Yang, M. Zhang, L. Su, *J. Appl. Polym. Sci.* 2016, 133;
20. P. Yang, D. Li, S. Jin, J. Ding, J. Guo, W. Shi, C. Wang, *Biomaterials.*  
2014, 35, 2079;
21. C. De Vasconcelos, d. P. Bezerril, D. Dos Santos, d. T. Dantas, M. Pereira,  
J. Fonseca, *Biomacromolecules.* 2006, 7, 1245;
22. R. Larson, E. Bookland, R. Williams, K. Yocom, D. Saucy, M. Freeman, G.  
Swift, *J. Environ. Polym. Degrad.* 1997, 5, 41;
23. S.-C. Luo, E. Mohamed Ali, N. C. Tansil, H.-h. Yu, S. Gao, E. A.



Kantchev, J. Y. Ying, Langmuir 2008, 24, 8071;

24. G. Cellot, P. Lagonegro, G. Tarabella, D. Scaini, F. Fabbri, S. Iannotta, M.

Prato, G. Salviati, L. Ballerini, Front. Neurosci. 2015, 9;

25. Y. Marois, R. Guidoin, 2013;

26. A. Tayal, S. A. Khan, Macromolecules 2000, 33, 9488.





Figures

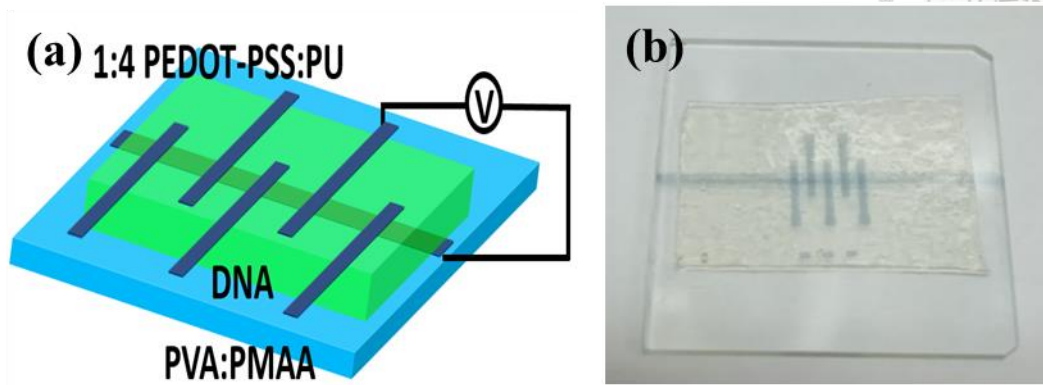


Figure 3-1. Schematic diagram (a) and picture (b) of stretchable DNA memory device.

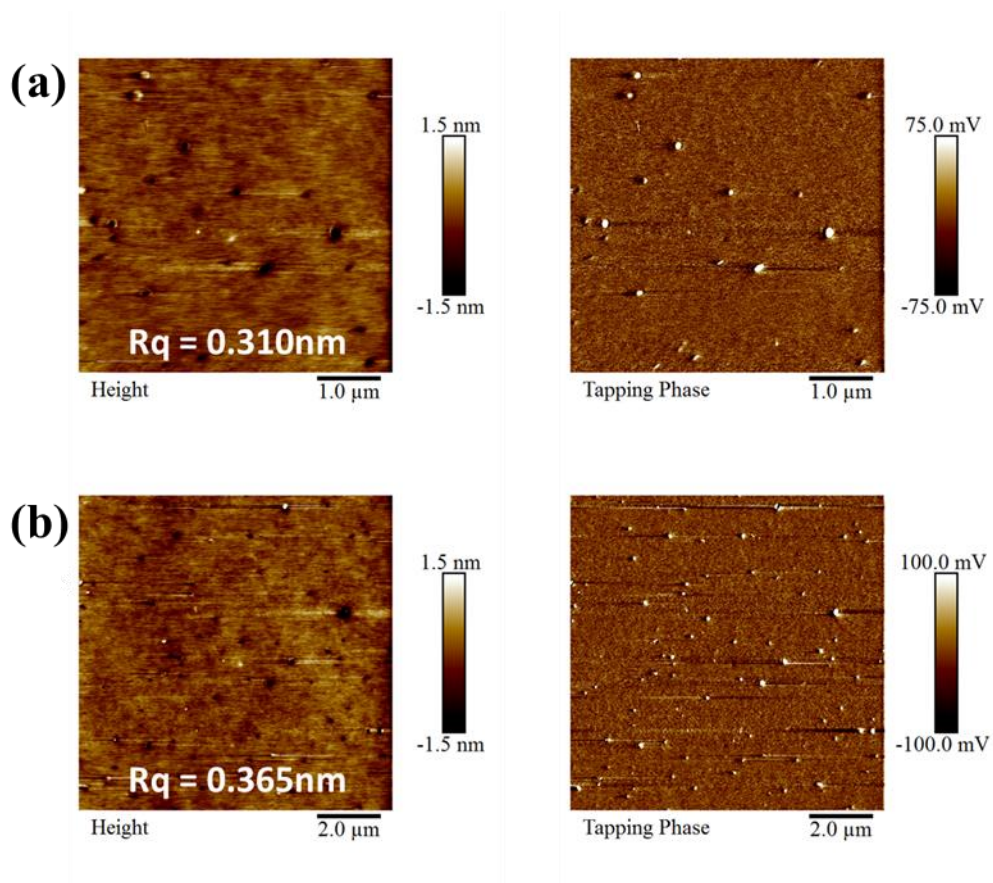
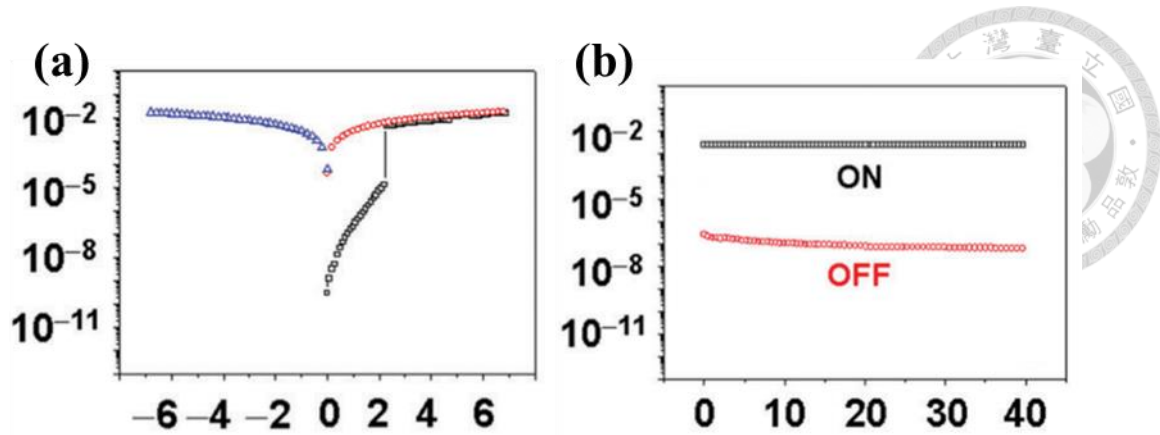
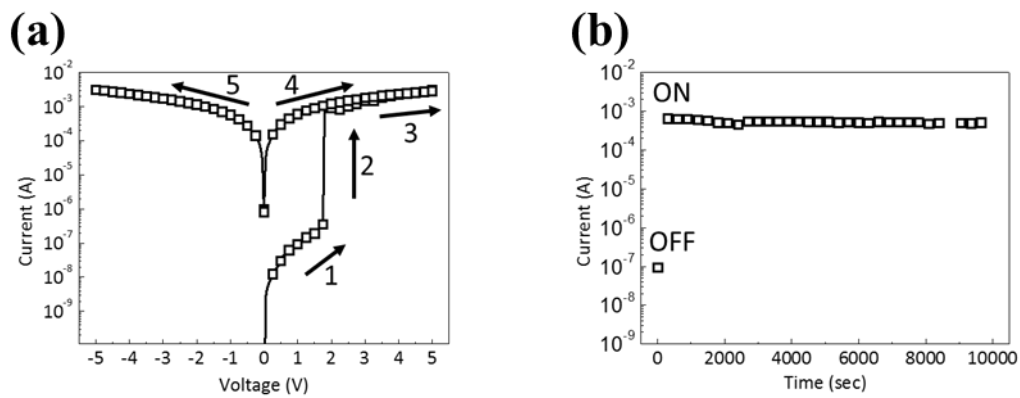


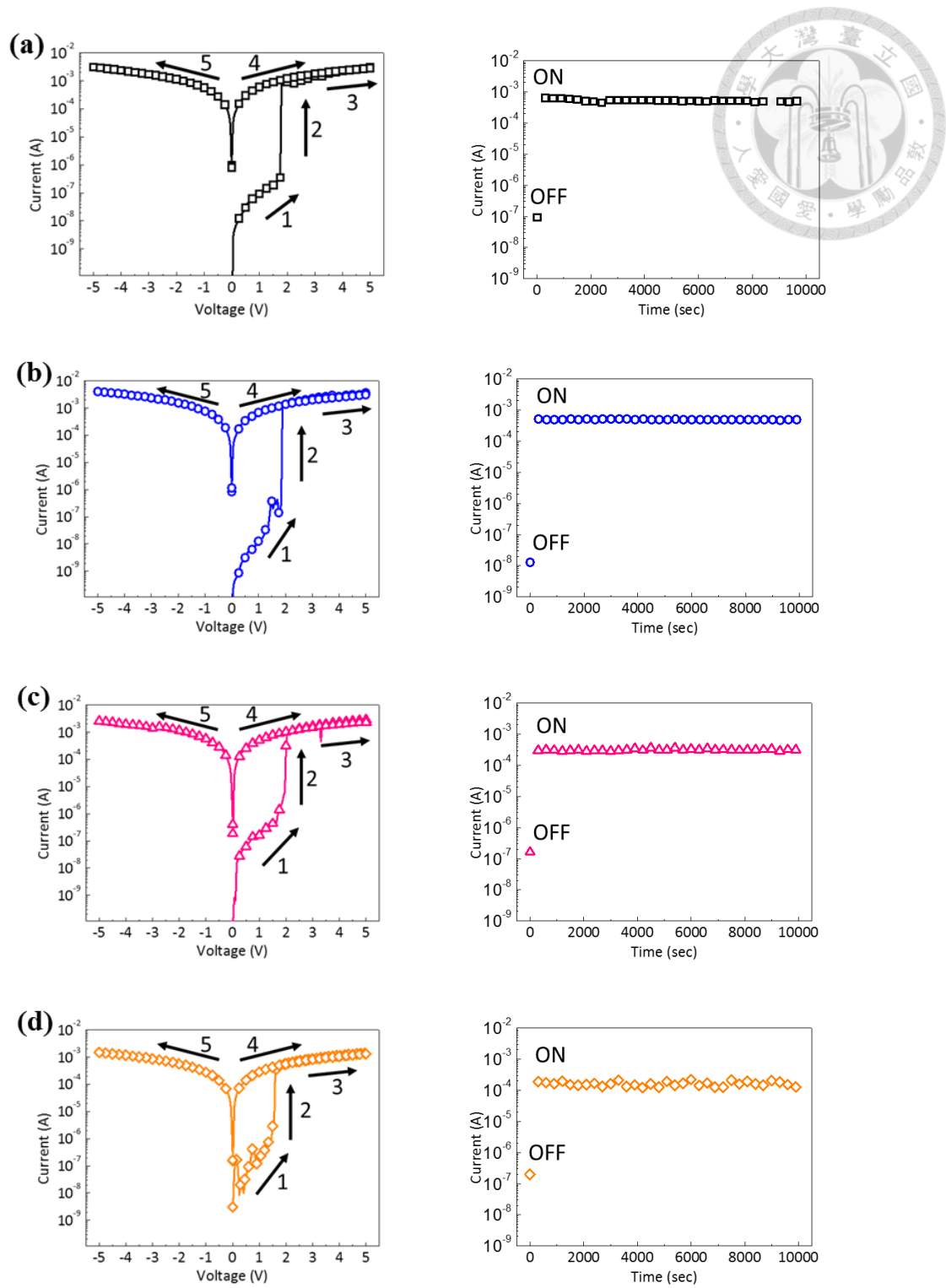
Figure 3-2. AFM topographies and phase images of 1:1 pseudo-hydrogel at an area of (a)  $25 \mu\text{m}^2$  and (b)  $100 \mu\text{m}^2$ .



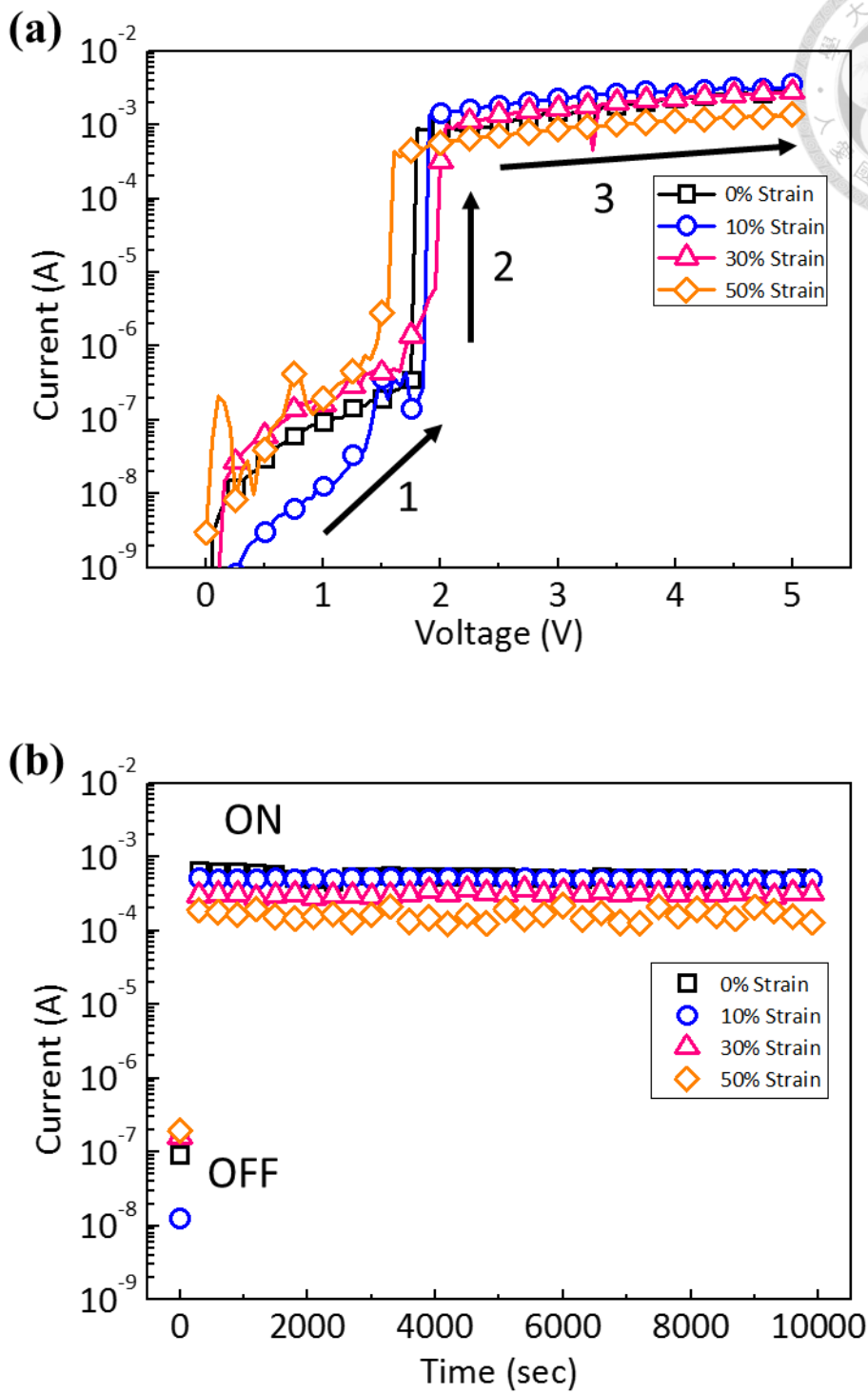
**Figure 3-3.** I-V curves (a) and retention times (b) of the St-DNA (sodium salt) memory devices fabricated on a device structure of 300nm silicon oxide/Al/St-DNA/Al.<sup>4</sup>



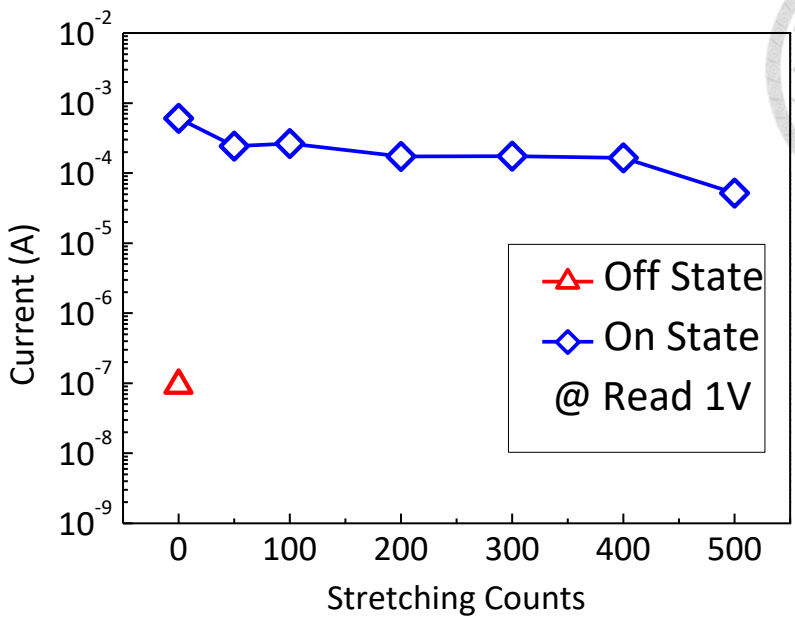
**Figure 3-4.** I-V curves (a) and retention times (b) of the St-DNA (sodium salt) memory devices fabricated on a device structure of 1:1 pseudo-hydrogel/1:4 PEDOT:PU/St-DNA/1:4 PEDOT:PU



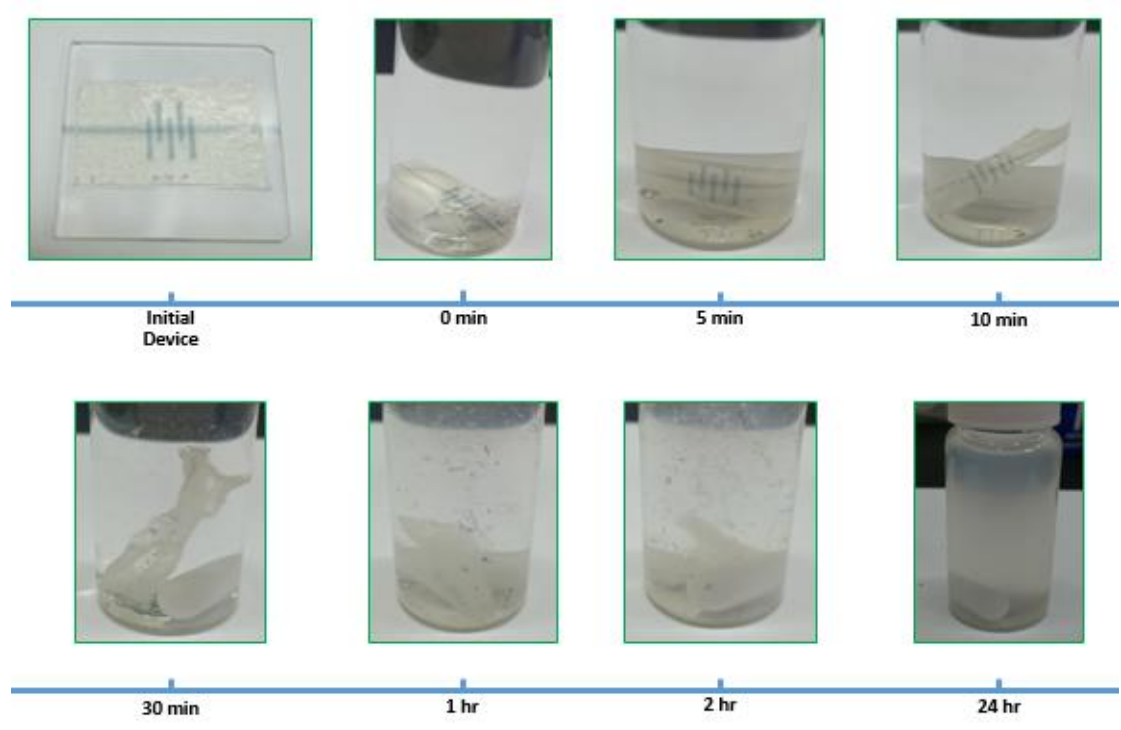
**Figure 3-5.** I-V curves and retention times (read at 1 V) of the St-DNA (sodium salt) memory devices fabricated on a device structure of 1:1 pseudo-hydrogel/1:4 PEDOT:PU/St-DNA/1:4 PEDOT:PU at 0% (a), 10% (b), 30% (c), and 50% (d) strain.



**Figure 3-6.** Compilation of I-V curves (a) and retention times (read at 1 V) (b) of the St-DNA (sodium salt) memory devices at 0%, 10%, 30%, and 50% strain.



**Figure 3-7.** ON state retention of stretchable DNA resistor device after 500 cycles of 30% strain and relax.



**Figure 3-8.** DNA device dissolution in DI water over 24 hours.

# Chapter 4



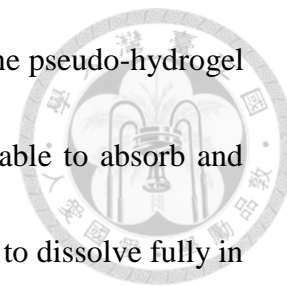
---

## Conclusion and Future Work

In this thesis, fabrication and characterization of a PVA:PMAA pseudo-hydrogel and application of said pseudo-hydrogel into a fully stretchable DNA resistive-memory device were reported. The pseudo-hydrogel was found to have several significant properties including: water vapor absorption and retention, good mechanical properties, self-healing, recyclability, and facile fabrication. Great care was taken to ensure that the subsequent DNA memory device fabricated on top the pseudo-hydrogel was stretchable, non-toxic, biocompatible, and water soluble while maintaining its high performance. The conclusions of each chapters are summarized below:

In chapter 2, a biocompatible, non-toxic, self-healing, mechanically tough, vapor absorbing and retaining, and recyclable PVA:PMAA pseudo-hydrogel is facilely fabricated. TGA, DSC, XRD, FTIR, and self-healing testing were used to confirm that the full blending of PVA and PMAA polymers as well as give insight on the strong hydrogen cross-link bonding between them. Stress-strain curves, relaxation times, loading and unloading mechanical testing revealed the high elongation, fast recovery, and tunable mechanical properties which helped confirm the 3D gel comprised of

mostly strong hydrogen bonds of the pseudo-hydrogel structure. The pseudo-hydrogel interactions with water were especially important as the gel was able to absorb and retain water vapor which is a novel property. The gel was also able to dissolve fully in water which is important for recycling and biodegradable pathways.



In chapter 3, we built upon the stretchable, biocompatible, nontoxic, and water-soluble nature of the pseudo-hydrogel and fabricated a high performance resistive DNA memory device using St-DNA as a charge trapping and transporting layer. The memory device was composed using a structure of 1:1 pseudo-hydrogel/1:4 PEDOT:PU/St-DNA/1:4 PEDOT:PU to preserve the “green” properties of the pseudo-hydrogel. The device exhibited WORM memory characteristics similar to literature findings with a  $V_{c,ON}$  of 2 V, a high ON/OFF current ratio up to  $10^4$  and a long retention time of  $10^4$ s. The device also retained these memory characteristics under 10, 30, and 50% strain as well as 500 strain cycles at 30% strain. The device could be easily dissolved in DI water which opens up bioresorbability and biodegradability potential.

From the above conclusions, some potential applications and projects using this pseudo-hydrogel could include: (1) Pyramid structured pseudo-hydrogel pressure sensors and the investigation of its performance compared to traditional PDMS pressure sensors. (2) Incorporation of ions into the pseudo-hydrogel to examine performance as an electrical double layer (EDL) dielectric in a “green” OTFT as well as examining the

effect an additional ion network to form a possible triple-network gel. (3). Gel blend of poly(lactic-co-glycolic acid) (PLGA) and PVA to form a fully biodegradable substrate and the eventual fabrication of a memory or TFT device using DNA to form a fully stretchable and biodegradable electronic device.

